ABSTRACT

Title of Document:	The Multiple Sulfur Isotopic Composition of Iron Meteorites: Implications for Nebular Evolution.
	Michael Ariel Antonelli, Master of Science, 2013.
Directed By:	Professor James Farquhar, Department of Geology and Earth System Sciences Interdisciplinary Center, University of Maryland-College Park

Multiple sulfur isotopic measurements of troilite from 61 different iron meteorites were undertaken in order to test for sulfur isotopic homogeneity within (and between) 8 different iron meteorite groups. It was found that different members within a given group of iron meteorites have homogeneous $\Delta^{33}S$ compositions, but that these $\Delta^{33}S$ compositions differ between groups. This thesis shows that iron meteorites from the groups IC, IIAB, IIIAB, IIIF, and IVA have small yet resolvable enrichments or depletions in $\Delta^{33}S$ relative to Canyon Diablo Troilite (CDT) and troilite from other non-magmatic (IAB and IIE) iron meteorites. The observed anomalous sulfur isotopic compositions in magmatic iron meteorites are most consistent with Lyman-α photolysis of H_2S, pointing towards inheritance of an unexpected photolytically-derived sulfur component in magmatic iron meteorite groups which is absent in non-magmatic iron meteorites, chondrites, and the Earth-Moon System.

THE MULTIPLE SULFUR ISOTOPIC COMPOSITION OF IRON METEORITES: IMPLICATIONS FOR NEBULAR EVOLUTION

By

Michael Ariel Antonelli

Thesis submitted to the Faculty of the Graduate School of the
University of Maryland, College Park, in partial fulfillment
of the requirements for the degree of
Master of Science
2013

Advisory Committee:
Prof. James Farquhar, Chair
Dr. Timothy J. McCoy
Prof. Richard J. Walker

Acknowledgements

First and foremost I would like to thank Professor James Farquhar for his endless advice and positive outlook, which have extended far past the research contained in this thesis. His approach to science and general disposition are truly inspirational. I would also like to thank Professor Richard J. Walker (UMD) and Dr. Timothy J. McCoy (Smithsonian Institution) for sharing their expertise in iron meteorites and helping greatly in my cosmochemical edification.

Professor John T. Wasson (UCLA) is also owed thanks for sharing his ideas and extensive INAA data on the iron meteorites analyzed in this study, while Prof. Mark H. Thiemens (UCSD) provided valuable humor and answers to many photochemical questions. Dr. Jabrane Labidi (IPGP) and Professor Pierre Cartigny (IPGP) made very helpful comments on several facets of this research, while Dr. Mathieu Touboul (UMD) provided great insights into the analysis of available Hf-W data. I would also like to thank fellow members of the Institute for Sulfur Isotope Studies (ISIS) at the University of Maryland (Daniel L. Eldridge, Brian S. Harms, and Dr. Joost Hoek) for their help in the lab and for late night discussions regarding the subtleties of isotopic fractionation. Finally, I would like to thank my parents and family for their endless support during my studies.

This research was partly funded by the Natural Sciences and Engineering Research Council of Canada (NSERC) through a Post Graduate Scholarship to M.A. Antonelli (PGS-M-420592-2012), and through a NASA Cosmochemistry grant to J. Farquhar.

Table of Contents

List of Tables

List of Figures

Chapter 1: Introduction

1.1 Meteorites and Cosmochemistry

The extraterrestrial origin of meteorites was first proposed by Ernst Chladni in 1794 upon his investigation of a stony-iron meteorite find. This proposition was later verified through the petrological analyses of observed meteorite falls in the following decades. The study of meteoritics progressed as new minerals were described from different meteorites and hypotheses regarding possible genetic models were gathered. Petrologic descriptions and paragenetic histories for different meteorites began to accumulate, and with the advent of geochemical tools such as isotope geochemistry in the early 20^{th} century, the study of cosmochemistry was born.

Chemical analyses of undifferentiated stony meteorites ("chondrites") revealed similar compositions to those deduced from spectroscopic studies of the solar spectrum (Palme and Jones, 2003), leading to the hypothesis that chondrites preserve the bulk starting composition of our solar system, and spurring interest in questions regarding the compositional differences between meteorites, the Earth, the Sun, and other planets in our solar system.

The gradual categorization of different meteorites into groups was based on different chemical and petrographic characteristics, which has resulted in over 50 known meteorite groups today, most of which are thought to represent fragments of different planetesimal bodies in our solar system. Over time it was deduced that meteorites do not originate solely from small planetary bodies within the asteroid belt, but also from larger planetary bodies such as Mars and the Moon.

Progressive refinements in radiogenic isotope dating techniques showed that (non-planetary) meteorites represent materials that pre-date the formation of the oldest rocks on Earth by over 500 million years, with the best recent measurements reporting age uncertainties on the order of only ~ ±1 Ma at 4567 Ma (*e.g.* Amelin *et al.*, 2002). Additional chronometric refinements from the identification of in-situ decay products of now-extinct short-lived radioisotopes (SLR) in meteorites have also contributed greatly to our unprecedented abilities in age-dating different types of extraterrestrial materials.

Although radiogenic isotope geochemistry has led to a tremendous wealth of chronometric knowledge, the incorporation of stable isotope geochemistry can begin to answer questions regarding the different types of processes that affected the different meteorites, and how these different processes occurred within the context of the early solar nebula.

1.2 Overview

The research contained within this thesis is an investigation into the sulfur isotopic compositions of different iron meteorites; it starts with an overview of iron meteorite classification and the general characteristics of each iron meteorite group, and is then followed by an introduction to sulfur isotope systematics and stable isotope geochemistry. A section describing previous work on sulfur isotopes in meteorites precedes a chapter on the methodology used to extract and analyze sulfur isotopes, followed by a description of the obtained results. In the later chapters of this study, the obtained data are evaluated in the context of other available meteoritic and sulfur isotopic data, and conclusions concerning the data are made; finally, the last

section of this thesis presents remaining questions and possible directions for future research.

This research builds on the prior studies of sulfur isotopes in iron meteorites by Hulston and Thode (1965b) and Gao and Thiemens (1991), and also aims to complement recent discoveries of mass-independent sulfur variations in meteorites, particularly the discoveries of $\Delta^{33}S$ variations in achondrites (Rai *et al.,* 2005; Farquhar *et al.*, 2000a) and in unidentified minor phases within certain chondrules (Rai and Thiemens, 2007). The documentation of sulfur isotopic compositions in iron meteorites adds to the existing data set, providing greater insight into the conditions affecting sulfur isotopic distributions in the solar nebula.

Chapter 2**:** Background

2.1 Iron Meteorites

Iron meteorites are dominantly composed of solid Fe-Ni metal, which upon slow cooling may exsolve into a high-Ni phase (taenite) and a low-Ni phase (kamacite) in a distinct octahedral pattern (Widmanstätten texture). The solid iron phase is also commonly accompanied by spherical nodules of troilite (FeS) and minor and variable amounts of schreibersite [$(Fe,Ni)_3P$], graphite (C), and cohenite [$(Fe,Ni)_3C$]. In certain iron meteorites ("non-magmatic" iron meteorites), there are abundant silicate inclusions. The silicate inclusions, embedded in the metal, tend to be angular, and are chondritic in composition (Benedix *et al.*, 2000, Benedix *et al.*, 2005). Many other trace minerals can also be found in iron meteorites, such as chromite ($FeCr_2O_4$), daubreelite ($FeCr_2S_4$), Copper (Cu^0), and haxonite [$(Fe, Ni)_{23}C_6$].

The classification of iron meteorites into different groups is based both on the textures and on the relationships between elements of different geochemical behavior, such as Ir, Ni, Ga, Ge, & Au (*e.g.* Wasson *et al.*, 1967a,b, 1969, 1970, 1971 1976, 1986, 1989, 1998, 1999, 2001, 2002, 2003, 2007, *etc.*). Different iron meteorite types can be grouped into distinct fields on plots of taxonomic element concentration (*Fig. 1*). The different groups are believed to each represent a different parent body in the Solar System, most of which are now thought to reside in the asteroid belt.

Certain groups of iron meteorites are known as magmatic iron meteorites (including the IIAB, IIIAB, IVA, IVB, IC, & IIIF groups examined in this study). These groups delineate elemental trends that are predictable through models of

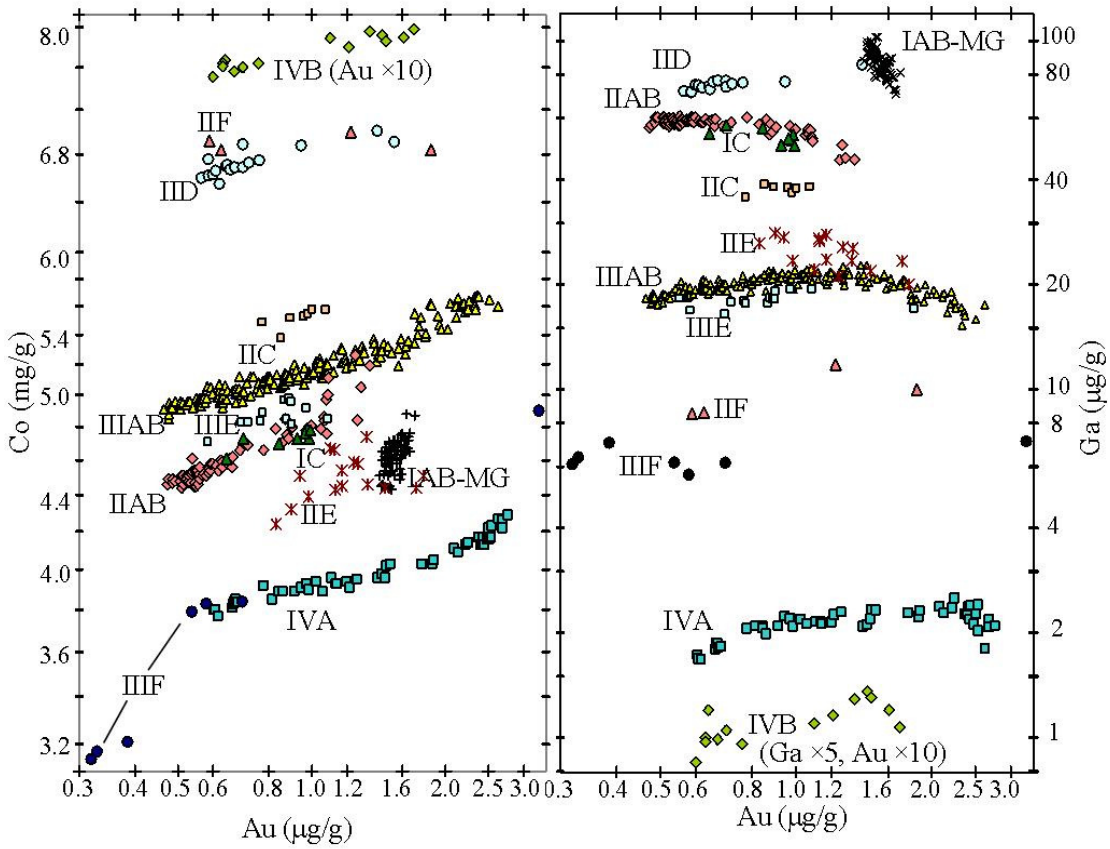

Fig. 1. Elemental compositions of iron meteorites from Instrumental Neutron Activation Analysis (INAA), Courtesy of J.T. Wasson (UCLA)

fractional crystallization within molten iron cores of variable starting composition (Scott *et al.*, 1996; Chabot *et al.*, 2004; Walker *et al.*, 2008). Other groups of irons are known as "non-magmatic" (IAB and IIE) and have compositions that cannot be modeled through the fractional crystallization of a molten core. Along with their abundant silicate inclusions, this is reason to believe that the non-magmatic irons formed as separate individual melt pockets (created by impacts) on a chondritic parent body (Wasson and Kallemeyn, 2002), or by the catastrophic disruption and reassembly of a partially differentiating parent body (Benedix *et al.*, 2000, 2005).

Recently, it has been found that magmatic iron meteorites probably underwent metal-silicate segregation earlier in solar system history than non-magmatic iron meteorites, based on ^{182}Hf-^{182}W constraints (Kleine *et al.*, 2005; Markowski *et al.*, 2006; Schersten *et al.*, 2006; Qin *et al.*, 2008; Schulz *et al.* 2009, 2012; Kruijer *et al.*, 2013a,b).

2.1.1 Magmatic Iron Meteorite Groups

2.1.1.1 The IIAB Irons

Group IIAB iron meteorites are classified as members of the magmatic iron meteorites, and are characterized by high sulfur concentrations, with estimates of 17 ± 1.5 wt% initial S, based upon highly siderophile element (HSE) partitioning models (as sulfur contents affect the distribution coefficients of other elements during crystallization) (Chabot, 2004). They also have the second highest average Ge content of all iron groups (Haack and McCoy, 2006). Like the IIIAB and IVA iron meteorites, the IIAB irons may have cooled in a core stripped of its silicate mantle (Yang *et al.*, 2008, Moskovitz and Walker, 2011), and have Hf-W metal-silicate

segregation ages within 2 million years of CAIs (Markowski *et al.,* 2006; Qin *et al.,* 2008; Kruijer *et al.,* 2013a,b).

However, linkage between the IIAB irons and their potential silicate counterparts have been hindered by their lack of oxygen-bearing silicates ($\Delta^{17}O$ measurements are currently the most well-established geochemical links between meteorite groups). Be that as it may, it has been noted that some oxides may exist, which could provide information on the IIAB parent body (Wasson *et al.*, 2007). The samples analyzed here span almost the entire range of highly siderophile element concentrations reported for IIAB iron meteorites, which enables an evaluation of possible sulfur isotope fractionation in troilite nodules trapped during various stages of core crystallization.

2.1.1.2 The IIIAB Irons

IIIAB iron meteorites are also considered to be magmatic, to be rich in sulfur, and to have differentiated within 2 million years of CAIs (Markowski *et al.,* 2006; Qin *et al.,* 2008; Kruijer *et al.,* 2013a,b). Estimates of the initial sulfur concentration in the IIIAB melts are 12 ± 1.5 wt% S (Chabot, 2004). However, unknown proportions and compositions of trapped melt complicate fractional crystallization models (Scott *et al.*, 1996; Wasson, 1999).

Meteorites from this group have been suggested to be associated with the main group pallasites (Clayton, 1993; Wasson and Choi, 2003, Greenwood *et al.,* 2006). It is also noted that IIIAB group iron meteorites have the oldest Re-Os crystallization ages, though the errors are relatively large, the Re-Os systematics imply crystallization for iron meteorites in the order IIIAB > IIAB > IVB > IVA

(Smoliar *et al.*, 1999). Early crystallization ages for the IIIAB group irons may be a result of rapid cooling and inward crystallization of a parent body stripped of its silicate mantle (Yang *et al.*, 2008).

2.1.1.3 The IVA Irons

Group IVA irons are magmatic, and are estimated to have had 3-9 wt% initial S (Chabot, 2004), this value is poorly constrained due to the different behaviour of Ir (compared to Ga and Ge) with reference to Au in members of this group. The compositional trends in the IVA irons are different than those seen in group IIIAB iron meteorites (Wasson and Richardson, 2001). A general depletion in volatile elements in IVA irons is suggested by low Ge contents (the second lowest in iron meteorite groups) (Haack and McCoy, 2006), whereas high Ni/Fe ratios coupled with chondritic Ni/Co ratios point towards an oxidized mantle (which would have retained oxidized Fe, along with other redox sensitive elements) (McCoy *et al.*, 2011).

In addition, highly variable cooling rates for the IVA iron meteorites are thought to reflect cooling of a core with virtually no silicate mantle, possibly crystallizing inwards from the outside after a grazing impact [like the previously discussed groups (Yang *et al.*, 2008)].

Although fractional crystallization models for this group, along with those previously discussed, appear to be complicated by the variable incorporations of trapped melt into crystallizing domains, the IVA iron meteorites can be well modeled *via* fractional crystallization (Wasson and Richardson, 2001). Like other magmatic iron meteorites, the group IVA parent body is thought to have undergone metal-silicate fractionation within the first few million years of CAIs (Markowski *et al.,*

2006, Qin *et al.,* 2008, Kruijer *et al.,* 2013a,b). Troilite from this group of meteorites has been dated to be 4565.3 ± 0.1 Ma using the Pb-Pb system (Blichert-Toft *et al.*, 2010), indicating crystallization very shortly after Hf-W core segregation ages and CAI formation. It has also been shown that the group IVA meteorites share oxygen isotopic compositions with the L and LL chondrites, implicating a possible genetic link between them (Clayton *et al.*, 1983; Clayton and Mayeda, 1996; Wang *et al.*, 2004; McCoy *et al.*, 2011).

2.1.1.4 The IVB Irons

Group IVB magmatic iron meteorites are estimated to have had even lower initial sulfur in their parental melts than the previous groups (1 ± 1 wt% Chabot, 2004), and are highly depleted in other volatile elements, with the lowest Ge contents of all iron groups (Haack and McCoy, 2006). Group IVB irons have been suggested to come from the same parent body as angrites (Campbell and Humayun, 2005) based on their complementary trace element compositions.

In terms of petrologic modeling, the trace element compositions of IVB irons are consistent with fractional crystallization of a low S and P parental melt (Walker *et al.*, 2008), however, the initial composition of this melt is very rich in Ni, requiring an oxidized mantle, and/or nebular processing prior to accretion of the parent body (Campbell and Humayun, 2005).

2.1.1.5 The IC and IIIF Irons

The IC group iron meteorites are magmatic, contain common troilite inclusions, typically shaped like cigars, and often contain mm-sized chromite crystals. Additionally, small schreibersite crystals are dispersed throughout most IC irons,

whereas graphite and silicates are not present (Scott, 1977). Other sulfur-bearing minerals found in the IC irons are daubreelite and sphalerite (Scott, 1977). It has been suggested that the IC parent body was disrupted after its core fractionally crystallized and was then reassembled early in its history, causing vastly different cooling rates for members of the group (Scott, 1977). Hf-W constraints on metal-silicate segregation in the IC parent body points towards ages similar to those of the more common magmatic iron meteorite groups, within the first few million years after CAIs (Markowski *et al.*, 2006; Qin *et al.*, 2008).

The IIIF iron meteorites are a rare group of magmatic iron meteorites (of which only nine are known) that have few troilite inclusions and grains of microscopic daubreelite (Scott and Wasson, 1976). Interestingly, Hf-W constraints on the age of metal-silicate segregation yield values similar to those for the non-magmatic iron meteorites, several million years after most other magmatic iron meteorite groups (Markowski *et al.*, 2006; Schersten *et al.*, 2006; Qin *et al.*, 2008).

2.1.2 Non-Magmatic Iron Meteorite Groups

2.1.2.1 The IAB Irons

The IAB iron meteorites are known as "non-magmatic" iron meteorites. These meteorites contain abundant angular silicate inclusions of generally chondritic composition (Benedix *et al.*, 2000), and their parent body is thought to have remained sufficiently cool such that it did not fully differentiate into a separate core and mantle (Haack and McCoy, 2006).

The geochemistry of this group of meteorites has been reviewed by Wasson and Kallemeyn (2002) who demonstrated, by examining variations in Ni with respect

to Au, that one could discern a main group (MG), five distinct subgroups, and two grouplets of IAB meteorites. IAB group iron meteorites are now referred to as IAB-MG or IAB-sXZ where X and Z are high (H), medium (M), or low (L) Au and Ni contents, respectively.

The IAB group iron meteorites have been proposed to be associated with the same parent body as the winonaite meteorites because of almost identical silicate mineralogy (Benedix *et al.*, 2000) and similar oxygen isotopic compositions ($\Delta^{17}O$) (Clayton and Mayeda, 1996). Another piece of evidence lays in the almost identical (and relatively late) Hf-W segregation ages of the IAB iron meteorites and the winonaite group meteorites (Schulz *et al.*, 2010, 2012). Wasson and Kallemeyn (2002) postulated that the group IAB irons formed in impact-melt pockets on a chondritic precursor, though the oxygen fugacities required for silicate formation appear to be more reduced than for ordinary chondrites (Benedix *et al.*, 2005). Group IAB iron meteorites also have the highest Ge content of any group (Haack and McCoy, 2006), pointing towards their general lack of depletion in volatile elements. Samples that were analyzed include members from the main group and also from several of the subgroups.

2.1.2.2 The IIE Irons

The group IIE iron meteorites are non-magmatic, like the IAB irons, containing abundant silicate inclusions. They are found to have $\Delta^{17}O$ values almost identical to H chondrites (Clayton and Mayeda, 1996; Clayton, 2003; McDermott *et al.*, 2010, 2011) suggesting a genetic link between them. The IIE irons also share other chemical similarities with H-chondrites (Teplyakova and Humayun, 2011),

even containing what are described as relict chondrules in the iron mesostasis (Roosbroek *et al.*, 2011). Hf-W constraints generally point to metal-silicate segregation ages of about 10 Ma after CAIs (Markowski *et al.*, 2006; Schersten *et al.*, 2006), however a recent study by (Schulz *et al.*, 2012) points to three probable stages of melt segregation, one around 3 Ma after CAIs (which could be from internal heating), and the other two at 13 Ma and 28 Ma (which are most likely impact-derived).

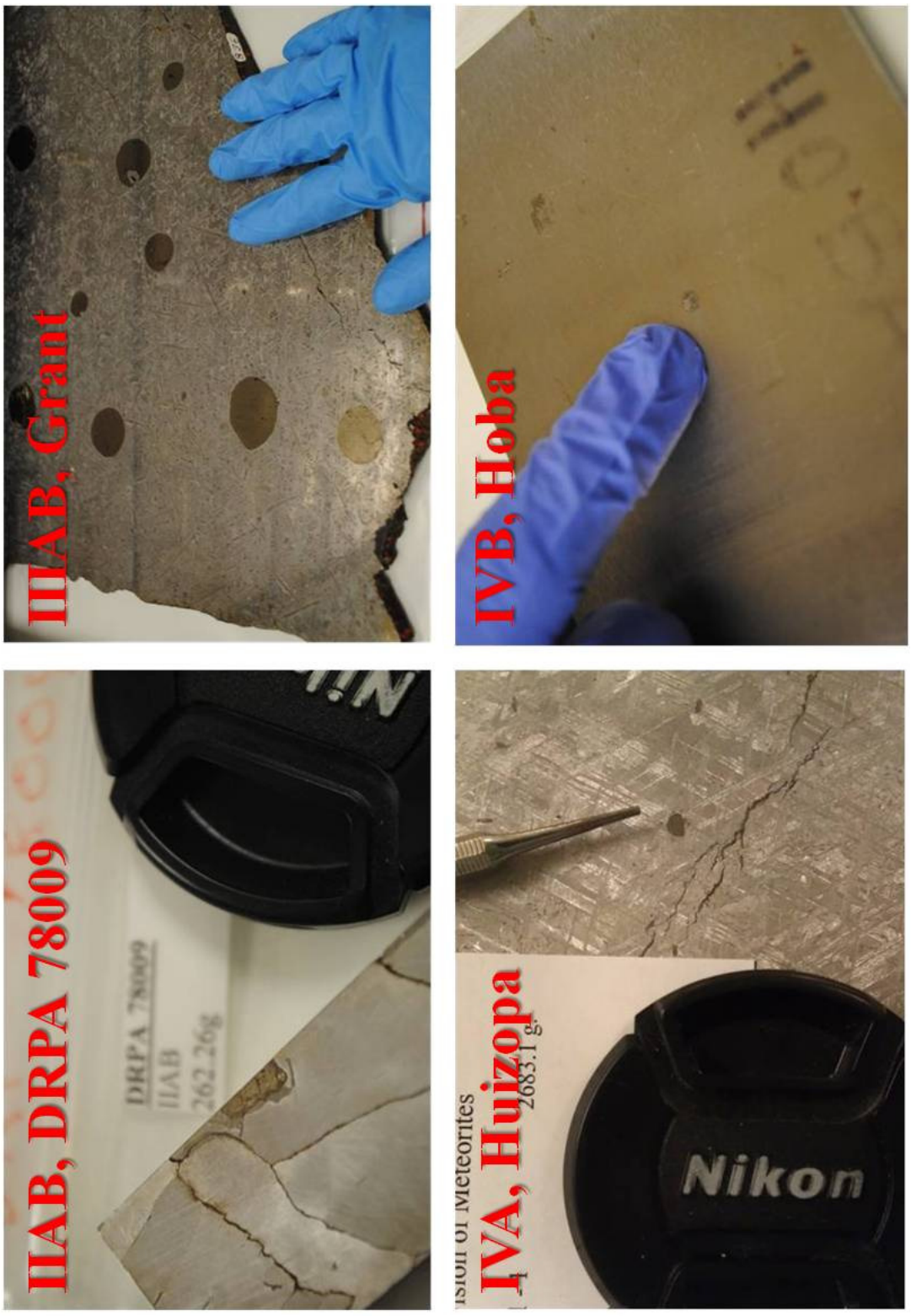

Plate 1 Troilite nodules in iron meteorites from groups IIAB, IIIAB, IVB, and IVA.

Plate 2 Troilite nodules in iron meteorites from groups IC, IIIF, IIE, and IAB.

2.2 Sulfur Isotope Systematics

All sulfur isotope data are reported with respect to a standard: Canyon Diablo Troilite (CDT). For the last 50 years (Ault and Jensen, 1962), troilite from the Canyon Diablo (IAB) iron meteorite has been used as a reference material for sulfur isotope analyses. However, studies have shown that the natural troilite has some slight variability in $\delta^{34}S$ (Beaudoin *et al.*, 1994) which has prompted the development of a synthetic standard reference material (V-CDT). In the study at hand, sulfur isotope values are normalized to our own measurements of CDT in the form:

$$(2.1)\quad \delta^{34}S = \left[\left(\left({}^{34}S / {}^{32}S\right)_{sample} / \left({}^{34}S / {}^{32}S\right)_{CDT}\right) - 1\right]$$

$$(2.2)\quad \delta^{33}S = \left[\left(\left({}^{33}S / {}^{32}S\right)_{sample} / \left({}^{33}S / {}^{32}S\right)_{CDT}\right) - 1\right]$$

$$(2.3)\quad \delta^{36}S = \left[\left(\left({}^{36}S / {}^{32}S\right)_{sample} / \left({}^{36}S / {}^{32}S\right)_{CDT}\right) - 1\right]$$

Thus, if a sample has a heavier isotopic composition than CDT it will have a positive $\delta^{3X}S$ value, and if it has a lighter isotopic composition it will have a negative $\delta^{3X}S$ value.

2.2.1 Mass-Dependent Fractionation

2.2.1.1 Equilibrium Isotope Fractionation

The relationship between isotopes in a substance tends to be dictated by the vibrational frequency differences between isotopically substituted versions of a molecule (isotopologues). The proportional difference in the masses of two isotopologues leads to lower zero point energies for the bonds containing heavier isotopes, with the difference in zero point energy growing as the bond to the isotope

gets tighter; this leads to a concentration of heavy isotopes in tighter bonds (lower free energy for the system) if equilibrium is attained ("equilibrium fractionation").

The reactivity of a molecule is based upon the breaking of one of its bonds. However, when these bonds are intact, they are in states of constant vibration. Like two masses on a spring (in the case of a diatomic molecule), a heavier mass will cause the amount of vibration to lessen. Only those bonds vibrating past the limit of their potential energy surface (*i.e.* the spring snapping) participate in a chemical reaction. Temperature augmentations cause the level of vibrations to increase in a quantized manner. However, at a value of absolute zero these atoms still have some energy, and this quantum concept ("zero point energy") is the difference in energy between the ideal resting position of the atom in a chemical bond and its n = 0 vibrational level (no nodes), and is a function of the molecule's intrinsic properties. It is the differences in zero point energy (ZPE) that dictate the partitioning of isotopes into certain molecular positions; *Figure 2* illustrates the lower ZPE of heavier isotopologues compared to lighter ones in the same chemical bond.

In many cases the bond between two atoms is modeled as a spring (simple harmonic oscillator). The vibrational frequency (ν) of a spring can be determined by Hooke's Law:

$$(2.4)\quad \nu = \frac{1}{2\pi}\sqrt{\frac{k}{\mu}}$$

where k is the force constant of the spring and μ is the reduced mass (m_1m_2/m_1+m_2) of the balls at the ends of the spring. Increasing the mass of one or both of the balls decreases the frequency at which the spring vibrates, all else being equal.

As the bond strength is controlled by electron interactions, and all isotopes of a substance are thought to have the same electron configurations in the same molecule, the shape of the potential well does not change when substituting isotopes ("Born-Oppenheimer approximation").

As the bond strength increases, the average distance between the atoms decreases and the potential energy well becomes narrower; during this process the difference in potential energy of the heavy and light isotopes in the well becomes greater (*Fig. 2*). Therefore, to achieve the lowest possible energy configuration a substance allocates heavy isotopes of an atom to its tightest bonds to achieve the lowest possible total energy state. In metamorphic reactions, for example, oxygen isotopes are exchanged between silicate minerals until equilibrium is reached. As the Si-O bond is one of the strongest, a mineral's enrichment in ^{18}O is a result of its Si-O bond content [with quartz (SiO_2) generally having the highest $\delta^{18}O$].

This effect decreases with increasing temperature, as the differences between the potential energy of isotopologues decreases at higher vibrational frequencies. At lower temperatures, the difference between the potential energy of isotopes is the greatest, approaching the zero point energy difference of the two isotopes.

Other ways in which energy is partitioned into gas-phase molecules is into translational movement and rotational movement. However, these are not as important in determining temperature-based isotope effects.

Given a general isotope exchange reaction of the form:

$$aA + bB^{*} = aA^{*} + bB$$

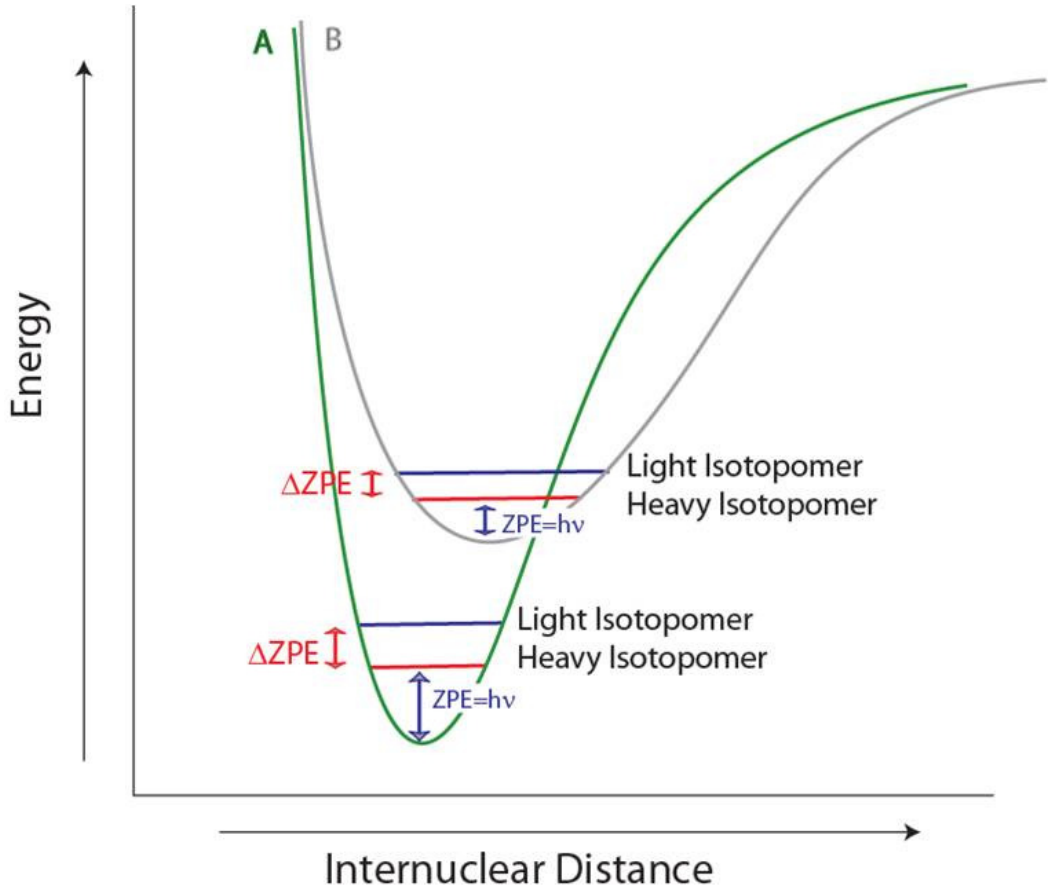

Fig. 2. Conceptual diagram illustrating the zero-point energy differences between heavy and light isotopologues of the same element in two different bonds (on a graph of potential energy versus displacement from the classical resting position). Tighter bonds result in greater zero-point energy differences between heavy and light isotopologues.

where the asterisks denote the molecule with the heavy isotope (being exchanged from substance A to substance B), the traditional equilibrium constant for this reaction is written:

$$(2.5)\quad \mathbf{K} = \frac{(\mathbf{a}_{A*})^{a}(\mathbf{a}_{B})^{b}}{(\mathbf{a}_{A})^{a}(\mathbf{a}_{B*})^{b}}$$

Where a is the activity of a substance raised to its stoichiometric coefficient. This equation can also be written using the substances' partition functions (Q), which are statistical-mechanical operators that depend on the total energy of a substance ("Hamiltonian"), and is, in some sense, equivalent to chemical activity.

$$(2.6)\quad \mathbf{K}_{A\text{-}B} = \frac{(\mathbf{Q}^{*})_{A}^{a}(\mathbf{Q})_{B}^{b}}{(\mathbf{Q})_{A}^{a}(\mathbf{Q}^{*})_{B}^{b}} = \frac{(\mathbf{Q}^{*}/\mathbf{Q})_{A}^{a}}{(\mathbf{Q}^{*}/\mathbf{Q})_{B}^{b}}$$

The classical total partition function of a molecule is the product of its partition functions for translational, rotational, and vibrational energy.

$$(2.7)\quad \mathbf{Q}_{T} = \mathbf{Q}_{tr}\mathbf{x}\,\mathbf{Q}_{rot}\mathbf{x}\,\mathbf{Q}_{vib}$$

In order to calculate fractionation, one must know the translational, rotational and vibrational partition functions of each isotopic substance. A molecule's translational energy can be described in the form:

$$(2.8)\quad \mathbf{Q}_{Tr} = \frac{(2\pi\,\mathbf{M}\,\mathbf{k}_{b}\mathbf{T})^{3/2}}{\mathbf{h}^{3}}\mathbf{V}$$

Where M is the molecular weight, k_b is the Boltzman constant, T is the temperature, V is the volume of the system, and h is plank's constant. The mechanics behind equation 2.8 are classical and not quantized, which is justified as a result of the relatively small energetic differences between the quanta describing different

translational states. Additionally, this equation does not need to be evaluated to study the isotope effect, as it is really the ratio of the partition functions for the heavy and light isotopologues that is of interest (Q*/Q). When calculating the ratio of two Q_{tr}, everything cancels out except the different mass terms, m* and m. Therefore, the translational motion differences between two isotopologues depend only on their relative masses.

$$(2.9)\quad \left(\mathbf{Q^* / Q}\right)_{\mathbf{tr}} = \left(\frac{\mathbf{M^*}}{\mathbf{M}}\right)^{3/2}$$

The rotational energy partition function ratio of two isotopologues is also defined classically, for the same reasons as translational motion, and can be determined using the equation:

$$(2.10)\quad \left(\mathbf{Q^* / Q}\right)_{rot} = \frac{\sigma}{\sigma^*}\left(\frac{\mathbf{I_A^* I_B^* I_C^*}}{\mathbf{I_A I_B I_C}}\right)^{1/2}$$

Where σ and σ* represent the symmetry number of a molecule (the number of equivalent ways of orienting it in space), and I and I* represent the three principle moments of inertia for the molecule.

Finally, to calculate the ratio of the partition functions for vibrational energy between two isotopologues, one uses the equation:

$$(2.11)\quad \left(\mathbf{Q^* / Q}\right)_{\mathbf{vib}} = \prod_{\mathbf{i}} \frac{\mathbf{e^{-U_i^*/2}}}{\mathbf{e^{-U_i/2}}} \frac{\mathbf{1 - e^{-U_i}}}{\mathbf{1 - e^{-U_i^*}}}$$

Where $(Q^*/Q)_{vib}$ is defined as the running product of the energy from all vibrational terms (i) for the heavy version of the molecule, divided by the same vibrational terms for the light version. In this equation, $U = h\nu_i/k_bT$, where ν_i is the vibrational

frequency for the bond in question. Therefore, vibrational energy depends only on the vibrational frequency and temperature of a molecule.

To calculate a partition function for a molecule, one simply combines the three equations to yield

$$(2.12)\ \left(\mathbf{Q}^{*}/\mathbf{Q}\right)_{\mathbf{T}} = \left(\frac{\mathbf{M}^{*}}{\mathbf{M}}\right)^{3/2} \frac{\sigma}{\sigma^{*}} \left(\frac{\mathbf{I}_{\mathbf{A}}^{*}\mathbf{I}_{\mathbf{B}}^{*}\mathbf{I}_{\mathbf{C}}^{*}}{\mathbf{I}_{\mathbf{A}}\mathbf{I}_{\mathbf{B}}\mathbf{I}_{\mathbf{C}}}\right)^{1/2} \prod_{\mathbf{i}} \frac{\mathbf{e}^{-\mathbf{U}_{\mathbf{i}}^{*}/2}}{\mathbf{e}^{-\mathbf{U}_{\mathbf{i}}/2}} \frac{\mathbf{1}-\mathbf{e}^{-\mathbf{U}_{\mathbf{i}}}}{\mathbf{1}-\mathbf{e}^{-\mathbf{U}_{\mathbf{i}}^{*}}}$$

Because of a constant relationship between ν_i, I, σ, and M, the Teller-Redlich spectroscopic approximation (Urey, 1947) may be applied to the above equation in order to remove all the terms for moment of inertia (I), yielding:

$$(2.13)\ \left(\mathbf{Q}^{*}/\mathbf{Q}\right)_{\mathbf{T}} = \left(\frac{\mathbf{m}^{*}}{\mathbf{m}}\right)^{3/2r} \frac{\sigma}{\sigma^{*}} \prod_{\mathbf{i}} \frac{\boldsymbol{\nu}_{\mathbf{i}}^{*}}{\boldsymbol{\nu}_{\mathbf{i}}} \frac{\mathbf{e}^{-\mathbf{U}_{\mathbf{i}}^{*}/2}}{\mathbf{e}^{-\mathbf{U}_{\mathbf{i}}/2}} \frac{\mathbf{1}-\mathbf{e}^{-\mathbf{U}_{\mathbf{i}}}}{\mathbf{1}-\mathbf{e}^{-\mathbf{U}_{\mathbf{i}}^{*}}}$$

where r is the number of atoms being exchanged in the molecule. The equilibrium constant (fractionation factor α) for a reaction is then calculated as the ratio of $(Q^*_A/Q_A)^a$ over $(Q^*_B/Q_B)^b$, usually yielding a ratio near unity. It is the deviations from unity (differences in free energy) that result in equilibrium isotope effects.

For many molecules, the mass terms and symmetry terms for the heavy and light isotope cancel out (along with the temperature terms); which leads to the "reduced partition function ratio", a simplification to facilitate calculation of equilibrium isotope effects.

$$(2.14)\ \boldsymbol{f} = \frac{\mathbf{Q}^{*}}{\mathbf{Q}} \left(\frac{\mathbf{m}}{\mathbf{m}^{*}}\right)^{3/2r}$$

The variable r is the number of atoms being exchanged in the molecule, as in the previous equation. In turn, these reduced partition functions are reported after taking the r^{th} root, leading one to a so called β value:

$$(2.15)\quad f^{1/r} = \beta$$

Finally, to obtain the equilibrium constant for an isotopic exchange reaction, one takes the ratios of these β values, leading to a "fractionation factor" known as α. For all intents and purposes α is just a different name for the equilibrium constant K, for any chemical reaction, but is used to signify that one is dealing with an isotopic exchange reaction with only one atom exchanged. However, this is not necessary for calculating α, as the ratio $(Q^*/Q)_A$ over $(Q^*/Q)_B$ is also equal to the fractionation factor as shown earlier.

$$(2.16)\quad \alpha_{(A\text{-}B)} = \beta_A / \beta_B \text{ and } 1000 \ln\alpha_{(A\text{-}B)} = 1000 \ln\beta_A - 1000 \ln\beta_B$$

Fractionations of isotopes during specific chemical reactions are typically reported in per mil units, by multiplying the natural logarithm of α by 1000.

2.2.1.2 Kinetic Isotope Fractionation

Kinetic isotope fractionation is the fractionation of isotopes during non-equilibrium chemical reactions. In these generally irreversible (unidirectional) reactions, it is the reaction rates, and not the final free energies of the molecules, that are important in controlling isotopic behavior.

Although kinetic effects are fundamentally different from equilibrium effects, they also depend on the mass differences between different isotopologues. The best model for explaining these effects is transition-state theory (*e.g.* Bigeleisen, 1952), in which a kinetic isotope effect depends on partitioning between the reactants and their transition-state, as opposed to between the reactants and their products. The final passage from the transition-state to the product state is controlled by a non-isotope

selective “leak-through” with a given rate.

More weakly bound transition-states (most common) lead to an equilibrium-like enrichment in light isotopes, resulting in a “normal kinetic effect” where the final products are enriched in the light isotopes of a substance. In the rarer case, where the transition-state provides a tighter bonding environment than the reactant state, “inverse kinetic fractionation” occurs and the heavy isotope is enriched in the products. In either case, the mechanisms depend on the same physics that describe equilibrium isotope effects, creating products and residual reactants that obey mass-dependent isotope fractionation laws.

The modeling of kinetic effects relies mostly on the vibrational frequencies of the molecules (and their transition-states) in a reaction, the ratio of rate constants for a reaction of a heavy versus light isotopologue is similar to the traditional partition function ratio equations for equilibrium reactions, but is calculated between the reactant and transition-states, and also includes a correction for the tunneling frequencies of each isotope.

$$(2.17)\ \mathbf{K_2/K_1} = ({}^{*}\boldsymbol{\nu}^{\ddagger}/\boldsymbol{\nu}^{\ddagger})((\mathbf{Q}_2/\mathbf{Q}_1)_{\text{tunneling}}({}^{*}\mathbf{Q}_{\text{vib}}/\mathbf{Q}_{\text{vib}})_{\text{TS}}/({}^{*}\mathbf{Q}_{\text{vib}}/\mathbf{Q}_{\text{vib}})_{\text{RS}}$$

Another subtlety in transition-state theory is the ratio of heavy versus light imaginary vibrational frequencies for the transition-state (represented as $^{*}\nu^{\ddagger}/\nu^{\ddagger}$), which are imaginary because they lie along the reaction path and accelerate as bond length in the transition-state structure increases or decreases (destabilizing), as opposed to

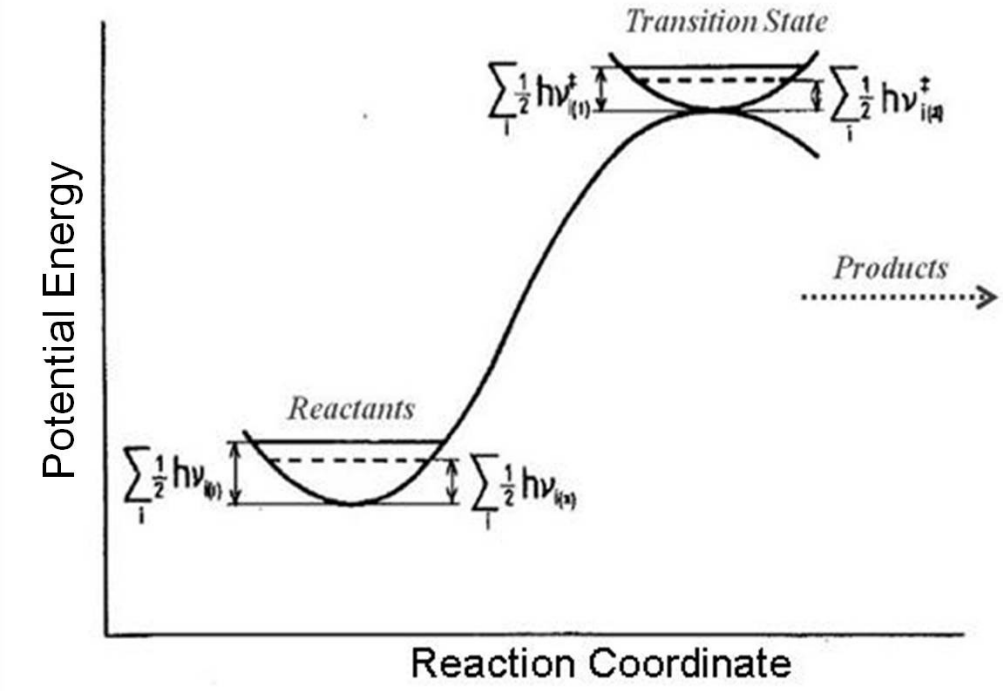

Fig. 3. Potential energy along the reaction coordinate for a kinetic chemical reaction (from transition-state theory). The solid lines represent zero-point energies (ZPE) for light isotopologues and the dotted lines represent ZPE for heavier isotopologues. (Modified from Bigeleisen, 1952).

decelerating as bond length increases or decreases from its equilibrium position in bound states (stabilizing).

In simpler terms, the ratio of the rates between two isotopologues in the same kinetic chemical reaction is:

$$(2.18)\quad \mathbf{K_{f,2}/K_{f,1}} = {}^{*}\boldsymbol{\nu}_2 / {}^{*}\boldsymbol{\nu}_1 (\int^{+}{}_{2/1} / \int^{\mathbf{react}}{}_{2/1})$$

Where $K_{f,2}$ and $K_{f,1}$ are the forward rate constants for identical reactions with a different isotopologue, $*\nu_2/*\nu_1$ are the vibrational frequencies for the bond that leads to formation of the activated complex (transition-state) when ruptured, and $(\int^{+}{}_{2/1}/\int^{react}{}_{2/1})$ is the equilibrium constant for the formation of the transition-state from the reactants.

2.2.2 Mass-Independent Fractionation

For sulfur isotopes, a predominance of natural equilibrium and kinetic isotope effects has resulted in $\delta^{33}S$, $\delta^{34}S$, and $\delta^{36}S$ values with characteristic logarithmic relationships between them. If material is derived purely from kinetic or equilibrium effects then the relationship between the isotopes will be approximately:

$$(2.19)\quad \boldsymbol{\delta^{33}S = \left(\delta^{34}S + 1\right)^{0.515} - 1}$$

$$(2.20)\quad \boldsymbol{\delta^{36}S = \left(\delta^{34}S + 1\right)^{1.9} - 1}$$

There may be slight variations in the exponents depending on the specific type of process and temperature involved, but these are less than ± 0.003 (Hulston and Thode, 1965). However, some chemical processes have been shown to fractionate isotopes in ways that cause significant deviations from the mass-dependent arrays

defined by equations 2.19 and 2.20. To quantify these effects one must calculate a sample's departure from the reference array:

$$\Delta^{33}S = \delta^{33}S_{measured} - \delta^{33}S_{predicted} = \delta^{33}S - \left(\left(\delta^{34}S + 1\right)^{0.515} - 1\right) \quad (2.21)$$

$$\Delta^{36}S = \delta^{36}S_{measured} - \delta^{36}S_{predicted} = \delta^{36}S - \left(\left(\delta^{34}S + 1\right)^{1.9} - 1\right) \quad (2.22)$$

A sample falling on the reference array will have a $\Delta^{3X}S$ of zero, whereas samples with anomalous enrichments or depletions in ^{33}S or ^{36}S will lead to positive or negative $\Delta^{3X}S$ values, respectively.

Samples enriched or depleted in $\Delta^{3X}S$ are commonly called "mass-independent" to signify their departures from the mass-dependent array, however, it has been found that mixing between pools of differentially enriched mass-dependent sulfur species can cause non-zero $\Delta^{3X}S$ values (as the reference array is curved and the mixing line between two samples is linear). This adds some confusion to the term "mass-independent", as small $\Delta^{3X}S$ variations can be generated by the typical mixing of mass-dependent components. However, for mixing reactions to cause any significant $\Delta^{3X}S$ variability they need to be the result of mixing between two reservoirs with highly different values of $\delta^{34}S$, as the curve of the mass-dependent array is not pronounced at the relevant scale, yielding a maximum $\Delta^{33}S$ value of about 0.2‰ when mass-dependent components with an 80‰ difference in $\delta^{34}S$ are mixed together (Farquhar *et al.*, 2007).

Truly mass-independent processes have been documented for several different isotopic systems. These include magnetic isotope effects involving odd-numbered nuclei (*e.g.* Turro and Kraeutler, 1980), nuclear volume effects in heavy elements

(*e.g.* Bigeleisen, 1996), and effects related to photochemical transformations (*e.g.* Thiemens and Heidenreich, 1983). By far, the largest recorded departures from mass-dependent isotope fractionation are those observed during gas-phase photolysis experiments. For example, it has been found that UV photolysis of sulfur-bearing gases leads to the formation of products enriched or depleted in $\Delta^{33}S$ (Colman *et al.*, 1996; Farquhar *et al.* 2000b, 2001; Chakraborty *et al.*, 2011; Masterson *et al.*, 2011, Chakraborty *et al.*, 2013), with greatly variable relationships between the $\Delta^{33}S$ and $\Delta^{36}S$ values of the products, depending on the type of sulfur-bearing gas, pressure, and wavelength of light that is used.

When an atom or molecule is subjected to light it absorbs energy at characteristic frequencies. These frequencies correspond to either increases in vibrational energy or to absorption of energy through the promotion of an electron to a higher orbital. When electrons are promoted to a higher orbital to form a stable species (*i.e.* without dissociation of the molecule), the molecule is said to be in a bound "excited-state".

A molecule in a bound excited-state has bonding characteristics that are very different than when it is in the ground-state, causing departures from the ground-state shape and bond strength, accompanied by changes to the $Q_{electronic}$ partition function, which are not considered in equation 2.13. The changes in the shape and position of the potential energy well for bonds in excited-states support the idea that large isotope fractionations are possible through reactions which involve them. These reactions are common when gas-phase molecules are subjected to UV light, such as in planetary atmospheres and in optically-penetrable gaseous zones of young protoplanetary

systems.

Absorption spectra provide a means of determining the energies for different electron transitions in an atom or molecule. In many cases there are discrete absorption bands above the energy associated with leaving the ground-state potential well of a given molecule (breaking its bond); as the molecule has not dissociated, there has been an electronic reconfiguration which has led to a change in the characteristics of its bonds, represented as a transition of the molecule from its ground-state to a new discrete vibrational level in a well of higher potential energy [bound excited-state (*e.g. Fig. 4*)].

Many different electronic configurations, and thus, many different excited-states may exist for a substance with a singular chemical composition. Different absorption bands reveal the discrete energies associated with electron transitions to higher molecular orbitals and the creation of many distinct excited-states.

Some of these absorption peaks, at energies above the dissociation limit for a substance in its ground-state, are broader than those which characterize lower energy transitions of electrons. These broad ("diffuse") peaks are thought to represent wavelengths which induce transitions between different excited-state potential wells (*Fig. 4a*). Some of these transitions are influenced by factors in addition to those in Q_T (*eq. 2.7 & 2.13*).

In these photochemical reactions, the non-classical isotope selection process is thought to occur either during transitions between different excited-states, or during initial excitation of the molecules to the excited-state.

The Frank-Condon effect, which applies to transitions of molecules from ground-state to a bound excited-state (*Fig. 4b*), is described as the greater probability of a transition from ground-state to excited-state, if the nuclear coordinates and probability density functions of the two states overlap (this is because electronic transitions are many orders of magnitude faster than nuclear motions). As the vibrational level shifts with increasing isotope mass, the average position of the vibrating atom also changes, which may cause preferential overlap in the nuclear positions required for ground-state to excited-state transitions, and an anomalously higher reaction rate for that isotopologue.

State-to-state transitions (revealed by diffuse bands) occur when there is rovibronic overlap between levels in different excited-state potential wells (*Fig. 4a, 4c*). As different isotopologues have different zero point energies within a given potential well, some of them may have preferential overlap with vibrational levels in adjacent potential wells, causing them to preferentially switch over to other potential energy surfaces at higher rates.

2.2.2.1 Shielding

Isotopic self-shielding in a column of gas will also lead to mass-independent fractionation as isotopomers of a substance have absorption peaks that are off-set from each other (*e.g.* Danielache *et al.*, 2012). In a column of gas, the wavelengths specifically absorbed by the most abundant isotopomer of a species will be filtered out with increasing distance from the source of light, eventually becoming completely absorbed. In regions further from the light source, where the column of gas has absorbed all frequencies of light that will photolyze the abundant isotopologues, there

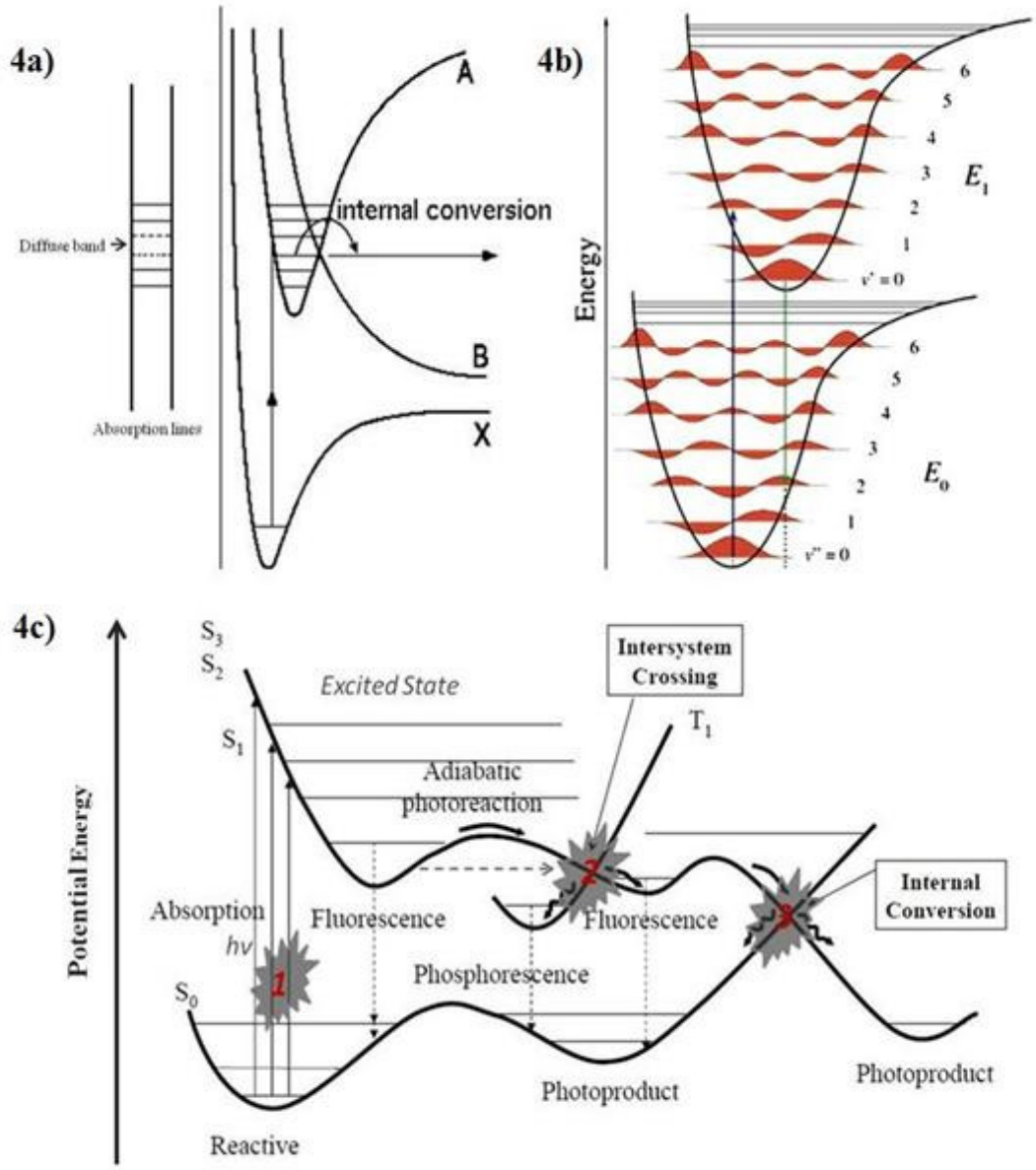

Fig. 4a. Schematic representation of initial excitation from a bound ground-state to a bound excited-state, and subsequent internal conversion to a dissociative surface. *Fig. 4b.* Schematic representation of Frank Condon overlap between n=0 and n=2 levels in the ground and excited-state, facilitating transitions between the two states. *Fig. 4c.* Schematic of possible photochemical reactions highlighting (numbered) processes which are suggested to cause non-traditional isotope selection.

will be a zone in which only the absorption spectra of minor isotopomers of a substance will match incident radiation, which will lead to products with mass-independent compositions within this zone (*e.g.* Lyons and Young, 2005).

2.2.2.2 Caveats

One important caveat to the above discussions is that the preservation of a pool of molecules that has been through an excited-state transition relies on the segregation of products from reactants through some sort of chemical/physical reaction other than the decay back to original ground-state.

2.2.2.3 Nuclear Effects

In addition to photochemical reactions, a few other scenarios leading to non-mass-dependent isotope enrichments need to be taken into account in nebular settings. For example, anomalous isotope enrichments may be the results of uneven contributions from different stellar sources ("nucleosynthetic anomalies") or from *in-situ* production through cosmic-ray induced spallation reactions.

2.3 Sulfur Isotopes in Meteorites

2.3.1 $\delta^{34}S$ in Meteoritic Materials

Sulfur-bearing minerals in meteorites are dominantly reduced, with the exception being those within carbonaceous chondrites, which have undergone post-formation aqueous alteration and oxidation. In a general sense, it has been found that sulfur is contained in water-soluble compounds, in acid soluble sulfides, as elemental sulfur, in water/acid soluble sulfates, and as unidentified sulfur minerals soluble only in aqua regia (Kaplan and Hulston, 1966). A list of sulfur-bearing minerals in

meteorites including reduced sulfur minerals such as troilite (FeS), oldhamite (CaS), ferroan alabandite ((Fe,Mn)S), and sphalerite (ZnS), intermediate oxidation sulfur minerals such as elemental sulfur (S_8), and oxidized sulfate minerals such as epsomite ($MgSO_4 \cdot 7H_2O$), and anhydrite ($CaSO_4$) has been compiled in several different sources (Rubin, 1997); however, the dominant sulfur mineral in meteorites is troilite (FeS) (Hulston and Thode, 1965; Gao and Thiemens, 1993a,b; Rubin, 1997).

It is also noted that oxidized sulfur minerals (sulfates) and elemental sulfur are present only in the carbonaceous chondrites, most likely derived from the oxidation of primary troilite during aqueous alteration on the parent body (Lewis, 1967). The grouping of $\delta^{34}S$ values seen within classes of carbonaceous chondrites [from most aqueously altered (type 1) to least aqueously altered (type 3)] show that the $\delta^{34}S$ of troilite increases with increasing degrees of aqueous alteration (Lewis, 1967). This lends greater weight to the idea that troilite (FeS) was the principal starting material from which other sulfur-bearing minerals were derived, and gradually became isotopically heavier as the residual reactant in kinetic oxidative processes. Other types of sulfur-bearing compounds exclusive to carbonaceous chondrites include insoluble organic matter (IOM), aliphatic sulfur, heterocyclic organic sulfur, and oxidized organic sulfur (Orthous-Daunay *et al.,* 2010). Daubreelite ($FeCr_2S_4$), which is known to form as exsolution lamellae within troilite (Buchwald, 1975), has been found in some iron meteorites, certain reduced achondrites, and in enstatite chondrites (Lewis, 1967), as it is likely to be unstable in the oxidizing conditions found within other meteorites.

In a pioneering multiple sulfur isotope study, Hulston and Thode (1965a) demonstrated the mass-dependent character of various meteoritic sulfur species (sulfide, sulfate, and elemental sulfur). Their work was specifically aimed at searching for possible anomalies of nucleosynthetic origin in meteoritic sulfur, which they did not find.

In other studies of sulfur in meteorites, it was found that sulfur isotope variability is also mass-dependent within meteoritic processes, whether it be during: (1) aqueous alteration/redox reactions of sulfides in carbonaceous chondrites (Monster *et al.*, 1965; Kaplan and Hulston, 1966, Bullock *et al.*, 2010), (2) evaporation/condensation of troilite (McEwing *et al.*, 1980; Tsuchiyama *et al.*, 1997; Tachibana and Huss, 2005), (3) metamorphism and partial melting in chondrites and achondrites (leading to $\delta^{34}S$ enrichments), or (4) impact metamorphism (Rubin, 2002). On top of this, both diffusional and crystallization processes are also thought to lead to mass-dependent partitioning of isotopes (Huang *et al.*, 2010). In all of the above situations, equilibrium and kinetic isotope effects dominate the distribution of sulfur isotopes. However, more recently, increased precision in mass-spectrometric methods has led to the identification of small yet resolvable $\Delta^{33}S$ anomalies in several meteorite groups.

2.3.2 Multiple Sulfur Isotope Measurements in Meteorites

In a study analyzing the multiple sulfur isotopic composition of ureilite meteorites, Farquhar *et al.* (2000a) found small $\Delta^{33}S$ enrichments in bulk samples with an average $\Delta^{33}S$ of +0.040 ± 0.006‰. Rai *et al.* (2005) reported enrichments in $\Delta^{33}S$ within several other achondrite groups, including acapulcoite-lodranites (+0.026

± 0.008‰), HED meteorites (+0.036 ± 0.016‰), and in one oldhamite (CaS) grain from the Norton County aubrite (+0.161 ± 0.012‰). Most of these $\Delta^{33}S$ enrichments are <0.1‰ but are resolvable with modern techniques.

Other enrichments have been found through the sequential sulfur extractions of certain chondrules from the Dhajala ordinary chondrite meteorite, where sulfur hosted in acid-resistant phases is enriched in ^{33}S ($\Delta^{33}S$ up to 0.113 ‰) (Rai and Thiemens, 2007). The largest $\Delta^{33}S$ enrichments reported were originally documented within ethane-, propane-, and butane- sulfonic acid extracts from the Murchison carbonaceous chondrite ($\Delta^{33}S$ up to 2.0‰) (Cooper *et al.*, 1997).

All of the $\Delta^{33}S$ enrichments found in meteoritic materials have been attributed to gas-phase photochemical reactions in the presolar nebula, rather than nucleosynthetic anomalies and spallation reactions, as these are thought to result in larger enrichments of ^{36}S over ^{33}S which have not been found (Cooper *et al.*, 1997; Farquhar *et al.*, 2000a; Rai *et al.*, 2005; Rai and Thiemens, 2007). Additionally, mixing reactions cannot create the $\Delta^{33}S$ values found because the range of documented $\delta^{34}S$ values is too small and magnetic isotope effects (*MIE*, which have also been observed to cause non-zero $\Delta^{33}S$) are favored principally in viscous solutions rather than in the solid or gas phase.

Despite the small enrichments found in organic materials and achondrites, bulk chondrites, lunar basalts, and the terrestrial mantle have $\Delta^{33}S$ values statistically indistinguishable from zero (CDT) (Gao and thiemens, 1993a,b; Wing and Farquhar, 2013; Labidi *et al.*, 2012, *Thesis*).

In iron meteorites, analyses of the four isotopes of sulfur in troilite have been reported by two different groups. In the first of these studies, Hulston and Thode (1965b) extracted small amounts of sulfur from the metal phase of iron meteorites and demonstrated that for some meteorites with long cosmic-ray exposure ages, excesses of ^{33}S and ^{36}S were present. They also showed that these excesses correlated with production rates of noble gases, and were most likely attributable to ^{56}Fe spallation reactions. However, sulfur found within the troilite nodules was isotopically indistinguishable from CDT (Hulston and Thode, 1965b)

In a later study, Gao and Thiemens (1991) confirmed homogeneity of sulfur isotopes in the troilite from iron meteorites, and demonstrated that the $\Delta^{33}S$ of troilite from iron meteorites yielded an average of 0.005‰ with a (1σ) standard deviation of ±0.025‰ relative to CDT. Gao and Thiemens (1991) also revisited sulfur in the metal phase of these meteorites, identifying two separate carriers of the anomaly, an acid volatile phase and an acid resistant phase (inferred to be daubreelite). They noted that the $^{36}S/^{33}S$ enrichments were a factor of two greater than their spallation modeling predicted, and called for further work that directly connected sulfur with the noble gas production rates in iron meteorites.

Chapter 3: Methods

3.1 Sample Acquisition

Of the 61 meteorites obtained for this study, 57 were successfully analyzed. There were also 3 duplicate samples which represented different troilite nodules from within the same meteorite [Mundrabilla-2 (IAB), Apoala-2 (IIIAB), and Santa Rosa-2 (IC)]. Of those successfully analyzed, 23 of the samples were from non-magmatic iron meteorite groups (22 IAB and 1 IIE) and 37 were from magmatic iron meteorite groups (2 IC, 8 IIAB, 17 IIIAB, 8 IVA, 1 IVB, & 1 IIIF). The samples which were not properly analyzed were Drum Mountains (IIIAB), which yielded no sulfur (likely due to the primary misidentification of a graphitic nodule for troilite), and Calico Rock (IIAB), Indian Valley (IIAB), and Djebel in Azzenne (IIIAB), which were affected due to errors or accidental contamination during sulfur extraction and subsequent purification.

Most of the samples were obtained from the National Museum of Natural History (Smithsonian Institution) by the author, using a fine chisel and hammer to chip out small pieces of troilite nodules. The samples were picked on a purely visual basis, and variable amounts of graphite and schreibersite, which are common in the troilite nodules, were included in the analyzed samples. Additional troilite was sent from several institutions as noted in *Table 1*.

Table 1. List of iron meteorites analyzed in this study.

Name	Group	Source	Name	Group	Source
Osseo	IAB-comp	USNM925	Old Woman	IIAB	USNM6359-17
ALHA77290	IAB-MG	USNM6361	Patos de Minas (Hex)	IIAB	USNM6844
Bogou	IAB-MG	USNM2245	Watson	IIE	USNM6483
Burkett	IAB-MG	USNM586	Acuna	IIIAB	NHM
Campo del Cielo	IAB-MG	USNM5615	Apoala	IIIAB	ME1009-1A
Canyon Diablo	IAB-MG	ME2108-1	Apoala 2	IIIAB	ME1009-3B
Deelfontain	IAB-MG	USNM3275	Loreto	IIIAB	USNM1507
Hope	IAB-MG	USNM3476	Wabar	IIIAB	USNM1564
Idaho	IAB-MG	USNM1652	Waingaromia	IIIAB	USNM5771
Wichita County	IAB-MG	ME885-1	Cape York	IIIAB	USNM5726
Mundrabilla 2	IAB-Mund	WAM13583	Grant	IIIAB	USNM836
Mundrabilla	IAB-Mund	USNM5914	Thule	IIIAB	USNM4856
Waterville	IAB-Mund	USNM1512	Kenton County	IIIAB	USNM2848
Pitts	IAB-Pitts	USNM1378	Costilla Peak	IIIAB	ME856-1
Woodbine	IAB-Pitts	USNM2169	La Porte	IIIAB	ME2269-2
Bischtube	IAB-sLL	USNM229	Sacramanto Mtns	IIIAB	AMNH4209
Goose Lake	IAB-sLL	USNM1332	Casas Grandes	IIIAB	USNM369A2
Toluca	IAB-sLL	USNM1214	Trenton	IIIAB	USNM2173
Lamesa, Texas	IAB-sLM	USNM6250	MET0040	IIIAB	USNM7080-2
Malta Hohe	IAB-sLM	USNM6482	Cerro del inca	IIIF	USNM7062
Mertzon	IAB-ung	USNM1435	Altonah	IVA	USNM863
Mesa Verde Park	IAB-Ung	USNM645	Bushman Land	IVA	USNM2515A22
Santa Rosa	IC	USNM457	Duchesne	IVA	USNM2181
Santa Rosa 2	IC	ME762-1	Gibeon	IVA	AMNH775
DRPA 78008/10	IIAB	UCSD	Harriman	IVA	USNM6072
DRPA 78009	IIAB	USNM6363	Huizopa	IVA	USNM871-1
Indian Valley	IIAB	USNM323	Maria Elena	IVA	USNM1221-32
Keen Mountain	IIAB	USNM1513	Mart	IVA	USNM221
Mayodan	IIAB	USNM1487	S.J. Nepomuceno	IVA	USNM6881
North Chile	IIAB	USNM2306	Hoba	IVB	USNM6506

*Abbreviations used: USNM = National Museum of Natural History (Smithsonian Institution), ME = Field Museum, Chicago, WAM = Museum of Western Australia, UCSD = University of California San Diego (Mark Thiemens), AMNH = American Museum of Natural History, NHM = Naturhistoriches Museum, Austria.

3.2 Sulfur Extraction and Analysis

3.2.1 Sulfur Extraction

Sulfur is extracted from different mineral phases in a sequential fashion. First, acid volatile sulfur (AVS) is obtained from crushed troilite samples: the samples (5-20 mg) are heated for three hours in two-necked 50ml boiling flasks with 20ml of nitrogen-flushed 5 N HCl through which nitrogen is continuously bubbled; the released $H_2S_{(g)}$ (from monosulfides) is carried through a condenser and an acid-trap, and is then chemically captured as Ag_2S in a slightly acidic trapping solution (containing HNO_3 and $AgNO_3$). The apparatus used is the same as described by Forrest and Newman (1977).

Chromium-reducible sulfur (CRS) is obtained by changing the capture solution and injecting a reduced Cr (II) solution into the boiling flasks (after the 3 hours of reaction with HCl) (Canfield *et al.*, 1986). The CRS solution is allowed to react with the acid-residues for an additional 3 hours. The small amount of product H_2S from chromium reduction of the troilite samples comes from acid-resistant phases within the troilite, possibly the mineral daubreelite in reduced iron groups ($FeCr_2S_4$) or other complex sulfides in other groups.

The precipitated Ag_2S is aged in the dark for one week (to remove impurities in the Ag_2S crystals) then centrifuged and rinsed with milli-Q water three times, after which it is allowed to sit overnight in 1 M NH_4OH solution to remove impurities, and then again rinsed three times before drying overnight in an oven (at 50°C).

3.2.2 Fluorination and Purification of SF_6

The fluorination line used in the production of SF_6 from Ag_2S is dedicated exclusively to meteorite analyses in order to avoid any possible contaminations from more highly-fractionated terrestrial samples. Aliquots of approximately 3 mg of Ag_2S are reacted with *ca.* 10 times stoichiometric excess of pure F_2 in nickel fluorination bombs (at 250 °C overnight), producing SF_6 gas and other fluorinated by-products. The excess fluorine is separated cryogenically, as it does not freeze at liquid N_2 temperatures (-196 °C) whereas both HF and SF_6 are trapped at this temperature. After all non-condensable gases are pumped away, the sample is thawed and subsequently re-frozen using an N_2-ethanol slurry (at -115°C), cryogenically trapping HF and thereby separating it from the SF_6. The SF_6 is then purified using gas chromatography on a 12' molecular sieve 5 Å/Hasep Q column with a thermal conductivity detector (TCD), and introduced cryogenically into the cold-finger of a ThermoFinnigan MAT 253 dual-inlet mass spectrometer.

3.2.3 Mass Spectrometry

SF_6 molecules from the sample and standard-gas are alternatively ionized to SF_5^+ ions in the source (electron impact), focused through lenses, and accelerated down the flight tube where they are deflected by a magnetic field. Heavier isotopologues of SF_5^+ are deflected by a smaller amount than lighter isotopologues of SF_5^+, allowing beams of each charged isotopologue to be separated according to their masses. The ion beams are collected in faraday cups at the detector-end of the mass spectrometer which are positioned to measure mass/charge ratios of 127, 128, 129, and 131 ($^{32}SF_5^+$, $^{33}SF_5^+$, $^{34}SF_5^+$, and $^{36}SF_5^+$ respectively)]. The number of ions hitting

each detector can be calculated (ions/sec) for each isotopologue by measuring the voltage drops across resistors of known conductance.

As the abundance of ^{36}S is the lowest of all stable sulfur isotopes (0.02% of natural abundance, versus 0.79% and 4.29% for ^{33}S and ^{34}S, respectively), its measurement is most susceptible to contamination from traces of other substances. A common source of isobaric interference on m/z station 131 includes contamination from $C_3F_5^+$. An attempt at monitoring this contamination is made through the repetitive analysis of IAEA S1 standard material between meteorite samples (an aliquot of which was fluorinated and processed with every batch of 6 samples, to also monitor the performance of the GC and fluorination-line). In some cases, m/z = 131 contaminations were observed in both the sample and a penecontemporaneously analyzed standard. As a result, samples with obvious contaminations were renormalized back to our long-term accepted values of IAEA S1 (based on their bracketing standard analyses). Measurements of $^{36}SF_5^+$ also succumb to greater amounts of instrumental noise because the resistor at m/z = 131 has the lowest conductivity, which is necessary in order to obtain a sufficient signal from an isotope of such low abundance.

For the dominant portion of iron meteorite measurements, the regular amounts of analyses performed per sample were tripled in order to decrease the uncertainty of our measurements. Each value reported is the average of 36 individual cycles, each measuring the isotopic difference between a sample and the standard-gas, which itself has a known isotopic composition relative to CDT. All results are finally converted to a known reference-frame by renormalizing to IAEA S1 analyses. This reference

frame is calibrated to the repeat analyses of CDT, which defines $\delta^{3X}S$ and $\Delta^{3X}S$ values of zero.

3.2.4 Sources of Uncertainty

The sources of uncertainty in the analyses performed in this study originate from various processes. The first source of uncertainty lies within the standard reference material for sulfur isotope analyses: troilite from the Canyon Diablo IAB iron meteorite. This material has been observed to posses $\delta^{34}S$ variations of ±0.2‰ in different nodules (Beaudoin *et al.,* 1994). However, the analyses made in this study were normalized to the average value for repeated measurements of CDT material from a single sample, and therefore provide an internally consistent reference material for this study; however, this factor translates into the external reproducibility of $\delta^{34}S$.

During the chemical extraction of sulfur from a sample, the incomplete reaction of sulfides would introduce a kinetic isotope fractionation effect into the captured Ag_2S. In addition, loss of any product H_2S during the extraction (through oxidation or leakage) would also lead to kinetic isotope fractionation. Due to these factors, a great deal of care is taken leak-checking the reaction apparatuses and purging them with N_2 for >30 minutes before introducing HCl acid (that has also been degassed separately with N_2 for the same amount of time). For subsequent CRS extractions, the Cr (II) solution is degassed with N_2 prior to its injection into the reaction flasks, in an ongoing effort to minimize oxygen in the system.

After the Ag_2S is collected, it is aged in the dark for a week, rinsed three times with ultrapure water, soaked in NH_4OH (to remove impurities), and rinsed three more times with ultrapure water. Incomplete rinsing could lead to impurities in the

subsequently fluorinated Ag_2S and could cause the conversions of Ag_2S to SF_6 to be non-quantitative, which would introduce a mass-dependent isotopic fractionation into the analyzed sample.

The dried Ag_2S samples are reacted with ~10x stoichiometric excess of F_2 at 250 °C overnight, in order to promote a full reaction. Although the bombs are degassed and checked for leaks prior to fluorine introduction, adsorbed water and oxygen (along with possible small leaks and temperature variations) may inhibit the completely quantitative reaction of Ag_2S to SF_6, in turn causing an isotopic fractionation.

Other sources of isotopic fractionation include the transfer of SF_6 from the bomb through the manifold to the primary separation volume, where it is allowed to freeze (along with HF and other condensable gases) at liquid N_2 temperatures for ten minutes. Leftover fluorine gas is slowly removed through the use of a KBr passivation column, trapping product bromine in a liquid N_2 cold trap after the column. Once all fluorine is gone, the frozen SF_6 and HF are allowed to thaw in the isolated primary separation volume, after which an N_2-ethanol slurry at ~-115 C is used to freeze the HF. The SF_6 is then frozen into the GC injection loop with liquid N_2 and allowed to transfer for 10 minutes while monitoring the temperature of the ethanol-N_2 slurry at the base of the primary separation volume.

Although small variations in temperature may introduce different compounds into the GC, they should not contribute to any isotopic fractionation, however, overly fast transfer speeds during the initial separation of F_2 from SF_6 may cause sample loss

through the entrainment of frozen SF_6 particles (transfer speeds kept under ~0.1 torr/sec to mitigate this effect).

Ultrapure He carrier gas is flowed through the GC and capture-end of the apparatus for ~20 minutes before a sample is introduced. When ready, a sample is allowed to thaw while flowing helium through the GC injection loop, and it is subsequently carried by helium through the GC columns. Several different small peaks are detected by the TCD as the different gas species from the sample pass through the column, which includes a consistent pre-peak of unknown composition that is immediately followed by the SF_6 peak at ~11 minutes.

When the SF_6 peak is detected, the flow of He is diverted through a channel which has two capture coils frozen by liquid N_2. Both the timing of the initial diversion and the cessation of flow at the end of the SF_6 peak may contribute to isotopic fractionation of the sample, as it has been observed that SF_6 peaks caught too late have isotopically light compositions indicative of kinetic fractionation during passage of gas through the column.

After it is captured, the sample of purified SF_6 is allowed to thaw, and its pressure is measured in order to determine how it matches an empirically based ideal fluorination yield, before it is allowed to freeze into the cold-finger of the mass spectrometer for ten minutes. The fluorination yields of all samples reported in this study are within analytical uncertainty of 100%.

Instrumental mass fractionation during the isotopic analysis of SF_6 affects both the sample-gas and the reference gas in the same way, and is therefore not likely to be a factor on dual-inlet mass spectrometers. Ionization efficiencies in the electron-

impact source are estimated to be approximately 1 in 1000 molecules. Though this is not likely to cause any isotopic fractionation, it has been noted that there are gradual shifts in the reference gas that may lead to uncertainties in the acquired data; this variation is taken into account by analyzing IAEA S1 material between the samples, and renormalizing the sample to our accepted long-term value for IAEA S1 if it is necessitated by the analyzed compositions of its bracketing standards.

Scattering of the beams in the analyzer- and detector-sectors of the mass spectrometer may also lead to erroneous measurements, along with environmental factors which influence electronic noise (such as Johnson noise). The current of the beam for $^{32}SF_5^+$ is approximately ~10nA (~6 billion ions/sec) for the average sample size in this study. Contamination by $C_3F_5^+$ and larger amounts of shot-noise due to the high resistance of the resistor at the mass station for $^{36}SF_5^+$ (m/z = 131) contribute the largest amount of uncertainties in the measurements of $\delta^{36}S$. The data (which are analyzed with respect to an SF_6 reference gas of known composition) is finally renormalized to the average long-term values for repeated analyses of CDT.

3.2.5 Evaluation of Uncertainty

Duplicate sulfur extractions of four different samples yielded average differences of only 0.08‰, 0.002‰, and 0.16‰ for $\delta^{34}S$, $\Delta^{33}S$, and $\Delta^{36}S$, respectively (*Table 5*), which serves to indicate that the total extraction, purification, and analysis procedures (described above) are well within the range of our reported long-term external reproducibilities. However, this data may not be extensive enough to fully confirm that these are the true internal reproducibilities of the performed analyses.

Due to long-term drift in the machine and isotopic differences reported in

CDT (Beaudoin *et al.,* 1994), along with differences in the methodology of individual operators, it is best to report the external reproducibilities of the measurements in this thesis based on the lab's long-term (2 year) reproducibility on IAEA S1 reference material, which is 0.3‰, 0.008‰, and 0.3‰ (2σ) for $\delta^{34}S$, $\Delta^{33}S$, and $\Delta^{36}S$, respectively, taking into account the improved counting statistics resulting from the tripled number of analyses performed on each sample in this study.

Chapter 4: Results

4.1 Sulfur Isotope Relationships in Troilite

It is found that values of $\Delta^{33}S$ in iron meteorite troilite range from -0.029‰ to +0.031‰ relative to CDT, with different iron groups forming discernible clusters in $\Delta^{33}S$ space (*Fig. 5*, 6). The data obtained for sulfur isotopic ratios in iron meteorite troilite nodules is shown in *Table 2*. Non-magmatic iron meteorites show a limited range in $\Delta^{33}S$: Group IAB (n=23) has an average $\Delta^{33}S$ of +0.004 ± 0.002‰ (2SE), while Watson, the single meteorite analyzed from group IIE has a $\Delta^{33}S$ of +0.009 ± 0.008‰ (2σ). Magmatic groups yield resolvable mass-independent compositions: group IC (n=2) has a mean value of +0.017 ± 0.008‰ (2σ), group IIAB (n=8) has a mean of +0.016 ± 0.004‰ (2SE), group IIIAB (n=18) has a mean of +0.018 ± 0.002‰ (2SE), and group IVA (n=8) has the highest mean value of all analyzed groups at +0.022 ± 0.004‰ (2SE). All of these groups are unresolvable from each other. Hoba, the only analyzed sample from group IVB, has a $\Delta^{33}S$ value of 0.000 ± 0.008‰ (2σ). Interestingly, the only observed depletions in ^{33}S were found in members of the rare magmatic group IIIF, with an average $\Delta^{33}S$ value of -0.028 ± 0.008‰ (2σ) (n=2)[1].

The measured samples have overlapping $\delta^{34}S$ values that fall within the range established by previous studies (Hulston and Thode, 1965b; Gao and Thiemens, 1991), ranging from -1.41‰ to +1.29‰ with an average of -0.01 ± 0.81‰ (2σ), this

[1] The measurement of St. Genevieve County (IIIF) from Gao and Thiemens, 1991, is similar to our measurement of Cerro Del Inca (IIIF), and was therefore considered in the discussion.

Table 2. Sulfur Isotopic Analyses of Iron Meteorite Troilite AVS

Name	Class	$\delta^{34}S$	$\Delta^{33}S$	$\Delta^{36}S$	Name	Class	$\delta^{34}S$	$\Delta^{33}S$	$\Delta^{36}S$
Osseo	IAB-comp	0.393	0.004	0.040	Acuna	IIIAB	0.004	0.024	-0.033
ALHA77290	IAB-MG	0.496	-0.001	0.134	Acuna (Fluo 2)	IIIAB	-0.146	0.014	-0.050
Bogou	IAB-MG	0.252	0.010	-0.006	Apoala	IIIAB	0.056	0.019	-0.299
Burkett	IAB-MG	0.132	0.001	0.112	Apoala 2	IIIAB	-0.179	0.021	0.018
Campo del Cielo	IAB-MG	-0.168	0.004	0.129	Loreto	IIIAB	0.272	0.011	0.005
Campo del Cielo (AVS2)	IAB-MG	-0.137	0.008	0.253	Wabar	IIIAB	-0.205	0.012	0.196
Canyon Diablo	IAB-MG	-0.277	0.003	0.209	Waingaromia	IIIAB	1.289	0.012	-0.053
Deelfontain	IAB-MG	-0.232	0.003	0.066	Cape York	IIIAB	0.367	0.013	-0.053
Deelfontein (Fluo2)	IAB-MG	-0.058	0.002	0.148	Grant	IIIAB	0.239	0.013	0.086
Hope	IAB-MG	-0.254	0.002	-0.092	Thule	IIIAB	0.287	0.014	-0.149
Idaho	IAB-MG	-0.069	0.001	0.012	Kenton County	IIIAB	-0.130	0.015	0.012
Wichita County	IAB-MG	-0.480	0.003	-0.209	Costilla Peak	IIIAB	-0.562	0.018	-0.053
Mundrabilla 2	IAB-Mund	0.128	-0.003	-0.036	La Porte	IIIAB	0.505	0.019	-0.095
Mundrabilla	IAB-Mund	-0.127	-0.007	0.110	Sacramanto Mtns	IIIAB	0.025	0.020	0.013
Waterville	IAB-Mund	-0.228	0.002	0.068	Grant	IIIAB	0.100	0.021	-0.038
Pitts	IAB-Pitts	-0.319	-0.002	0.207	Casas Grandes	IIIAB	-0.141	0.022	-0.040
Woodbine	IAB-Pitts	0.099	0.007	0.047	Trenton	IIIAB	0.128	0.027	-0.072
Woodbine (Fluo2)	IAB-Pitts	0.086	0.004	0.044	MET0040	IIIAB	0.294	0.028	-0.200
Bischtube	IAB-sLL	0.245	0.001	0.054		**IIIAB Average**	**0.122**	**0.018**	**-0.045**
Goose Lake	IAB-sLL	-0.167	0.003	0.181					
Goose Lake (AVS2)	IAB-sLL	-0.247	0.006	0.282	Cerro del inca	IIIF	-0.117	-0.027	-0.233
Toluca	IAB-sLL	0.546	0.000	0.209	Cerro del Inca-re	IIIF	0.253	-0.029	-0.136
Lamesa, Texas	IAB-sLM	0.752	0.013	0.225	Cerro del inca-re2	IIIF	0.207	-0.031	-0.110
Malta Hohe	IAB-sLM	0.644	0.011	0.135	St. Genevieve Cnty°	IIIF	0.240	-0.024	-0.256
Mertzon	IAB-ung	-0.171	0.010	0.124		**IIIF Average**	**0.146**	**-0.028**	**-0.184**
Mertzon (AVS2)	IAB-ung	-0.277	0.009	0.277					
Mesa Verde Park	IAB-Ung	0.139	0.007	0.226	Altonah	IVA	-0.405	0.019	0.025
	IAB Average	**0.026**	**0.004**	**0.109**	Bushman Land	IVA	-0.480	0.020	0.185
					Duchesne	IVA	-0.255	0.023	0.017
Santa Rosa	IC	0.008	0.017	-0.070	Gibeon	IVA	0.097	0.021	-0.017
Santa Rosa 2	IC	-0.087	0.017	-0.064	Harriman	IVA	-0.799	0.031	-0.212
					Huizopa	IVA	-0.775	0.025	-0.066
DRPA 78008/10	IIAB	0.022	0.026	-0.115	Maria Elena	IVA	-1.414	0.027	0.047
DRPA 78008/10 (Fluo2)	IIAB	-0.057	0.020	-0.134	S.J. Nepomuceno	IVA	-0.505	0.013	0.055
DRPA 78009	IIAB	0.888	0.018	-0.019	S.J. Nepomuceno (Fluo2)	IVA	0.294	0.017	-0.031
Indian Valley	IIAB	-0.343	0.007	-0.034		**IVA Average**	**-0.471**	**0.022**	**0.000**
Keen Mountain	IIAB	0.131	0.014	-0.112					
Mayodan	IIAB	0.059	0.016	-0.337	Hoba	IVB	-0.485	0.000	0.128
North Chile	IIAB	0.143	0.018	-0.087					
Old Woman	IIAB	-0.096	0.009	-0.155	10057.271	Lunar basalt	0.697	0.001	-0.022
Patos de Minas (Hex)	IIAB	-0.151	0.018	-0.066	12022.281	Lunar basalt	0.473	-0.009	-0.027
Patos de Minas (Hex) (AVS2)	IIAB	-0.068	0.017	0.190	70017.598.67	Lunar basalt	0.667	-0.004	0.434
	IIAB Average	**0.053**	**0.016**	**-0.087**		**Lunar Average**	**0.612**	**-0.004**	**0.128**
Watson	IIE	-0.361	0.009	0.106	MORB Glasses[†]	**Mantle Average**[‡]	**-1.1**	**0.005**	**0.05**
Watson-re	IIE	-0.025	0.011	-0.020					

Note: AVS2 = duplicate extraction of initial troilite, Fluo2 = duplicate fluorination of Ag_2S, re = re-measurement of stored SF_6, ‡ mantle average from Labidi et al., 2012 & Labidi (*IPGP*, *thesis*), °St. Genevieve County data from Gao and Thiemens, 1991. Long-Term uncertainties for individual measurements are 0.3‰, 0.008‰, 0.3‰ (2σ) for $\delta^{34}S$, $\Delta^{33}S$, and $\Delta^{36}S$, respectively.

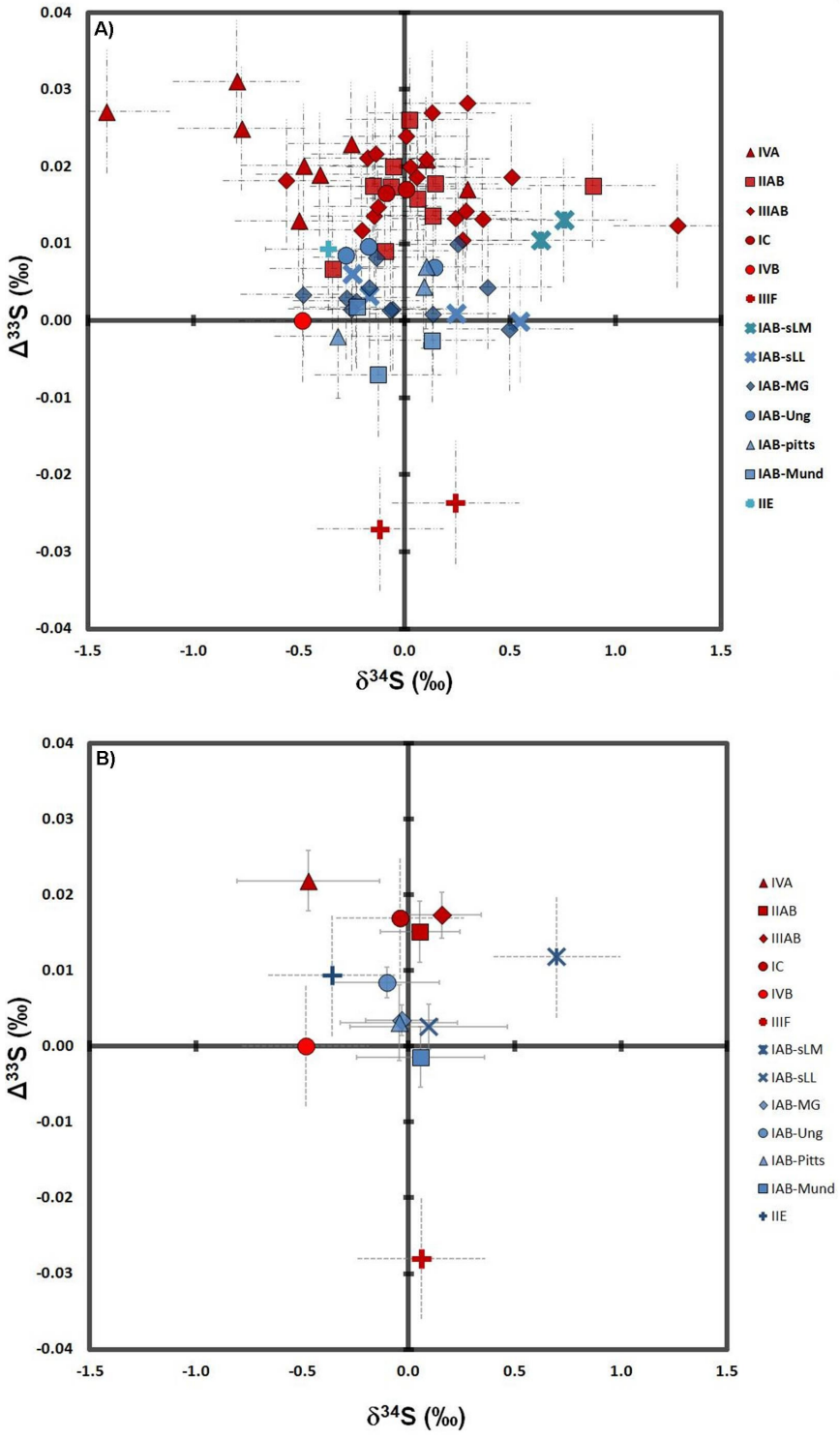

Fig. 5a,b. Measurements of (a) $\Delta^{33}S$ vs. $\delta^{34}S$ and (b) average values of $\Delta^{33}S$ vs. $\delta^{34}S$ for AVS fractions of troilite from 57 iron meteorites belonging to the groups IAB, IC, IIAB, IIE, IIIAB, IIIF, IVA, and IVB. Non-Magmatic and Magmatic groups are in blue and red, respectively. Error bars represent 2σ uncertainties (dotted) and 2σ std. errors (solid).

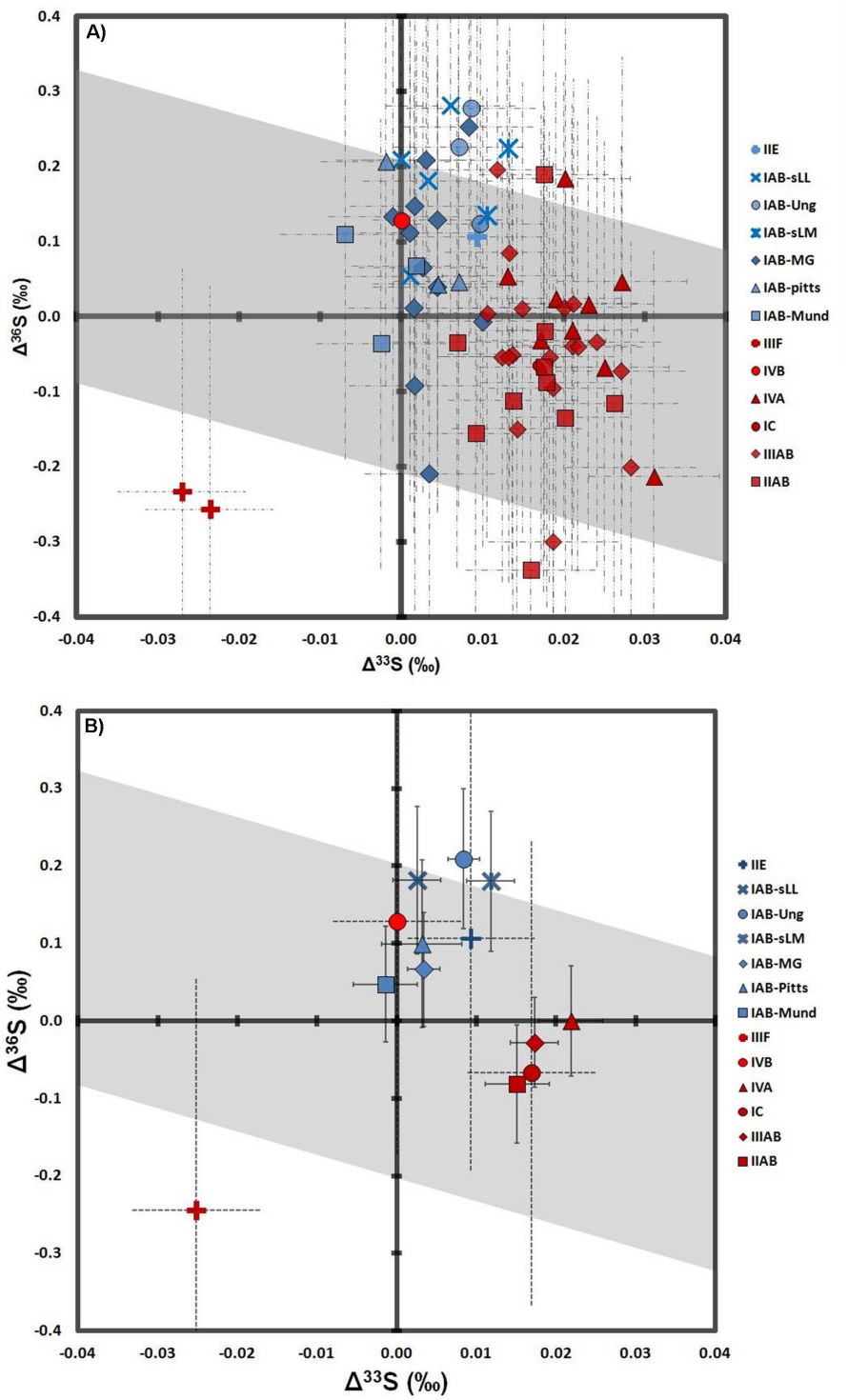

Fig. 6a,b. Plots of (a) $\Delta^{36}S$ vs. $\Delta^{33}S$ and (b) average values of $\Delta^{36}S$ vs. $\Delta^{33}S$ for AVS fractions of troilite from 57 iron meteorites. Non-Magmatic and Magmatic groups are in blue and red, respectively. Error bars represent 2σ uncertainties (dotted) and 2σ std. errors (solid). Linear regression of data (*excl.* IIIF) yields slope of ~ -7. Grey band represents photolysis of H_2S from Chakraborty *et al.,* 2013.

variation is thought to reflect mass-dependent isotopic fractionation during parent body processing. Individual groups also have average $\delta^{34}S$ values falling within error of zero, with the exceptions of group IVA, which tends towards negative values, having an average $\delta^{34}S$ of -0.471 ± 0.337‰ (2SE) (n=8) and group IAB-sLM with an average of +0.698 ± 0.3‰ (2σ) (n=2).

Average $\Delta^{36}S$ measurements also overlap greatly for most iron meteorite groups (*Fig. 6*) and are within error of zero, ranging from -0.337‰ to +0.282‰. However, the non-magmatic iron meteorites appear to have slightly elevated $\Delta^{36}S$ values with an average of +0.109 ± 0.227‰ (2SD), while the magmatic irons tend to have more negative values with an average of -0.044 ± 0.252‰ (2SD).

4.2 Chromium-Reducible Sulfur

Few samples yielded enough chromium-reducible sulfur (CRS) to analyze with the same precision as the AVS samples. Chromium-reduction is an established method for extracting sulfur from pyrite and other disulfide minerals (Canfield *et al.,* 1986). Five samples of CRS from different troilite nodules were analyzed in this study (*Table 3*). The sulfur in the CRS products of the extractions derives from minor amounts of acid-resistant sulfide phases (such as daubreelite or other complex sulfides).

The results for the CRS data indicate resolvable (but not unidirectional) differences in $\delta^{34}S$ when compared to their corresponding AVS fractions, but almost no variability in $\Delta^{33}S$ or $\Delta^{36}S$. This is not surprising, as the carrier of CRS sulfur is likely to have exsolved from the troilite during sub-solidus cooling, and therefore, probably comes from the same parental sulfur pool as the troilite nodule. Exsolution

of daubreelite, for example, would likely have had an effect on $\delta^{34}S$ (diffusional fractionation), however, the differences between the AVS and CRS fractions in our data set do not appear to be systematic and requires further investigation.

4.3 Measurement Reproducibility

The variability between different non-proximal troilite nodules from the same iron meteorites was investigated for three different meteorites (*Table 4).* Our results show that $\Delta^{33}S$ and $\Delta^{36}S$ do not vary significantly between different troilite nodules in a single meteorite; however, there are differences in $\delta^{34}S$ as a possible result of mass-dependent isotope fractionation processes during sulfide segregation and crystallization, or possibly due to differing amounts of terrestrial alteration between the nodules.

Separate AVS extractions were made of the same troilite samples for four different iron meteorites (*Table 5).* This was done in order to test the reproducibility of the processing methods on sulfur isotope measurements. All duplicate analyses produce results well within the estimates of our long-term reproducibilities.

The variability in $\Delta^{33}S$ is less than 0.004‰ in all duplicate samples, whereas the maximum variability in $\Delta^{36}S$ is 0.3‰. The variability in $\delta^{34}S$ is inferred to be the highest, as the processes used to extract sulfur are themselves mass-dependent; however, variability in duplicate extractions of the four different troilite samples was less than 0.1‰. It is also shown that there is no correlation between the percent yield of a sulfur extraction (based on assumption of pure troilite, *Appendix A*) and its $\delta^{34}S$, $\Delta^{33}S$, and $\Delta^{36}S$ values (*Appendix B*). The product ideal yield was always less than

Table 3. Chromium-reducible sulfur analyses

Name	Group	$\delta^{34}S$	$\Delta^{33}S$	$\Delta^{36}S$	$\delta^{34}S_{(CRS-AVS)}$	$\Delta^{33}S_{(CRS-AVS)}$	$\Delta^{36}S_{(CRS-AVS)}$	Sf_6 (torr)
Goose Lake CRS	IAB-sLL	1.248	0.006	-	1.455	0.001	-	0.282
Mertzon CRS	IAB-Ung	-0.528	0.009	-	-0.304	0.000	-	0.485
Santa Rosa CRS	IC	0.803	0.014	0.073	0.842	-0.003	0.141	3.454
Acuna CRS	IIIAB	0.129	0.021	-0.007	0.125	-0.003	0.026	1.522
Apoala 2 CRS	IIIAB	-0.511	0.015	-0.030	-0.450	-0.005	0.110	3.228
Average difference (CRS-AVS)					**0.635**	**0.002**	**0.092**	
Std Dev. (1σ)					0.803	0.003	0.059	

*Notes: Samples with SF_6 pressures of less than 1 torr do not yield reliable $\Delta^{36}S$ data, average differences are from absolute values

Table 4. Different nodules from the same meteorites

Name	Group	$\delta^{34}S$	$\Delta^{33}S$	$\Delta^{36}S$	$\delta^{34}S_{(1-2)}$	$\Delta^{33}S_{(1-2)}$	$\Delta^{36}S_{(1-2)}$
Mundrabilla	IAB-Mund	-0.127	-0.007	0.110	-	-	-
Mundrabilla 2	IAB-Mund	0.128	-0.003	-0.036	-0.255	-0.004	0.146
Santa Rosa	IC	0.008	0.017	-0.070	-	-	-
Santa Rosa 2	IC	-0.087	0.017	-0.064	0.094	0.000	-0.006
Apoala	IIIAB	0.056	0.019	-0.299	-	-	-
Apoala 2	IIIAB	-0.179	0.021	0.018	0.235	-0.003	-0.318
Average difference (different nodules)					**0.195**	**0.002**	**0.156**
Std Dev. (1σ)					0.252	0.002	0.236

*Note: average differences are calculated from absolute values

Table. 5 Sulfur Extraction Duplicates

Name	Group	$\delta^{34}S$	$\Delta^{33}S$	$\Delta^{36}S$	$\delta^{34}S_{(AVS1-AVS2)}$	$\Delta^{33}S_{(AVS1-AVS2)}$	$\Delta^{36}S_{(AVS1-AVS2)}$
Campo del Cielo	IAB-MG	-0.168	0.004	0.129	-	-	-
Campo del Cielo (AVS2)	IAB-MG	-0.137	0.008	0.253	-0.031	-0.004	-0.124
Goose Lake	IAB-sLL	-0.167	0.003	0.181	-	-	-
Goose Lake (AVS2)	IAB-sLL	-0.247	0.006	0.282	0.080	-0.003	-0.100
Mertzon	IAB-ung	-0.171	0.010	0.124	-	-	-
Mertzon (AVS2)	IAB-ung	-0.277	0.009	0.277	0.106	0.001	-0.154
Patos de Minas (Hex)	IIAB	-0.151	0.018	-0.066	-	-	-
Patos de Minas (Hex) (AVS2)	IIAB	-0.068	0.017	0.190	-0.084	0.000	-0.256
Average difference (sulfur extractions)					**0.075**	**0.002**	**0.159**
Std Dev. (1σ)					0.090	0.002	0.069

*Note: average differences are calculated from absolute values

100% in all measurements[2], which supports the idea that it was the impurity of the samples that lead to Ag_2S yields less than those predicted from pure troilite, as opposed to loss of product through oxidation, leakage, or incomplete reactions during sample preparation.

[2] The product ideal yield was over 100% in only one sample (likely due to added mass from a broken Pasteur pipette tip used during the extraction).

Chapter 5: Discussion

Variations in the $\Delta^{33}S$ and $\Delta^{36}S$ compositions on the scale identified in this study could be generated through many possible mechanisms. The evaluation of these different processes can be done using relationships between the different isotopes of sulfur. Possible sources for $\Delta^{33}S$ anomalies in iron meteorites include post-formational effects, such as spallation, or pre-formational effects such as nucleosynthetic anomalies and photolysis. Additionally, for such small $\Delta^{33}S$ variations (up to +0.031‰), possible $\Delta^{33}S$ sources including mixing and variations in the exponent defining $\Delta^{33}S$ must also be considered, as they have been shown to have relevance in the interpretation of small $\Delta^{33}S$ (*e.g.* Farquhar and Wing, 2007).

5.1 Evaluation of the Sulfur Isotopic Signals

5.1.1 Mixing and the Definition of $\Delta^{33}S$

As discussed above, mixing of different mass-dependent sulfur pools can create deviations from the mass-dependent array. The size of the variations measured in $\Delta^{33}S$ merits a discussion of mixing as a possible source of the anomalies, as mixing of sulfide and sulfate pools (*e.g.* within the cell of a sulfate-reducing bacterium or in other complex reaction networks) is known to lead to $\Delta^{33}S$ values between 0 and 0.2‰, with a starting $\delta^{34}S$ difference of ~ 80‰ between the sulfate and sulfide (Farquhar *et al.*, 2007)].

The largest $\delta^{34}S$ deviations found in carbonaceous chondrite sulfides are ±8‰ (Bullock *et al.*, 2010). By mixing these extreme end-members, it is possible to

generate $\Delta^{33}S$ values from 0 to -0.008‰ (*Appendix C*). However, the range of $\delta^{34}S$ found in iron meteorites is almost an order of magnitude less. Mixing between two mass-dependent pools with $\delta^{34}S$ of +1‰ and -1‰ causes a very small maximum $\Delta^{33}S$ of only 0.0001‰. Likewise, variability in the exponent used to calculate mass independence (between 0.512 and 0.518) yields $\Delta^{33}S$ variation of less than 0.004‰ within the small $\delta^{34}S$ range of this study (*Appendix D*).

One other interesting possibility is $\Delta^{33}S$ enrichment through mixing of sulfur pools created through the evaporation of troilite (Rayleigh distillation). McEwing *et al.* (1980) reported results of an experiment in which troilite was evaporated at low-pressure and high temperature, condensing product elemental sulfur and dissociated troilite at the opposite end of a sealed tube. Measuring $\delta^{34}S$, they then calculated the fractionation factors associated with the branched reaction of evaporation of troilite to elemental sulfur ($1000\ln\alpha = -13$‰) and to dissociated troilite ($1000\ln\alpha = -5.4$‰). Using their data and assuming mass dependence, the $\Delta^{33}S$ variations due to mixing between the products and reactants at different stages during Rayleigh distillation of troilite to elemental sulfur were calculated. The maximum attainable value of $\Delta^{33}S$ for the pooled-product from mass-dependent Rayleigh processes during evaporation is less than 0.010‰ (*Appendix E*) and decreases as the reaction's branching ratio increases towards dissociated troilite.

As physical mixing processes are not sufficient to account for the anomalous sulfur compositions found in this study, there must have been other processes at work. The best way in which one can discern between different mechanisms of mass-

independent fractionation and/or anomalous isotope enrichments is by examining the relationships between $\Delta^{33}S$ and $\Delta^{36}S$.

5.1.2 Post-Disruption Spallation Reactions

Spallation reactions that occur near the surface of an iron meteorite during cosmic-ray bombardment can also cause mass-independent isotope variations. The metal phase of different iron meteorites has been shown to contain several ppm of sulfur with large changes in $\Delta^{33}S$ and $\Delta^{36}S$ that increase with increasing cosmic-ray exposure age (Hulston and Thode, 1965b; Gao and Thiemens, 1991). The enrichment of different isotopes in these cases depends on the flux of cosmic-rays, the location of material relative to the surface of its parent body, and on the probability of a given atom interacting with a bombarding particle and becoming an isotope of sulfur.

The creation of ^{33}S and ^{36}S in iron meteorites would be dominated by the spallation of ^{56}Fe, which could create ^{20}Ne along with an isobar of mass 36 [with a certain probability that it will be ^{36}S, and a lower probability that it will be ^{33}S along with another element or isotope (to balance the reaction)]. The spallogenic production of sulfur isotopes was shown to lead to ratios of $\Delta^{36}S/\Delta^{33}S$ of ~8 (Gao and Thiemens, 1991).

With necessary caution due to the limited spread of our data and analytical uncertainties on $\Delta^{36}S$, the $\Delta^{36}S/\Delta^{33}S$ slope associated with troilite from the major groups analyzed in this study is approximately -7.3 (R^2=0.23, *Appendix F*).
The observation that there are no relationships between published exposure ages (excluding largest meteorites) and $\Delta^{33}S$, along with different observed ratios for $\Delta^{36}S/\Delta^{33}S$, do not support the production of ^{33}S anomalies in troilite through

spallation.

Furthermore, sulfur with highly enriched $\Delta^{36}S/\Delta^{33}S$, derived from spallation, is only observed in concentrations of several ppm (Gao and Thiemens, 1991). Mass balance calculations indicate that a troilite nodule would need to exchange sulfur with 10^3 times its own volume of metal ($\Delta^{33}S$ of ~2) to obtain the enrichments observed in the magmatic iron meteorite groups, which is unlikely to happen in the solid-state and would make a larger effect on $\Delta^{36}S$ than observed here.

Likewise, homogeneous $\Delta^{33}S$ values (within uncertainty) for each group are not what would be expected if the anomalies were spallation-derived, as they would likely differ depending on the size of the piece broken from the parent body. Evidence for ^{33}S-depletions in the IIIF iron meteorite group compared to the inferred $\Delta^{33}S$ of the bulk inner solar system [chondrites, IAB iron meteorites, and the Earth-Moon system (Gao and Thiemens, 1993a,b; Rai *et al.*, 2007; Antonelli *et al.*, 2012, 2013, *this study;* Wing and Farquhar, 2013; Labidi *et al.*, 2012; Labidi *et al.*, *Thesis*)] also argues against an origin associated with the (unidirectional) spallogenic production of sulfur in the analyzed meteorites.

5.1.3 Nucleosynthetic Sulfur Anomalies

Since mixing processes and post-disruption spallation reactions do not appear to create the observed sulfur isotope signatures; it is most likely that the observed signatures were inherited from materials that pre-dated the assembly of the iron meteorite parent bodies. Two possibilities exist for this scenario, in which anomalous sulfur is either (1) created through the uneven contributions of different stellar sources to individual parent bodies or (2) created through gas-phase photochemical

processes in discrete regions of the early solar nebula.

A weak, but coherent, negative relationship between $\Delta^{36}S$ and $\Delta^{33}S$ is inconsistent with early nucleosynthetic models, but may be allowed by recent SIMS measurements of nucleosynthetic anomalies in presolar SiC grains (Hoppe *et al.*, 2012; Heck *et al.*, 2012).

^{32}S, ^{33}S, and ^{34}S are created in related stellar environments, through hydrostatic oxygen- and silicon- burning and explosive oxygen- and neon- burning (Chin *et al.*, 1996; Heger *et al.*, 2002). This generally happens through the repeated capture of alpha particles onto oxygen, neon, magnesium, and silicon (and subsequent neutron reactions to create ^{33}S and ^{34}S). On the other hand ^{36}S, the rarest of the sulfur isotopes, is created purely through the s-process (slow neutron capture), making it unlike the other sulfur isotopes; ^{36}S is created mostly in the hydrostatic carbon-burning shell of massive stars prior to SNII supernova explosion (Mauersburger *et al.*, 1996; Woosley & Weaver, 1995; Woosley & Hager, 2007). Clayton and Ramadurai (1977) argued that measurements of $\Delta^{36}S$ would be important because of the very low natural abundance of this isotope (which would make any heterogeneity more apparent), and suggested that nucleosynthetic anomalies would be most likely manifested by variations in $\Delta^{36}S$. To date, no variations in $\Delta^{36}S$ attributable to different nucleosynthetic sources have been found at the bulk scale in analyzed meteorite groups.

Recent work by Hoppe *et al.* (2012) has documented several presolar SiC grains with very large ^{32}S enrichments (*Fig. 7*). These grains are thought to originate from the Si/S zones of SNII supernovas and have large ^{32}S enrichments with $\delta^{33}S \cong$

$\delta^{34}S$ and $\Delta^{33}S$ values as low as ~ -200‰. Simple dilution of sulfur by ^{32}S yields a negative $\Delta^{36}S/\Delta^{33}S$ (~-1.9) about the origin (*Appendix G*), which is allowed by our observations. However, the observation of both positive and negative deviations from inferred average solar system $\Delta^{33}S$ (= 0.00‰) are difficult to reconcile with the addition of sulfur from a single nucleosynthetic source.

There are also proposals that sulfur with enrichments in ^{33}S may be a possible product of nucleosynthesis in the He/C zones of SNII supernovas (Rauscher *et al.,* 2002), but these zones are modeled to produce significantly larger enrichments in $\Delta^{36}S$ than in $\Delta^{33}S$ (Woosley and Heger, 2007), and poor mixing of several weakly anomalous presolar (nucleosynthetic) sulfur pools appears unlikely.

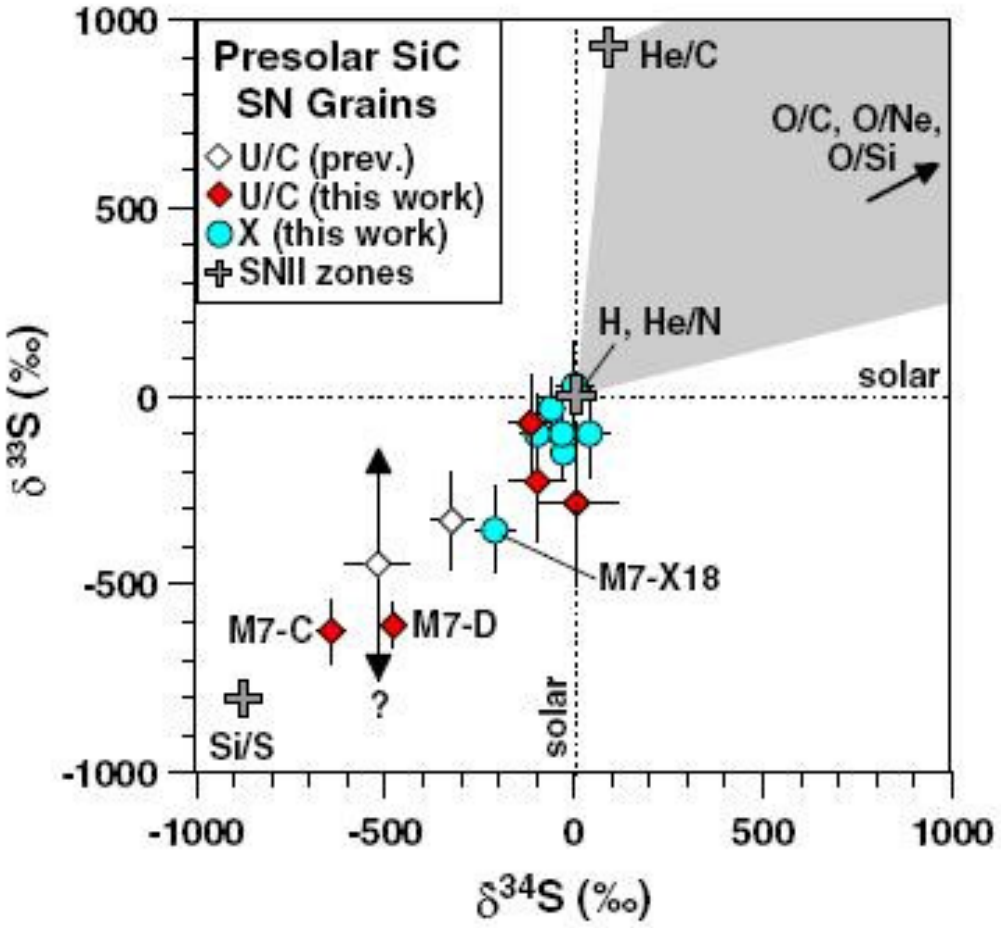

Fig. 7. Secondary Ion Mass Spectrometry (SIMS) measurements of $\delta^{33}S$ versus $\delta^{34}S$ in presolar SiC grains, demonstrating progressively more negative values on a slope of approximately 1. (From Hoppe *et al.*, 2012).

5.1.4 Photolysis in the Early Solar Nebula

The first convincing arguments that photochemical reactions generated meteoritic mass-independent sulfur isotope signatures were made by Cooper *et al.,* (1997) who demonstrated that the sulfur isotopes in methane-, ethane-, and propane-sulfonic acids in the Murchison meteorite reveal mass-independent relationships. In work that followed, studies of the ureilite, aubrite, HED, and acapulcoite-lodranite achondrite meteorite groups revealed small enrichments in ^{33}S (positive $\Delta^{33}S$) that were also attributed to photochemical origins (Farquhar *et al.*, 2000a; Rai *et al.,* 2005). A photochemical origin has also been attributed to $\Delta^{33}S$ enriched sulfur in an unidentified minor mineral fraction held within rare chondrule rims (but that is absent from bulk sulfur in chondrites), isolated through a time-series extraction (Rai and Thiemens, 2007).

A difficulty with making a strong case for a photochemical origin for mass-independent sulfur isotope signatures in meteorites has been the paucity of photochemical studies undertaken at relevant conditions. Work by Farquhar *et al.*, (2000b) documented that products derived from hydrogen sulfide photolysis by UV radiation with wavelengths longer than ~220 nm yielded a slightly positive $\Delta^{36}S/\Delta^{33}S$ (~1.7) which does not match the observations made here (though it may have some relevance in explaining the outlier IIIF data). However, a series of recent photolysis experiments of H_2S using Lyman α radiation (thought to be the most prominent wavelength of UV during the sun's T-Tauri phase) provide a possible match to the observed sulfur isotopic values in iron meteorites, with an array between products and reactants having a $\Delta^{36}S/\Delta^{33}S$ value of ~ -3 (Chakraborty *et al.*, 2013). This

roughly consistent $\Delta^{36}S/\Delta^{33}S$ supports a possible pre-accretionary photochemical origin for the sulfur isotope signatures seen in iron meteorite troilite.

As opposed to addition of anomalous sulfur from a specific source, the chemical fractionation of a nebular sulfur reservoir would make isotopically complementary components, and could possibly explain both the enrichments and depletions observed in our samples, relative to chondrites and IAB iron meteorites. Interestingly, the relationship between the IIIF measurements and the other magmatic iron meteorites have a best fit slope that is slightly positive (~1.7, which is similar to H_2S photolysis by wavelengths >220nm), but with a very low R^2 value of only 0.02 (*Appendix F*). While it is tempting to call on another process, the sample set is too small to do so, and the most constructive statement that can presently be made is that inheritance of sulfur from a photolytic source is the most parsimonious explanation for the obtained data.

5.2 Geochemical Considerations

5.2.1 Hf-W Model Ages

The short lived isotope ^{182}Hf decayed to ^{182}W with a half life of 9 Ma for the first ~60 Ma of solar system history. Hafnium is a lithophile element, whereas tungsten is a siderophile element, therefore most W in a planetesimal body is incorporated into the metal phase during the process of core formation, whereas Hf is left in the silicate mantle. Any ^{182}Hf left in the mantle after core formation will finish decaying to ^{182}W which will then remain in the silicates (and have a much higher $^{182}W/^{180}W$ ratio due to prior depletion of tungsten during core formation), whereas the ^{182}W composition of the core is frozen at the time of core formation, and is

necessarily less than that in chondrites, which have more radiogenic ^{182}W compositions because they did not undergo core-mantle differentiation.

These data can then be used to estimate the time of core formation by comparing the $\varepsilon^{182}W$ ratios in the sample to those of reference samples of known age, such as CAIs [which are Pb-Pb dated to 4567 ± 1 Ma (Amelin *et al.*, 2002)] and can then be used to obtain Hf-W core segregation ages for iron meteorites.

It is found that magmatic iron meteorites (IC, IIAB, IIIAB, IVA, IVB) segregated their cores in the first couple million years after CAIs, whereas most non-magmatic iron meteorites segregated their cores approximately 3-5 million years after CAI formation (Kleine *et al.*, 2005; Markowski *et al.*, 2006; Schersten *et al.*, 2006; Qin *et al.*, 2008; Schulz *et al.* 2009, 2012; Kruijer *et al.*, 2013a,b). Interestingly, the magmatic IIIF group iron meteorites are the only group that have late core-segregation ages similar to the non-magmatic irons (Qin *et al.*, 2008)[3].

To get a value of $\varepsilon^{182}W$ that accurately reflects the age of mantle-core segregation from a chondritic reservoir, it is necessary to correct for the cosmogenic production of ^{182}W from neutron capture reactions. Recently, Kruijer *et al.* (2013a,b) have proposed a method for pre-exposure age dating of different iron meteorite groups based on the use of platinum isotopes as a neutron dosimeter. Due to different exposure ages for different members within a given group of iron meteorites, there is a linear relationship between ^{182}W and the cosmogenically produced isotopes of Pt. The regression of this line yields an intercept equal to the pre-exposure $\varepsilon^{182}W$ value (Kruijer *et al.,* 2013a,b). Prior to the use of Pt isotopes, other studies reported values

[3] it is noted that in this study a slightly different CAI initial value was used, but the correction is very slight, pushing the IIIF group further away (later in time) from CAIs.

corrected with Sm isotopes as a neutron dosimeter, or with both no correction and with a maximum cosmogenic ^{182}W correction based on production calculations using other cosmic-ray exposure age proxies (Markowski *et al.*, 2006; Qin *et al.*, 2008; Schultz *et al.*, 2012).

Through advances in measurement and correction techniques, it now appears that differences between different magmatic iron meteorite groups can also be resolved. The most recent efforts in dating core-segregation in magmatic iron meteorites has placed them in the order (IC<IIAB<IIIAB<IVA<IVB<IIIF). However, the overlap between groups, other than those with the earliest and latest core segregation ages, makes their ages difficult to resolve from each other. What can be resolved is that the IVB iron meteorites have later ages than the IIAB iron meteorites, and the IIIF, IIE, and IAB formed later than all the others (Qin *et al.,* 2008; Kruijer *et al.*, 2013a, b; Schulz *et al.,* 2009, 2012).

Our results for the average $\Delta^{33}S$ of iron meteorite groups are plotted against their different Hf-W ages in Figure 8. There is a weak relationship between the Hf-W ages of the different magmatic iron meteorites and their $\Delta^{33}S$ values, which decreases with increasing Hf-W metal-silicate differentiation age (*Fig.* 8). Only corrected data are plotted, but the most accurate values are assumed to be those from Kruijer *et al.,* (2013a,b), which appear to plot closest to the theoretical "max-correction" values from earlier literature.

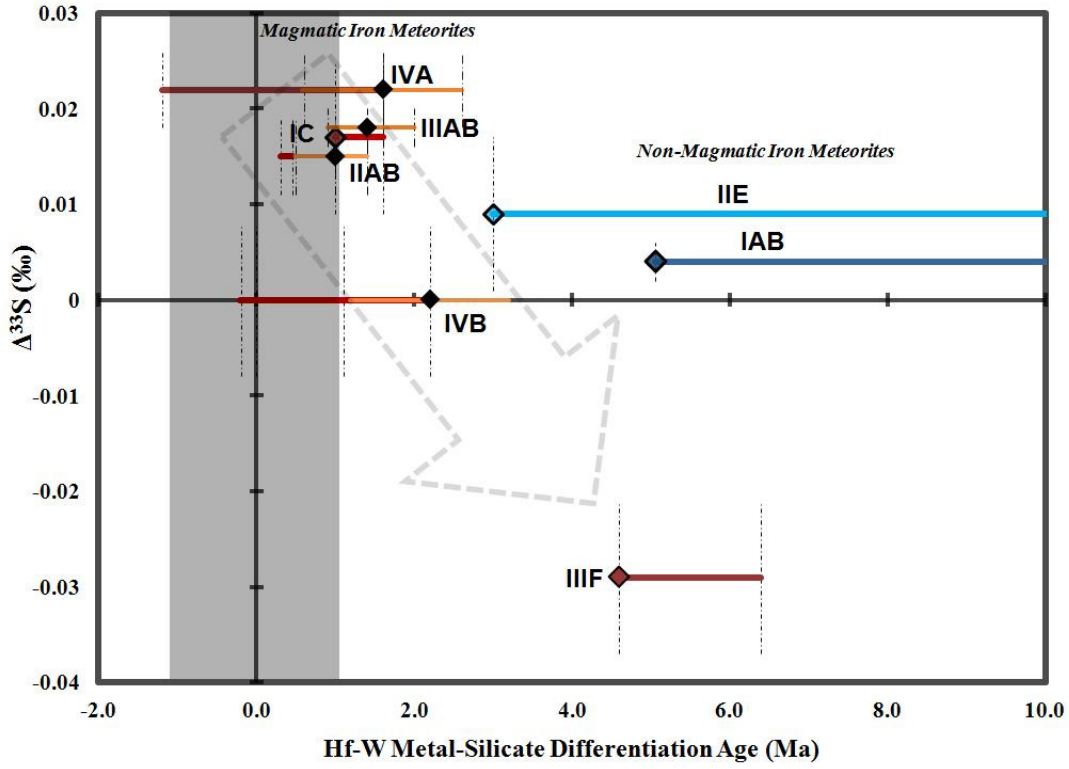

Fig. 8 Measured Average $\Delta^{33}S$ for each group of iron meteorites plotted against various Hf-W age studies. Solid black diamonds and their orange uncertainties represent pre-exposure $\varepsilon^{182}W$ values from Kruijer *et al.* (2013). Hollow diamonds represent maximum calculated cosmogenic exposure corrections on groups IC and IIIF (from Qin *et al.,* 2008), and Sm-based corrections on IAB and IIE data, respectively (Schulz *et al.,* 2009, 2012). Solid colored lines span the range of max-corrected values from Markowski *et al.* (2006), Qin *et al.* (2008), Schulz *et al.* (2009, 2012), and Kruijer *et al.* (2013). Error bars in y-direction represent 2SE for groups IAB, IVA, IIAB, & IIIAB, and long-term 2SD reproducibility for groups with less than 8 measurements (IC, IVB, IIIF, & IIE). Grey band represents uncertainty in CAI initial, grey arrow demarcates a possible trend in the magmatic irons.

5.2.2 Volatile Element Content

A crude linear relationship is also observed between the $\Delta^{33}S$ of different iron meteorite groups (other than the IIIF iron meteorites) and their Ni-normalized volatile element abundances (such as Ga, Ge, and Sb) (Wasson *et al.*, 2007; Wasson and Kallemeyn, 2002) (*Fig.* 9a,b,c). The normalization to Ni better reflects the starting Ga, Ge, and Sb concentrations of the different iron meteorite parent bodies prior to fractional crystallization (though this process does not change $\Delta^{33}S$). Graphs were also constructed of the average $\Delta^{33}S$ and average Ga/Ni, Ge/Ni, and Sb/Ni ratios for the different groups, but are not used due to the improper weighting of average values in the calculated linear regression. While there appears to be a rough variation in $\Delta^{33}S$ versus these normalized elemental values, this may or may not imply an actual relationship. To explore the possibility of a causal connection, several models of volatile element depletion in iron meteorites are discussed below.

Contrasting models used to explain the relative volatile element depletions in different iron meteorite groups include: (1) variable loss during impact processes between different parent bodies (Wasson, *Pers. Comm.* 2013) and (2) volatile depletion through the incomplete condensation of early solar system materials as a function of temperature [which decreases with increasing heliocentric distance and time (Wasson, 1976; Bland and Ciesla 2010, 2012)].

As the Sun is a large source of energy in the early solar nebula, it is likely that at any given time, temperature decreased with increasing heliocentric distance.

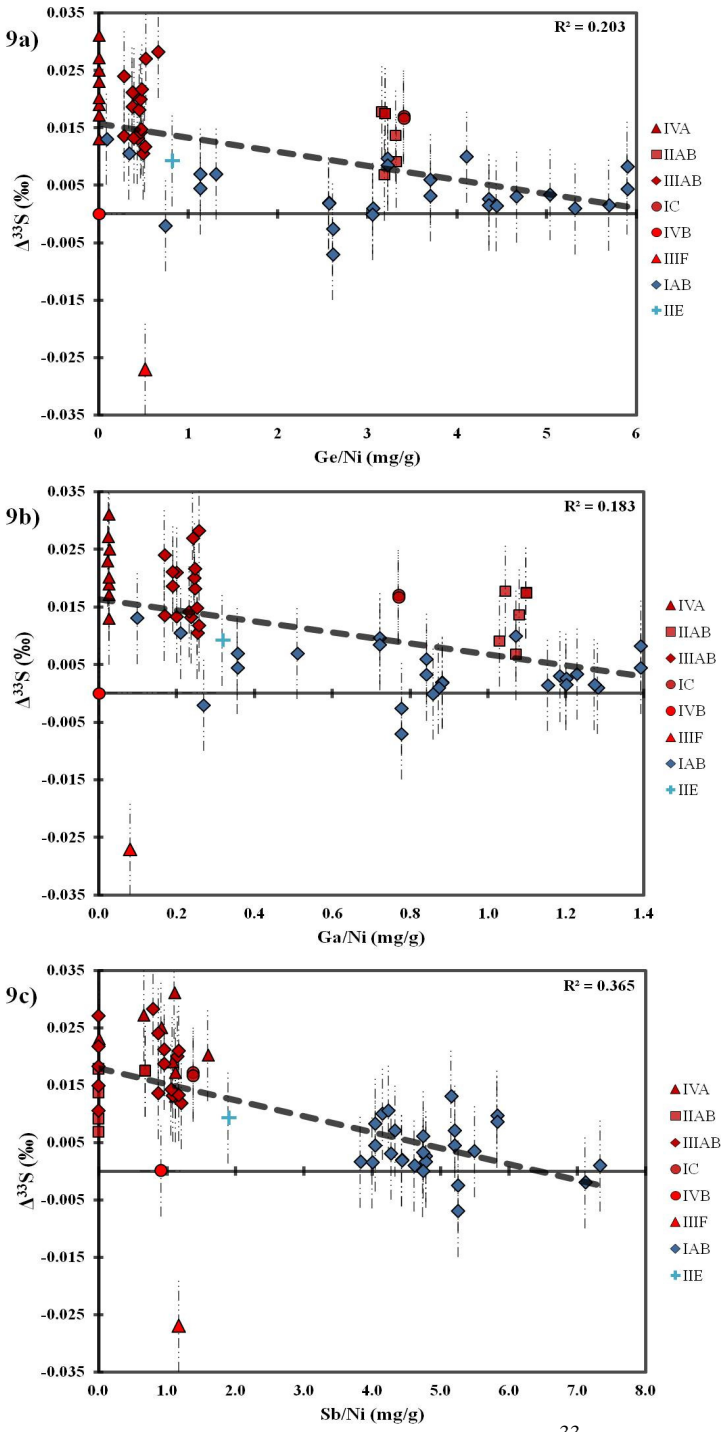

Fig. 9a Ni-normalized Ge concentrations *versus* $\Delta^{33}S$ in individual iron meteorites. *Fig. 9b* Ni-Normalized Ga concentrations *versus* $\Delta^{33}S$ in individual iron meteorites. *Fig. 9c* Ni-Normalized Sb concentrations *versus* $\Delta^{33}S$ in individual iron meteorites. Concentration data are INAA results from J.T. Wasson. Linear regressions of all data are shown as dotted lines and their R^2 values are plotted in the upper right corner of each graph.

Correspondingly, volatile content in iron meteorite groups would increase with increasing heliocentric distance and decreasing temperature (Bland and Ciesla, 2010, 2012), predicting that chondritic meteorites formed at greater distances than the iron meteorite parent bodies (and complementary achondrites). However, the volatile depletions may also be explained by differing amounts of impact metamorphism on the parent bodies, which would cause devolatilization, and a purely heliocentric explanation of volatile contents is likely to be over-simplistic.

If the anomalous $\Delta^{33}S$ values are indeed derived from Lyman-α photolysis of H_2S near the early sun, then both volatile depletion models are consistent with the correlations between the $\Delta^{33}S$ and Ni-normalized Ga, Ge, and Sb abundances, as both high temperatures and greater collisional frequencies are expected at smaller heliocentric distances.

Comparisons between $\delta^{34}S$ of samples and chemical proxies for extent of fractional crystallization were made in order to test the potential relationship between core-crystallization and $\delta^{34}S$ composition in trapped troilite nodules (*Appendix H*). In the magmatic iron meteorite groups, which are thought to have undergone relatively well-behaved fractional crystallization, no significant relationships were observed between $\delta^{34}S$ and Ni, Ge, or Ga. However, in the IAB iron meteorites there does appear to be a weak correlation between Ni, Ge, and Ga contents and the $\delta^{34}S$ values, with the high-Ni, low-Ge, low-Ga end-members having more positive $\delta^{34}S$ values (*Appendix H*).

As the IAB iron meteorites cannot be modeled through simple fractional crystallization, the $\delta^{34}S$ variations are probably best explained by different degrees of

devolatilization during the different impact events that created the IAB main group and its sub-groups. Larger impacts would cause greater amounts of devolatilization and would increase the $\delta^{34}S$ of residual sulfur[4] and Ni contents, and decrease the concentrations of volatile elements such as Ge and Ga. As a result, $\delta^{34}S$ measurements in IAB iron meteorites might represent a proxy for the extent of devolatilization in different group members.

5.3 Models of Sulfur Isotopic Distribution in the Early Solar Nebula

The coherent $\Delta^{33}S$ of iron meteorites belonging to the same group, combined with the different $\Delta^{33}S$ for different groups, suggests a link with materials that accreted to form the differentiated early solar system planetesimals, rather than an effect related to planetary processes or post-disruption cosmic-ray spallation reactions. Photolysis in the early solar nebula has been proposed to explain ^{33}S enrichments found in bulk achondrites, rare chondrule components, and sulfonic acids extracted from the Murchison carbonaceous chondrite (Farquhar *et al.*, 2000a; Rai *et al.*, 2005; Rai and Thiemens, 2007; Cooper *et al.*, 1997). This study demonstrates that the anomalous sulfur in magmatic iron meteorites was most likely inherited from early nebular photolysis of H_2S.

A pre-accretionary photochemical origin for the sulfur isotope signatures seen in iron meteorite troilite implies the involvement of a gas phase sulfur species as well as a source of photolytic radiation in the early solar nebula. Ciesla (2013) and Pasek *et al.* (2005) have argued that hydrogen sulfide would have been present within the

[4] It is also reassuring to note that there is no relationship between the $\Delta^{33}S$ and the Ni, Ge, and Ga values in IAB irons supporting the idea that devolatilization reactions do not affect $\Delta^{33}S$ values (*Appendix I*).

inner ~ 1-2 AU of the young solar nebula because nebular temperatures were higher than ~ 570 to 690 K [the temperature at which sulfidation of metallic iron consumes hydrogen sulfide to produce troilite (Woods and Hashimoto, 1993)]. If some of this hydrogen sulfide was exposed to radiation either at the surface of the disk, or in the inner parts of the disk, it may have undergone photolysis reactions similar to those studied by Chakraborty *et al.*, (2013). Lyman α radiation would have been highest during the sun's T-Tauri phase, which lasts approximately 1-2 Ma for a star of solar mass (Wolk *et al.*, 2005), and is likely to be responsible for ejecting high temperature components (CAIs) into distal regions of the early solar nebula to be mixed with lower temperature components (*e.g.* Shu *et al.*, 1996). As magmatic iron meteorites are suggested to have formed in the terrestrial planet region (Bottke *et al.*, 2006), and have core segregation ages within 2 Ma of CAIs, it is not unlikely that they accreted materials previously subjected to Lyman-α radiation.

Trapping of photolytic product sulfur into chemical phases distinct from hydrogen sulfide would be required to preserve and transfer an anomalous $\Delta^{33}S$ signal to precursor materials for the magmatic iron meteorite parent bodies. The largest positive $\Delta^{33}S$ deviation (+0.161‰) in achondrite meteorites was recorded within the oldhamite (CaS) of the Norton Country aubrite (Rai *et al.*, 2005), and it may be the case that similar refractory sulfides could have acted as the early (transient) carriers of anomalous ^{33}S in iron meteorite parent bodies, condensing in hotter areas with greater amounts of gas (possibly closer to the Sun).

Studies of carbonaceous chondrites provide evidence for variable ^{33}S enrichments in some rare organic and mineral phases compared to the bulk sulfur in

chondrites (Cooper *et al.*, 1997; Rai and Thiemens, 2007; Gao and Thiemens, 1993a,b), which raises the possibility that the different materials accreting to form the iron meteorite parent bodies also possessed some variability in $\Delta^{33}S$.

5.3.1 Variable Preservation of a Homogeneously Distributed $\Delta^{33}S$ Carrier

While it is not clear whether similar precursor phases were present in the parent bodies of different magmatic iron meteorites, it could be possible that the variability observed in $\Delta^{33}S$ reflects the differential incorporation of an otherwise homogeneously-distributed precursor component, during the segregation of metal and sulfides on different parent bodies.

However, the IAB iron meteorites, which have been proposed to originate from separate impact-derived melt pools on a chondritic precursor in order to explain their very different compositions (Wasson and Kallemeyn, 2002), span a smaller range of $\Delta^{33}S$ values than the magmatic groups, which is the opposite of what would be expected if it was indeed the differential incorporation of anomalous but homogenously-distributed ^{33}S carriers in the parent bodies causing the observed variability in $\Delta^{33}S$ (as variable impact energies would have caused the differential volatilization of various sulfur-bearing minerals in different melt pools on the IAB parent body).

The Earth's mantle, lunar basalts, bulk chondrites, and IAB iron meteorites have $\Delta^{33}S$ values of ~0.00‰ (*Table 2*). If this composition does indeed represent the bulk solar system, then it would be difficult to explain the details of how different preservation or volatilization reactions on an otherwise homogenous starting

substance could lead to both the positive and negative $\Delta^{33}S$ values observed in our data set.

5.3.2 Photolytic Depletion of an Inner Solar System Reservoir

An attractive alternative for the $\Delta^{33}S$ variation among magmatic iron meteorite groups is through secular variation in the composition of an inner-solar system sulfur reservoir undergoing progressive photolysis (if it is indeed the age of metal-silicate segregation that is dated by the different $\varepsilon^{182}W$ compositions of the iron meteorite groups, and not deviations in their original Hf/W ratios).

The previously discussed Hf-W data suggest that core segregation of magmatic iron meteorite parent bodies occurred within the first two million years after CAI formation, earlier than the ages of most chondrules and several million years earlier than ages for the non-magmatic iron meteorite groups. A weakly defined decrease from slightly positive $\Delta^{33}S$ values to slightly negative $\Delta^{33}S$ values for magmatic iron groups with later Hf-W segregation ages appears to exist (*Fig.* 8), which allows for the possibility that the anomalous sulfur isotope signals evolved from a single reservoir, progressively distilled by photolysis during the early stages of the solar nebula.

A similar relationship between $\Delta^{33}S$ and ^{26}Al-^{26}Mg ages is revealed when one considers ^{26}Al-^{26}Mg (Kita *et al.*, 2003; Goodrich *et al.*, 2010) and $\Delta^{33}S$ (Farquhar *et al.*, 2000a; Rai *et al.*, 2005) data for different achondrite groups (ureilites, aubrites, and HED).

The proposed link between early inner solar system processes and $\Delta^{33}S$ may also be supported by recent dynamical modeling which suggests that the fastest

accretion rates occur where densities are highest, near the center of protoplanetary disks, and that iron meteorite parent bodies in our solar system formed in the terrestrial-planet region, before being displaced into the asteroid belt (Bottke *et al.*, 2006). More rapid accretion rates would lead to greater incorporation of short-lived heat-producing radionuclides, which would cause earlier magmatic differentiation in parent bodies with shorter orbital periods. This may in turn suggest that magmatic iron meteorites and achondrites (which underwent greater amounts of magmatic differentiation and have generally older ages than chondrites and IAB irons) formed earlier and closer to the sun than chondrites and undifferentiated meteorites.

The crude linear relationship observed between the $\Delta^{33}S$ of different iron meteorite groups and their Ni-normalized volatile element abundances is also consistent with this model. At shorter heliocentric distances there would be greater collisional rates (due to greater densities) and higher ambient temperatures, both of which could lead to volatile depletion[5].

A working model emerges that links the gas phase photolysis of hydrogen sulfide, possibly by Lyman α radiation occurring in the inner ~1 – 2 AU of the young solar nebula, to the evolution of mass-independent sulfur isotope signatures that were captured by early-forming planetesimals (*Fig.* 10). The non-magmatic iron parent bodies probably formed in more distal parts of the solar nebula, past the optical penetration depth of UV light and at lower temperatures, decreasing the availability of $H_2S_{(g)}$ (*Fig.* 10). The slower accretion rates and lower ambient temperatures at greater heliocentric distances would have led to lesser amounts of internal heating,

[5] However, It is uncertain whether the greater number of collisions at shorter heliocentric distances would lead to greater amounts of devolatilization compared to the different collisional energies of planetesimals with longer free-paths (at greater heliocentric distances).

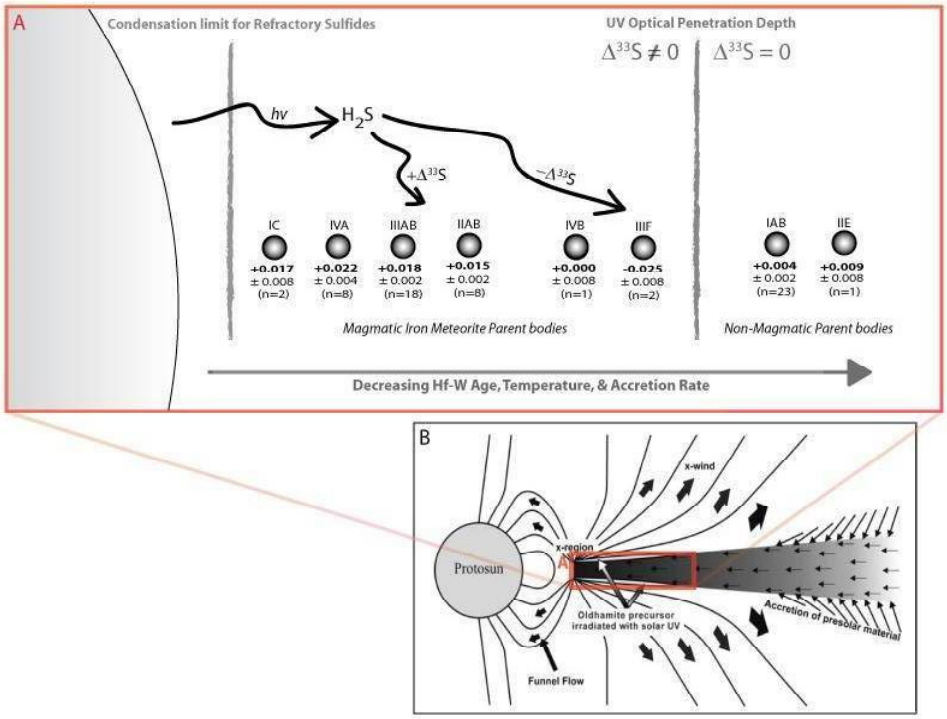

Fig. 10. Possible model for the early solar nebular generation of the sulfur isotopic distributions in magmatic and non-magmatic iron meteorites. In this working model, Hf-W age, temperature, and accretion rate roughly decrease to the right with increasing heliocentric distances (*e.g.* Bland and Ciesla, 2010, 2012; Bottke *et al.*, 2006). Irradiation of H_2S could lead to anomalous sulfur fractionations in the regions between the limit for refractory sulfide condensation and the penetration depth of UV light. The main magmatic iron meteorites form from this inner-solar system reservoir that is gradually distilled by photolysis, imparting a residual composition to late forming magmatic irons (IVB & IIIF). The IAB and IIE iron meteorites are suggested to have formed at greater heliocentric distances, later in time, past the penetration depth for UV light. Inset B is an expanded view of the solar nebula during T-Tauri phase showing the likely formational zone of the oldhamite precursor suggested by Rai *et al.* (2005) to have carried anomalous sulfur to achondrites.

later Hf-W segregation ages (>5 Ma after CAIs), and greater incorporation of volatile elements for the IAB iron meteorites.

The existence of an average inner solar system $\Delta^{33}S$ of ~0.00‰ (defined by chondrites, IABs, and the Earth-Moon system) that is intermediate between the ^{33}S-enriched and ^{33}S-depleted compositions of magmatic iron meteorites and achondrites may be a critical piece of information because it implies a process that either (1) remixed the sulfur pools during the formation of larger planetary embryos and planets in the terrestrial-planet region or (2) prevented the anomalous signatures from being produced in the region where the Earth was formed. The first scenario is considered here to be more likely because the iron meteorites are suggested to have come from the terrestrial-planet forming region, and the anomalous sulfur components identified within iron meteorites and achondrites were likely to have been re-homogenized or overwhelmed by isotopically normal (chondritic) sulfur during the accretion of the Earth.

Chapter 6: Conclusions

Our results show that the magmatic iron meteorite groups IC, IIAB, IIIAB, IIIF, & IVA, have resolvable variations in $\Delta^{33}S$ which are attributed to the inheritance of components sourced from the photolysis of H_2S in the early solar nebula. This is consistent with the hypothesis that these groups formed in proximity to the sun, near an optically-thin zone of the protoplanetary disk where photolysis could take place. Non-Magmatic iron meteorite groups, which do not have resolvable $\Delta^{33}S$ variations, are interpreted to have formed at greater heliocentric distances where anomalous $\Delta^{33}S$ materials were rare, being past the optical penetration depth of UV light and/or after the end of the Sun's T-Tauri phase, when its UV output was greatly reduced (Wolk *et al.*, 2005; Chakraborty *et al.*, 2013).

In summary, the work described in this thesis has shown that:

1. The sulfur isotopic composition of troilite in the different groups of iron meteorites analyzed covers only a very small range in $\delta^{34}S$, $\Delta^{33}S$, and $\Delta^{36}S$, which is consistent with previous studies (Hulston and Thode, 1965b; Gao and Thiemens, 1991).
2. There are newly-identified resolvable differences in the $\Delta^{33}S$ of troilite from different iron meteorite groups (ranging from -0.029‰ to +0.031‰), especially between the non-magmatic (IAB and IIE; average $\Delta^{33}S$ of +0.004‰) and magmatic groups [IC, IIAB, IIIAB, IVA, and IIIF (which tend to have enrichments or depletions on the order of ~0.020‰ relative to IAB)].
3. Generation of anomalous ^{33}S through cosmic-ray induced spallation reactions is ruled out as the cause of the observed $\Delta^{33}S$ variations based on the different

slope for $\Delta^{36}S/\Delta^{33}S$ and the consistent $\Delta^{33}S$ values observed for members within each group. Both known and hypothesized nucleosynthetic sulfur anomalies are also considered to be unlikely as the sources of the observed $\Delta^{33}S$, but are not fully ruled out.

4. The slope identified for $\Delta^{36}S/\Delta^{33}S$ (~ -7) for the major groups analyzed in this study (*excl.* IIIF) may be explained by experiments described by Chakraborty *et al.* (2013) for photolysis of H_2S by Lyman-α radiation (~ -3), given the small spread of our data and our uncertainties on $\Delta^{36}S$.
5. Published Hf-W ages appear to be weakly correlated with $\Delta^{33}S$ in magmatic iron meteorite groups, with $\Delta^{33}S$ gradually decreasing from positive (+0.022‰) to negative values (-0.028‰) in magmatic iron meteorites with later metal-silicate segregation ages.
6. Anomalous $\Delta^{33}S$ compositions in magmatic iron meteorite parent bodies were most likely inherited from components created through the photolysis of H_2S in the early solar nebula, while $\Delta^{33}S$ compositions in non-magmatic iron meteorite groups are chondritic and do not require this history.
7. A model in which the sulfur compositions of different magmatic iron meteorite parent bodies are inherited at different times/locations within an inner-solar system H_2S reservoir, gradually depleted by photolysis, is consistent with the observed $\Delta^{33}S$ variability within the different magmatic iron meteorite groups.
    a. This model is also consistent with dynamical models of early solar system formation where planetesimal accretion begins at short

heliocentric distances and progresses outwards (Bottke *et al.*, 2006), providing a potential synthesis between Hf-W, $\Delta^{33}S$, and volatile element data for different iron meteorite groups.

8. Non-magmatic iron meteorites have average $\Delta^{33}S$ values statistically indistinguishable from analyzed lunar basalts (-0.004‰) (*this study*; Wing and Farquhar, 2013) and from published values for Earth's mantle compiled from MORB glasses (+0.005‰) (Labidi *et al.*, 2012, *Thesis*).
    a. As the anomalous inner solar system sulfur reservoir from which the magmatic irons are thought to have derived is assumed to loosely coincide in space with the hypothesized formation distance of iron meteorites groups (1-2 AU; Bottke *et al.,* 2006) and the Earth-Moon system, it may be the case that larger planetary embryos and planets both re-homogenized the anomalous $\Delta^{33}S$ signals and drowned them out through the incorporation of isotopically normal (chondritic/IAB) sulfur from greater heliocentric distances.
9. Variability in the $\delta^{34}S$ of magmatic iron meteorites (ranging from -1.41‰ to +1.29‰) does not appear to be related to any other geochemical parameters considered in this study, but does appear to have a weak correlation with volatile elements within different IAB group iron meteorites (*Appendix H*), increasing with decreasing volatile contents as a possible result of impact processes on the parent body.

6.1 Future Work

Based on the work presented in this thesis, several questions and uncertainties lead to a multitude of directions for future work. The most prevalent questions and ideas for future work are summarized as follows:

1. The relationship observed between different age proxies (Hf-W & Al-Mg) and $\Delta^{33}S$ in iron meteorites and achondrites may support a model invoking the secular evolution of an inner solar system sulfur reservoir, however, the resolution of most published age measurements is not currently sufficient to decipher any detailed relationships between age and sulfur isotopic composition. Therefore, the current investigation would be greatly benefitted by refined age proxies, along with greater numbers of sulfur analyses from meteorite groups (with different ages) that have not been previously measured, such as pallasites, angrites, and brachinites.
2. Specifically regarding iron meteorite analyses, it would be especially useful to measure more members from groups IIE, IIIF, and IVB, to confirm whether or not the few members which were analyzed from each group truly represent the sulfur isotopic compositions of each whole group. Interestingly, IID irons have elemental composition close to group IIIF and may yield interesting sulfur isotopic results if measured, while other minor magmatic iron meteorite groups still remain to be analyzed in order to complete the full set of sulfur isotope measurements in iron meteorites.
3. A major setback in the definition of a precise $\Delta^{36}S/\Delta^{33}S$ slope for the data in this thesis is due to the lower precision of mass spectrometric measurements

of ^{36}S relative to ^{33}S. This is mostly due to low abundances of ^{36}S and isobaric interferences from $C_3F_5^+$, which may be resolved through modifications to the mass spectrometer (removal of additional inlets or possible addition of an electron multiplier), higher mass resolution, or through repeated gas chromatography (GC) runs.

4. The sulfur isotopic compositions produced during the photolysis of different gases at various conditions relevant to the early solar nebula still remains poorly understood. Although H_2S was likely to be the most abundant sulfur-bearing gas in the early solar nebula, and the recent experimental photolysis results of Chakraborty *et al.* (2013) provide reasonable agreement with the iron meteorite data, SiS has been predicted to be the main sulfur-bearing gas in reducing regions of the early solar nebula (with C/O > 0.95) at temperatures above 900 K (Pasek *et al.*, 2005). In addition to SiS, gases such as HS, S, PS, S_2, and AlS, are also predicted to have existed in reducing areas of the early solar nebula, and despite the difficulty of high-temperature photolysis experiments, they are the only way to test the effects of photolysis on these exotic sulfur-bearing gases, which is a necessary stepping-stone in the understanding of multiple sulfur isotope behaviors in the early solar nebula.
5. Further constraints on the capture cross sections of sulfur, relevant to spallation reactions and neutron capture reactions (although not thought to have created the anomalous sulfur signatures contained in the analyzed samples), could lead to the development of important cosmic-ray exposure

corrections on future sulfur isotopic measurements in meteoritic materials, and could be refined through greater amounts of experimental work and modeling.

6. Sulfur isotope fractionation during the evaporation of troilite in the early solar nebula was experimentally reproduced by McEwing *et al.* (1980), however, they did not measure the minor isotopes of sulfur. Assuming the $\Delta^{33}S$ compositions to be mass-dependent, modeled $\Delta^{33}S$ variations due to Rayleigh fractionation only produced $\Delta^{33}S$ signatures of up to +0.010‰ (*Appendix E*). However, the actual minor isotope measurements of this process may reveal fractionation factors different from those assumed, and lead to greater variations in $\Delta^{33}S$. Therefore, a more extensive investigation into sulfur isotope fractionation during the evaporation of troilite would be of great assistance in evaluating Rayleigh fractionation as a possible source of $\Delta^{33}S$ in early solar system materials.
7. To the author's knowledge, there are no sulfur isotopic measurements of CAIs, which is likely due to their very low concentrations of primary sulfur, but may perhaps be accomplished by using a technique such as SIMS. CAIs are generally thought to be the earliest formed solids in the solar system, condensing at high temperatures in regions proximal to the early sun, therefore, the working model described in this thesis predicts that they would have anomalous sulfur isotopic compositions. Therefore, measurements of $\Delta^{33}S$ and $\Delta^{36}S$ in CAIs may help constrain the proposed model for sulfur isotopic distribution and evolution in the early solar nebula.

8. The most enriched $\Delta^{33}S$ material found so far in achondrites is the oldhamite (CaS) from the Norton County aubrite (Rai *et al.*, 2005), but no similarly enriched oldhamite has been investigated within other meteorites. Interestingly, enstatite chondrites were not observed to have $\Delta^{33}S$ anomalies in previous investigations (Gao and Thiemens, 1993b), but this could possibly be due to limitations in the available resolution of isotopic measurements at the time of the study. Regardless, mineralogical separation of the different components in different achondrites (and chondrites) could potentially lead to the identification of the ^{33}S-carrier phase(s) that was likely to have transferred the different anomalous signals into the different magmatic iron and achondrite parent bodies.
9. An interesting possibility that has not been discussed in this paper is that of a solar $\Delta^{33}S$ composition differing from that of the planets, as has been demonstrated for oxygen isotopes (McKeegan *et al.,* 2011). In this case, the $\Delta^{33}S$ in achondrites and magmatic irons could represent greater amounts of contamination from a solar sulfur source. However, the case for sulfur may not be as simple as the case of oxygen isotopes, the data for which lie on a line of approximately slope-1 (consistent with addition of ^{16}O) on triple oxygen isotope plots (*e.g.* Clayton, 1993). The evaluation of this hypothesis could be accomplished through analyses of multiple sulfur isotopes in samples of the solar wind, using a technique such as SIMS.
10. The question regarding whether or not the anomalous sulfur isotopic signals in the presolar nebula were inherited from earlier galactic cosmic-ray photolysis

in the pre-existing molecular cloud from which the sun (and solar system) was derived (*i.e.* carbon-monoxide in Lyons and Young, 2005), or whether it was created within the solar system itself by solar radiation around the young sun, as is proposed in this thesis, may be addressed through refined spectroscopic techniques for measuring sulfur isotope ratios in other nebulae and molecular clouds. The model proposed in this thesis predicts that anomalous sulfur compositions should exist in the disks around young stars in other planetary systems. However, a successful deconvolution of the spectral bands for different isotopologues of H_2S is required in order to accurately make these measurements.

11. Finally, new models for the chemical evolution of H_2S and iron grains in a dynamical protoplanetary disk now include particle-tracking methods (Ciesla, 2013), and suggest that H_2S concentrations were highest in the innermost <1 AU of the early solar system, decreasing with time. A few modifications to this model (including optical thicknesses and solar UV outputs with respect to time) might allow one to predict the formation region(s) for anomalous sulfur in the early solar nebula, along with the possible migration-paths and final resting places of particles which gained their sulfur from within these regions.

Appendix A

a) Sulfur Extraction yields

Name	Class	Mass	Ideal Yield	AVS yield	CRS yield	Percent yield (AVS)	CRS/AVS	Ref
Bischtube	IAB	16.2	45.4	32.3	0.600	71.1	0.019	.MP2011
Bogou	IAB	6.7	18.8	15.8		84.0	0.000	.MP2011
Mesa Verde Park	IAB	6.5	18.2	17.3		94.8	0.000	.MP2011
Mundrabilla	IAB							.MP2011
Pitts	IAB	12.5	35.0	20.7	0.770	59.2	0.037	.MP2011
Woodbine	IAB	8.2	23.0	11.5	0.790	49.9	0.069	.MP2011
DRPA78009,8	IIAB	16.0	44.8	37.0		82.6	0.000	.MP2011
Acuna	IIIAB	8.4	23.5	26.0	1.770	110.7	0.068	.MP2011
Grant	IIIAB	8.0	22.4	16.3		72.8	0.000	.MP2011
Sacramanto Mtns	IIIAB							.MP2011
Trenton	IIIAB	12.5	35.0	31.2		89.1	0.000	.MP2011
Altonah	IVA	6.6	18.5	12.3	2.490	66.7	0.202	.MP2011
Duchesne	IVA	9.5	26.6	26.6		99.9	0.000	.MP2011
Gibeon	IVA							.MP2011
S.J. Nepomuceno	IVA	5.5	15.4	3.2		20.9	0.000	.MP2011
ALH77290	IAB-MG	18.135	50.8	39.013	0.000	76.8	0.000	MAA
Burkett	IAB-MG	13.237	37.1	30.460		82.2	0.000	MAA
Campo Del Cielo	IAB-MG	16.3		6.963			0.000	MAA
Campo Del Cielo	IAB-MG	10.3	28.8	2.545	0.020	8.8	0.008	MAA
Canyon diablo (FM)	IAB-MG	10.256	28.7	25.870		90.1	0.000	MAA
Deelfontain	IAB-MG	11.565	32.4	9.597		29.6	0.000	MAA
Goose Lake	IAB-sLL	9.2		21.624			0.000	MAA
Goose Lake	IAB-sLL	8.6	24.0	20.290	0.345	84.7	0.017	MAA
Hope	IAB-MG	7.945	22.2	18.003	0.826	80.9	0.046	MAA
Idaho	IAB-MG	19.765	55.3	29.594		53.5	0.000	MAA
Lamesa, Texas	IAB-sLM	18.884	52.9	45.812		86.6	0.000	MAA
Malta Hohe	IAB-sLM	21.899	61.3	50.472	1.102	82.3	0.022	MAA
Mertzon	IAB	9.1		16.181			0.000	MAA
Mertzon	IAB	6.6	18.6	14.302	0.599	77.1	0.042	MAA
Mesa Verde Park	IAB		0.0					MAA
Mundrabilla	IAB		0.0					MAA
Mudrabilla-2 (WAM)	IAB	18.404	51.5	46.811		90.8	0.000	MAA
Osseo	IAB	14.774	41.4	33.521		81.0	0.000	MAA
Pitts	IAB		0.0					MAA
Toluca	IAB-sLL	20.317	56.9	39.250	0.101	69.0	0.003	MAA
Waterville	IAB	18.276	51.2	15.106	0.000	29.5	0.000	MAA
Wichita County	IAB-MG	10.597	29.7	22.097	1.185	74.5	0.054	MAA

Woodbine-re	IAB	16.679	46.7	34.485	1.694	73.8	0.049	MAA
Santa Rosa	IC	16.964	47.5	36.562	4.049	77.0	0.111	MAA
Santa rosa-2 (FM)	IC	5.306	14.9	12.128		81.6	0.000	MAA
Calico Rock	IIAB	9.824	27.5	25.470		92.6	0.000	MAA
DRPA 78008/10	IIAB		0.0					MAA
DRPA 78009	IIAB	9.563	26.8	23.015		86.0	0.000	MAA
Indian Valley	IIAB	11.113	31.1	6.067		19.5	0.000	MAA
Keen Mountain	IIAB	12.136	34.0	19.511		57.4	0.000	MAA
Mayodan	IIAB	15.329	42.9	15.562		36.3	0.000	MAA
North Chile	IIAB	8.72	24.4	20.729	0.190	84.9	0.009	MAA
Old Woman	IIAB	10.163	28.5	9.093	0.000	32.0	0.000	MAA
Patos de Minas (hex)	IIAB	8.9		17.821			0.000	MAA
Patos de Minas (hex)	IIAB	5.8	16.1	13.691		84.8	0.000	MAA
Watson	IIE	17.691	49.5	18.529	0.000	37.4	0.000	MAA
Acuna	IIIAB		0.0					MAA
Apoala (FM)	IIIAB	7.178	20.1	4.553		22.7	0.000	MAA
Apoala-2 (FM)	IIIAB	15.086	42.2	27.673	3.683	65.5	0.133	MAA
Cape York	IIIAB	12.13	34.0	31.024	0.000	91.3	0.000	MAA
Casas Grandes	IIIAB	12.275	34.4	28.072	0.000	81.7	0.000	MAA
Costilla Peak (FM)	IIIAB	10.072	28.2	23.859	1.055	84.6	0.044	MAA
Djebel In Azzene	IIIAB	10.17	28.5	20.712		72.7	0.000	MAA
Drum Mountains	IIIAB	9.677	27.1	0.0		0.0		MAA
Kenton County	IIIAB	8.894	24.9	17.869		71.8	0.000	MAA
La Porte	IIIAB	8.916	25.0	16.228	0.000	65.0	0.000	MAA
Loreto	IIIAB	13.938	39.0	29.271		75.0	0.000	MAA
MET0040	IIIAB	8.076	22.6	6.865		30.4	0.000	MAA
Thule	IIIAB	7.519	21.1	16.985		80.7	0.000	MAA
Tieraco Creek	IIIAB	12.402	34.7	11.829		34.1	0.000	MAA
Trenton	IIIAB		0.0					MAA
Wabar	IIIAB	2.005	5.6	2.453		43.7	0.000	MAA
Waingaromia	IIIAB	16.961	47.5	39.049		82.2	0.000	MAA
Wonnyulgunna	IIIAB	11.039	30.9	25.085		81.2	0.000	MAA
Cerro del inca	IIIF	14.279	40.0	33.666	0.665	84.2	0.020	MAA
Bushman Land	IVA	13.798	38.6	2.199		5.7	0.000	MAA
Harriman	IVA	4.027	11.3	8.732		77.4	0.000	MAA
Huizopa	IVA	17.814	49.9	34.138	1.465	68.4	0.043	MAA
Maria Elena	IVA	7.074	19.8	5.631		28.4	0.000	MAA
Mart	IVA	4.506	12.6	0.776		6.2	0.000	MAA
S.J. Nepomuceno-re	IVA	15.035	42.1	20.883	0.760	49.6	0.036	MAA
Hoba	IVB	7.88	22.1	16.774		76.0	0.000	MAA

Appendix B

b) Percent ideal yields vs. Sulfur isotopic Composition

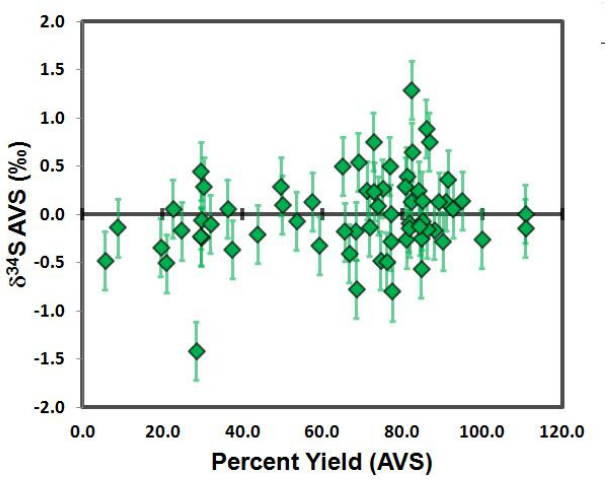

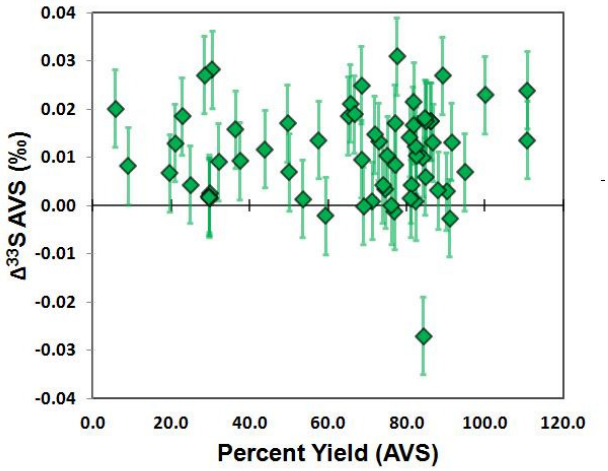

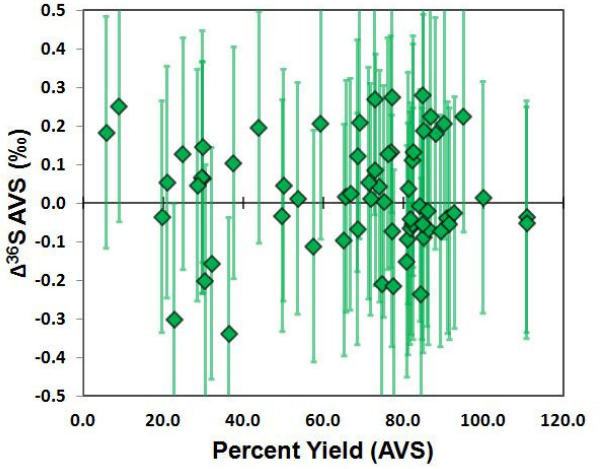

Appendix C

c) $\Delta^{33}S$ from mixing most enriched and depleted troilite found in meteorites

$\delta^{34}S$	Calculated $\delta^{33}S$	$\delta^{33}S$ of mixing line	$\Delta^{33}S$
8.000	**4.112**	**4.112**	**0.0000**
7.000	3.599	3.597	0.0019
6.000	3.086	3.082	0.0035
5.000	2.572	2.567	0.0049
4.000	2.058	2.052	0.0060
3.000	1.544	1.537	0.0069
2.000	1.030	1.022	0.0075
1.000	0.515	0.507	0.0079
0.000	**0.000**	**-0.008**	**0.0080**
-1.000	-0.515	-0.523	0.0079
-2.000	-1.031	-1.038	0.0075
-3.000	-1.546	-1.553	0.0069
-4.000	-2.062	-2.068	0.0060
-5.000	-2.578	-2.583	0.0049
-6.000	-3.095	-3.098	0.0035
-7.000	-3.611	-3.613	0.0019
-8.000	**-4.128**	**-4.128**	**0.0000**

Appendix D

d) Exponent differences in $\Delta^{33}S$ values

$\delta^{34}S$	$\delta^{33}S$ exp = 0.512	$\delta^{33}S$ exp = 0.518	$\delta^{33}S$ exp = 0.515	$\Delta^{33}S$ exp = 0.512	$\Delta^{33}S$ exp = 0.518
-1.2	-0.6146	-0.6218	-0.6182	0.0036	-0.0036
-1.1	-0.5634	-0.5700	-0.5667	0.0033	-0.0033
-1	-0.5121	-0.5181	-0.5151	0.0030	-0.0030
-0.9	-0.4609	-0.4663	-0.4636	0.0027	-0.0027
-0.8	-0.4097	-0.4145	-0.4121	0.0024	-0.0024
-0.7	-0.3585	-0.3627	-0.3606	0.0021	-0.0021
-0.6	-0.3072	-0.3108	-0.3090	0.0018	-0.0018
-0.5	-0.2560	-0.2590	-0.2575	0.0015	-0.0015
-0.4	-0.2048	-0.2072	-0.2060	0.0012	-0.0012
-0.3	-0.1536	-0.1554	-0.1545	0.0009	-0.0009
-0.2	-0.1024	-0.1036	-0.1030	0.0006	-0.0006
-0.1	-0.0512	-0.0518	-0.0515	0.0003	-0.0003
0	**0.0000**	**0.0000**	**0.0000**	**0.0000**	**0.0000**
0.1	0.0512	0.0518	0.0515	-0.0003	0.0003
0.2	0.1024	0.1036	0.1030	-0.0006	0.0006
0.3	0.1536	0.1554	0.1545	-0.0009	0.0009
0.4	0.2048	0.2072	0.2060	-0.0012	0.0012
0.5	0.2560	0.2590	0.2575	-0.0015	0.0015
0.6	0.3072	0.3108	0.3090	-0.0018	0.0018
0.7	0.3583	0.3625	0.3604	-0.0021	0.0021
0.8	0.4095	0.4143	0.4119	-0.0024	0.0024
0.9	0.4607	0.4661	0.4634	-0.0027	0.0027
1	0.5119	0.5179	0.5149	-0.0030	0.0030
1.1	0.5630	0.5696	0.5663	-0.0033	0.0033
1.2	0.6142	0.6214	0.6178	-0.0036	0.0036

Appendix E

e) $\Delta^{33}S$ from Mixing of Rayleigh Fractionation Pools during Troilite Evaporation

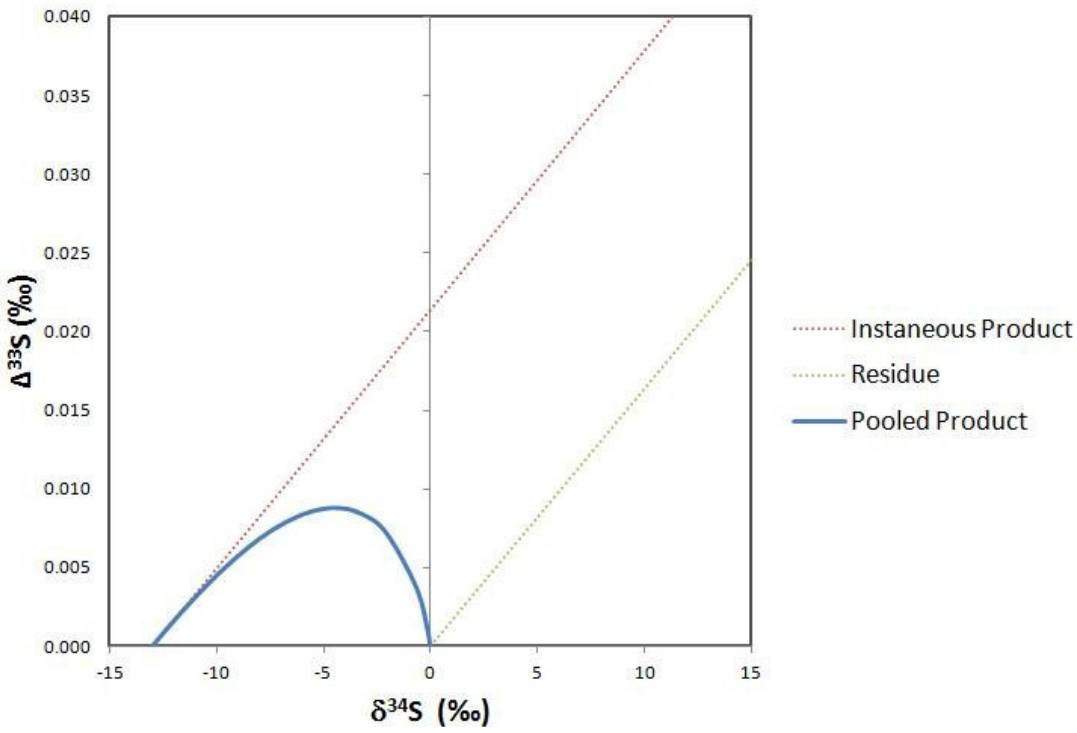

Appendix F

f) Sulfur isotope relationships among different groupings of Irons

i) All data excluding IIIF

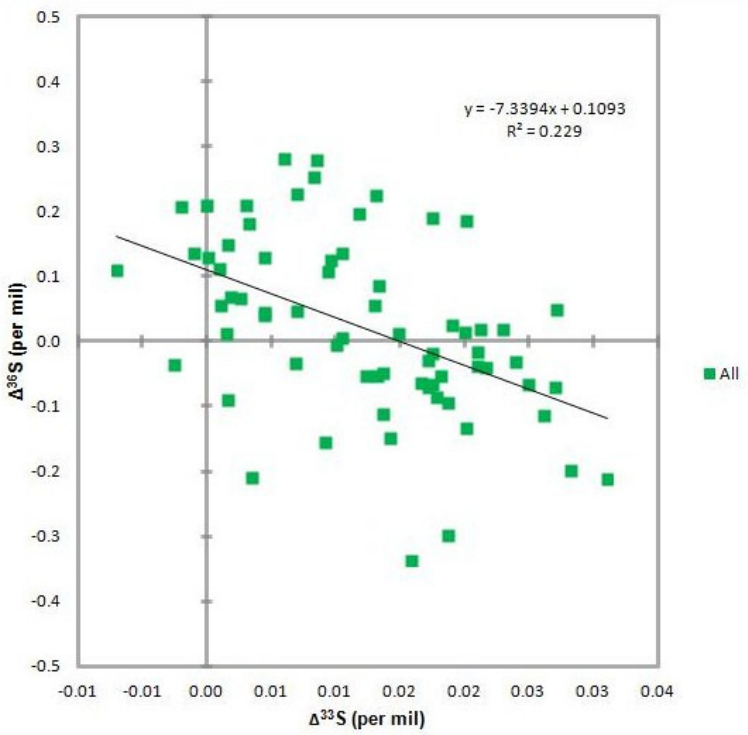

ii) All Data

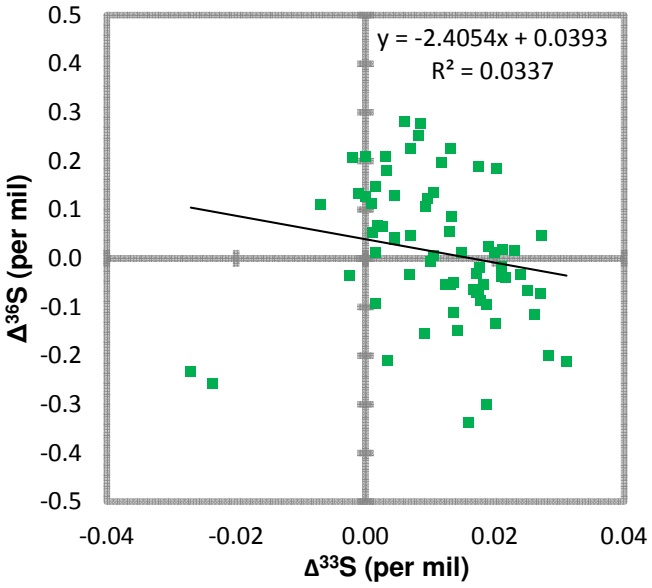

iii) All Magmatic Irons

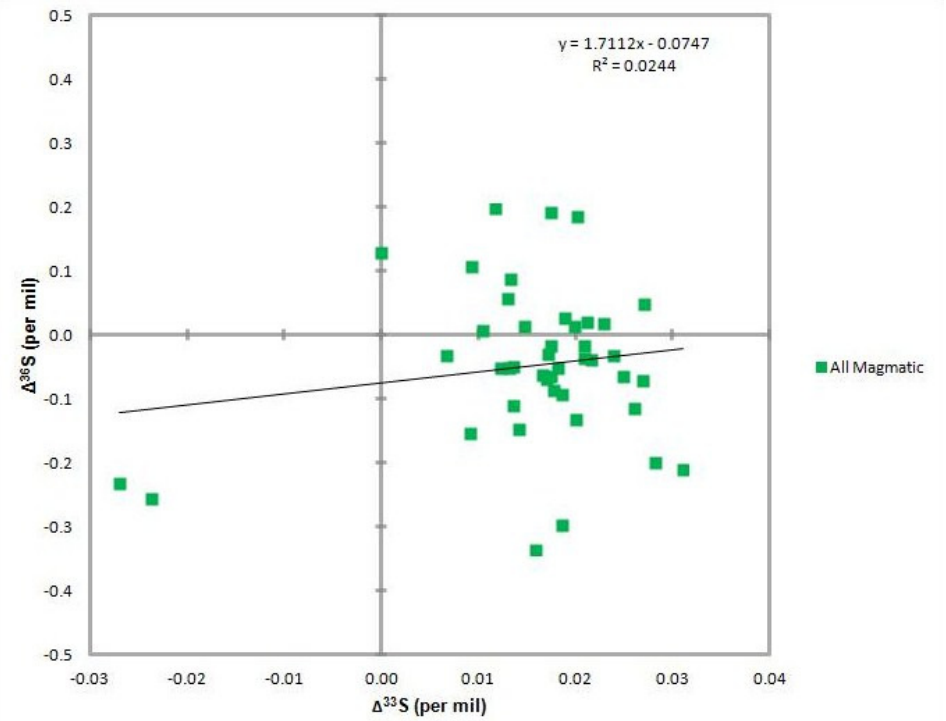

iv) All magmatic irons excluding IIIF

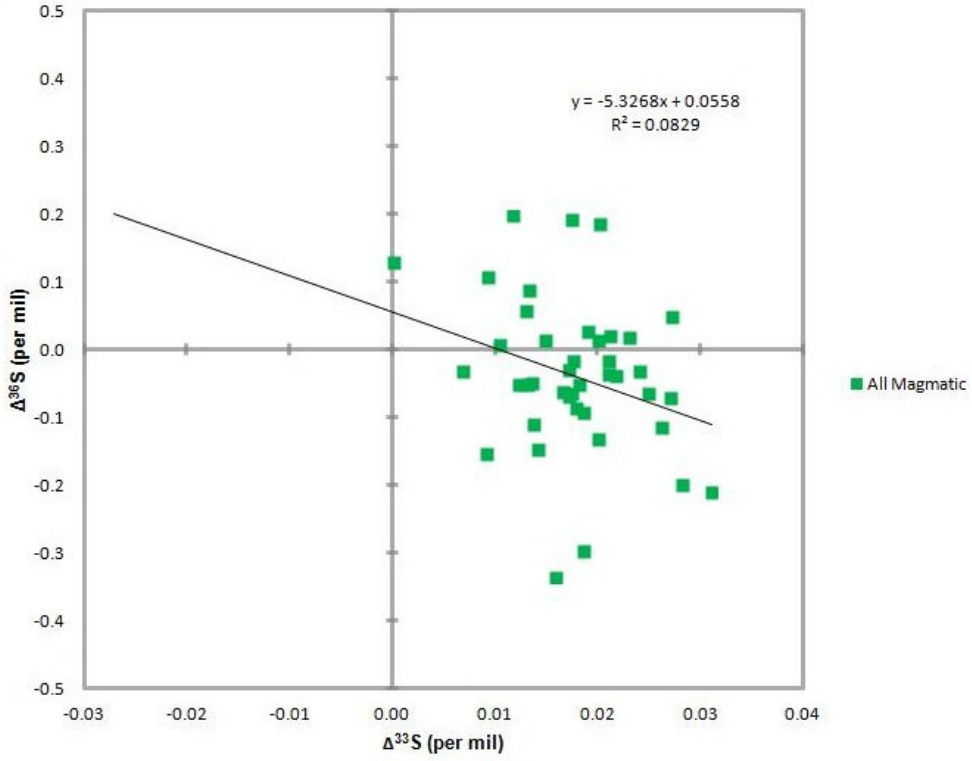

Appendix G

g) Modeled Nucleosynthetic injection of ^{32}S

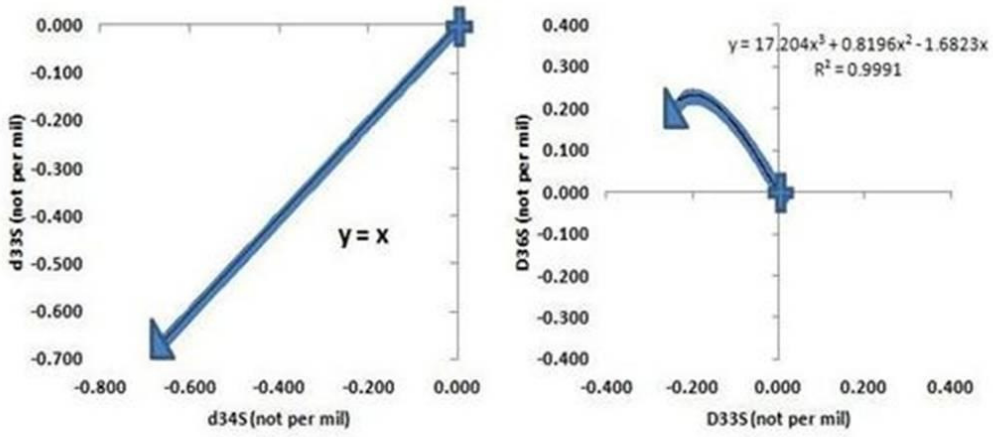

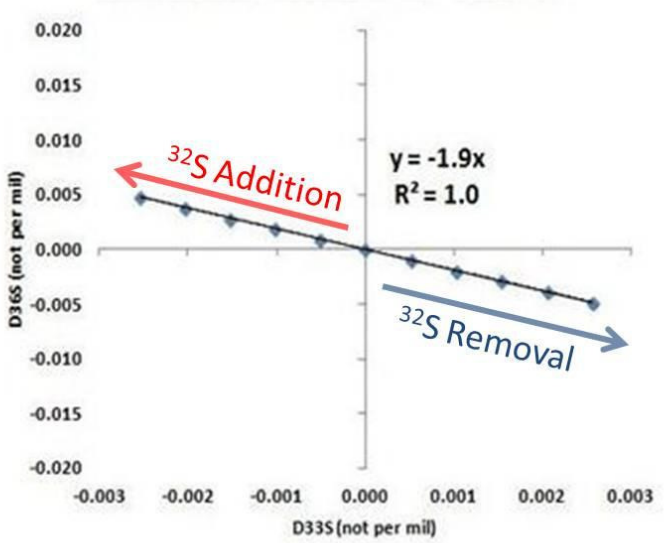

Appendix H

h) $\delta^{34}S$ relationships with Ni, Ge, and Ga (regressions of only IAB irons)

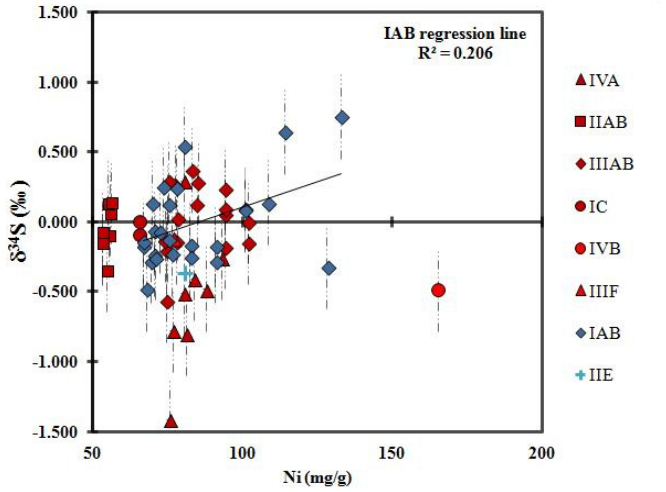

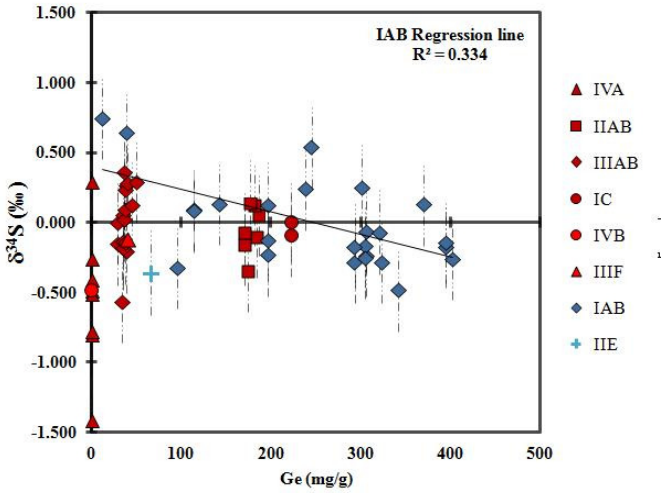

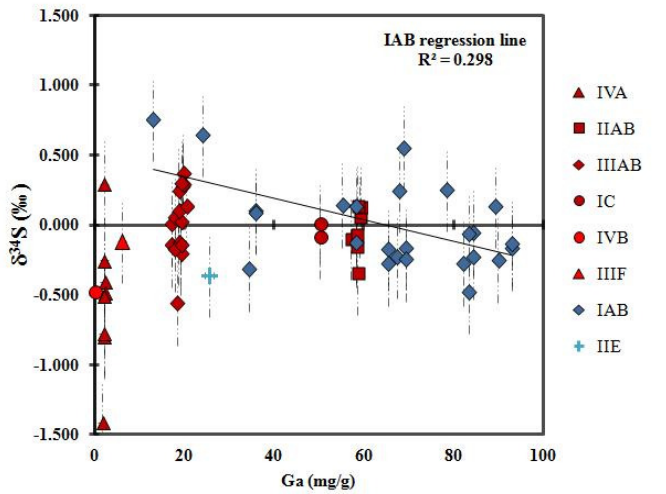

Appendix I

i) $\Delta^{33}S$ relationships with Ge, and Ga (no relationship for IAB groups)

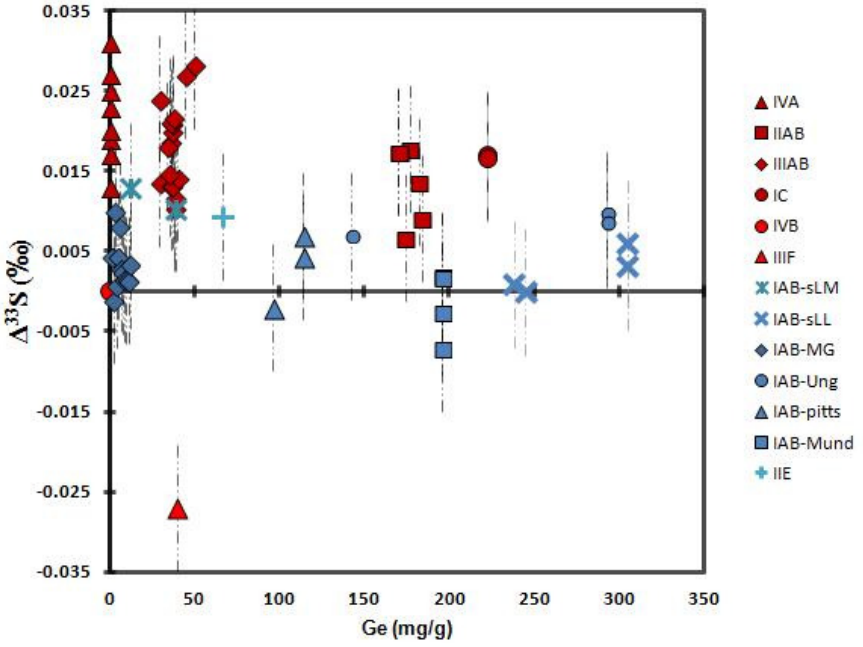

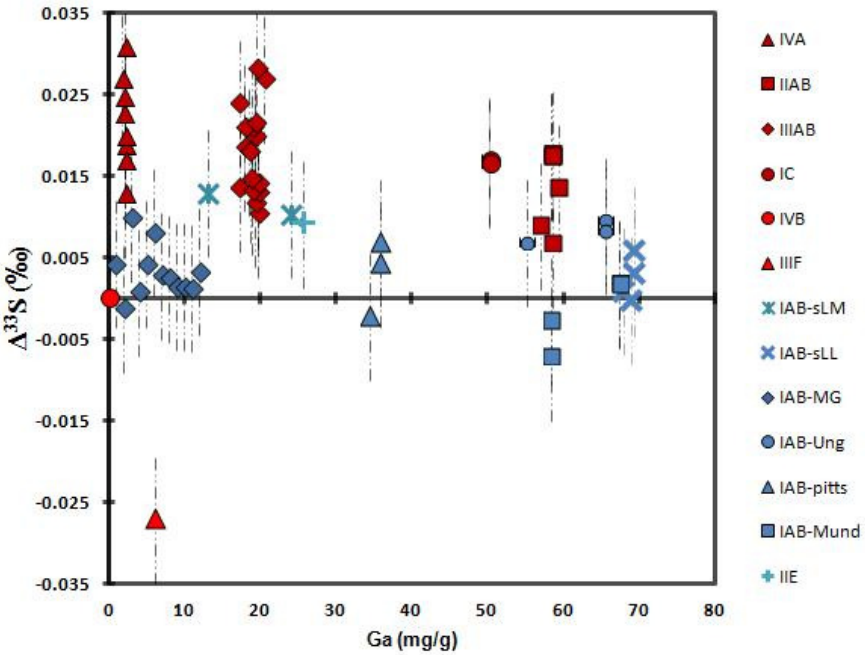

Bibliography

Amelin, Y., Krot, A.N., Hutcheon, I.D., Ulyanov, A.A. (2002). "Lead isotopic ages of chondrules and calcium-aluminum-rich inclusions" *Science, vol. 297*, pp. 1678-1683.

Antonelli, M.A., Peters, M., Farquhar, J. (2013). "Multiple Sulfur Isotopes in Iron Meteorites: Implications for Nebular Evolution." *44th Lunar and Planetary Science Conference*, #1279. The Lunar and Planetary Institute, Houston.

Antonelli, M.A., Peters, M., Farquhar, J. (2012). "Sulfur isotopic compositions of magmatic and non-magmatic iron meteorites." *43rd Lunar and Planetary Science Conference*, #2081. The Lunar and Planetary Institute, Houston.

Ault, W.U. and Jensen, M.L. (1962). "Summary of sulfur isotopic standards." Biogeochemistry of sulfur isotopes (Ed. M.L. Jensen), *Symposium of N.S.F* Yale University.

Beaudoin, G., Taylor, B.E., Rumble III, D., Thiemens, M.H. (1994). "Variations in the sulfur isotope composition of troilite from the Cañon Diablo iron meteorite." *Geochimica et Cosmochimica Acta, vol. 58*, pp. 4253-4255.

Benedix, G. K., Lauretta, D. S., McCoy, T.J. (2005). "Thermodynamic constraints on the formation conditions of winonaites and silicate-bearing IAB irons." *Geochimica et Cosmochimica Acta 69 (21)*, pp. 5123-5131.

Benedix, G. K., McCoy, T.J., Keil, K., Love, S.G. (2000). "A petrologic study of the IAB iron meteorites: Constraints on the formation of the IAB-Winonaite parent body." *Meteoritics & Planetary Science 35(6)*, pp. 1127-1141.

Bigeleisen, J. (1996). "Nuclear size and shape effects in chemical reactions. Isotope chemistry of the heavy elements." *Journal of the American Chemical Society vol. 188*, pp. 3676.

Bigeleisen, J. (1952). "The effects of isotopic substitution on the rates of chemical reactions." *Journal of Physical Chemistry 56(7)*, pp. 823-828.

Bland, P.A. and Ciesla, F.J. (2010) "The impact of nebular evolution on volatile depletion trends observed in differentiated objects." *41st Lunar and Planetary Science Conference,* #1817. The Lunar and Planetary Institute, Houston.

Bland, P.A. and Ciesla F.J. (2012) "Nebular Evolution and Volatile Depletion in the Inner Solar System." *75th Annual Meteoritical Society Meeting*, #5188.

Blichert-Toft, J., Moynier, F., Lee, C-.T.A, Telouk, P., Albarede, F. (2010). "The

early formation of the IVA iron meteorite parent body." *Earth and Planetary Science Letters 296*, pp. 469-480.

Bogard, D.D., Garrison, D.H., Takeda, H. (2005). "Ar-Ar and I-Xe ages and the thermal history of IAB meteorites." *Meteoritics and Planetary Science 40*, pp. 207-224.

Bottke, W.F., Nesvomy, D., Grimm, R.E., Morbidelli,A., O'Brien. D.P. (2006). "Iron meteorites as remnants of planetesimals formed in the terrestrial planet region." *Nature vol. 439*, pp. 821-824.

Bottke W. F., Durda D. D., Nesvorny´ D., Jedicke R., Morbidelli, A., Vokrouhlicky´ D. and Levison H. F. (2005). "Linking the collisional history of the main asteroid belt to its dynamical excitation and depletion." *Icarus 179*, pp. 63–94.

Buchwald, V.F. (1975). "The Handbook of Iron Meteorites vol. 1 - 3." Edited by G. Boyd, *University of California Press*, Berkeley and Los Angeles, California.

Bullock, E.S., McKeegan, K.D., Gounelle, M., Grady, M.M., Russel, S.S. (2010). "Sulfur isotopic composition of Fe-Ni sulfide grains in CI and CM carbonaceous chondrites." *Meteoritics and Planetary Science 45, n. 5*, pp. 885-898.

Cameron, A. G. W. (1979). "Neutron-Rich Silicon-Burning and Equilibrium Processes of Nucleosynthesis." *Astrophysical Journal 230(1):* L53-L57.

Campbell, A. J. and M. Humayun (2005). "Compositions of group IVB iron meteorites and their parent melt." *Geochimica et Cosmochimica Acta 69(19),* pp. 4733-4744.

Canfield, D.E., Raiswell, R., Westrich, J.T., Reaves, C.M., Berner, R.A. (1986). "The use of chromium reduction in the analysis of reduced inorganic sulfur in sediments and shales." *Chemical Geology*, 54, pp. 149-155.

Chabot, N. L. (2004). "Sulfur contents of the parental metallic cores of magmatic iron meteorites." *Geochimica et Cosmochimica Acta 68(17),* pp. 3607-3618.

Chakraborty, S., Jackson, T.L., Ahmed, M., Thiemens, M.H. (2013) "Sulfur Isotopic Fractionation in Vacuum UV photodissociation of hydrogen sulfide and its potential relevance to meteorite analysis." *Proceedings of the National Academy of Sciences*, *Special Edition.*

Chin, Y.N., Henkel, C., Whiteoak, J.B., Langer, N., Churchwell,, E.B. (1996). "Interstellar sulfur isotopes and stellar oxygen burning." *Astron. Astrophys. 305*, pp. 960-969.

Ciesla, F.J. (2013) “Sulfidization of iron in a dynamic solar nebula and the implications for planetary compositions.” *44th Lunar and Planetary Science Conference*, #1315. The Lunar and Planetary Institute, Houston.

Clayton, D. D. and S. Ramadurai (1977). "Pre-Solar Meteoritic Sulfides.” *Nature 265 (5593)*, pp. 427-428.

Clayton, R.N. “Oxygen isotopes in the Solar System.” (2003) *Space Science Reviews 106*, pp. 19-32. Kluwer Academic Publishers.

Clayton, R.N. and Mayeda, T.K. (1996). “Oxygen isotope studies of achondrites”. *Geochimica et Cosmochimica Acta, vol. 60*, no. 11, pp. 1999-2017.

Clayton, R. N. (1993). "Oxygen Isotopes in Meteorites.” *Annual Review of Earth and Planetary Sciences 21*, pp. 115-149.

Clayton, R. N., T. K. Mayeda, *et al.* (1983). "Oxygen Isotope Relationships in Iron-Meteorites.” *Earth and Planetary Science Letters 65(2),* pp. 229-232.

Cobb, J.C., (1966). “Iron meteorites with low cosmic-ray exposure ages.” *Science, vol. 151, no. 3717*, p. 1524

Colman, J.J., Xu, X., Thiemens, M.H., Trogler, W.C. (1996). “Photopolymerization and mass-independent sulfur isotope fractionations in carbon disulfide.” *Science, vol. 273, no. 5276*, pp. 774-776.

Cooper, G.W., Thiemens, M.H., Jackson, T.L., Chang, S. (1997). “Sulfur and hydrogen isotope anomalies in meteorite sulfonic acids.” *Science, vol. 277*, pp. 1072-1074.

Danielache, S.O., Hattori, S., Johnson, M.S., Ueno, Y., Nanbu, S., Yoshida, N. (2012) “Photoabsorption cross-section measurements of ^{32}S, ^{33}S, ^{34}S, and ^{36}S sulfur dioxide for the B^1B_1-X^1A_1 absorption band” *Journal of Geophysical Research 117,* D24301, doi:10.1029/2012JD017464.

Eugster, O., Herzog, G.F., Marti, K., Caffee, M.W. (2006). “Irradiation records, cosmic-ray exposure ages, and transfer times of meteorites.” *Meteorites and the Early Solar System II*, pp. 829-851.

Farquhar, J., Johnston, D.T., Wing, B.A. (2007). “Implications of conservation of mass effects on mass-dependent isotope fractionations: influence of network structure on sulfur isotope phase space of dissimilatory sulfate reduction.” *Geochimica et Cosmochimica Acta 71*, pp. 5862-5875.

Farquhar, J., Savarino, J., Airieau, S., Thiemens, M.H. (2001). “Observation of wavelength-sensitive mass-independent sulfur isotope effects during SO_2

photolysis: Implications for the early atmosphere. *Journal of Geophysical Research 106*, pp. 32829–32839.

Farquhar, J., Jackson, T.L., Thiemens, M.H. (2000a). "A ^{33}S enrichment in ureilite meteorites: Evidence for a nebular sulfur component." *Geochimica et Cosmochimica Acta vol. 64*, *no. 10*, pp. 1819-1825.

Farquhar, J., Savarino, J., Jackson, T.L., Thiemens, M.H., (2000b). "Evidence of atmospheric sulphur in the martian regolith from sulphur isotopes in meteorites. *Nature 404,* pp. 50–52.

Forrest, J. and Newman L. (1977). "Silver-110 microgram sulfate analysis for the short time resolution of ambient levels of sulfur aerosol." Analyical Chemistry, 49 pp. 1579–1584.

Gao, X. and M. H. Thiemens (1993a). "Isotopic Composition and Concentration of Sulfur in Carbonaceous Chondrites." *Geochimica Et Cosmochimica Acta 57(13)*, pp. 3159-3169.

Gao, X. and M. H. Thiemens (1993b). "Variations of the Isotopic Composition of Sulfur in Enstatite and Ordinary Chondrites." *Geochimica Et Cosmochimica Acta 57(13),* pp. 3171-3176.

Gao, X.. and M. H. Thiemens (1991). "Systematic Study of Sulfur Isotopic Composition in Iron-Meteorites and the Occurrence of Excess ^{33}S and ^{36}S." *Geochimica Et Cosmochimica Acta 55(9)*, pp. 2671-2679.

Goodrich C.A., Hutcheon, I.D., Kita, N.T., Huss, G.R., Cohen, B.A., Keil, K. (2010). "^{53}Mn-^{53}Cr and ^{26}Al-^{26}Mg ages of a feldspathic lithology in polymict ureilites." *Earth and Planetary Science Letters, 295*, 531-540.

Greenwood, R.C., Franchi, I.A., Jambon, A., Barrat, J.A., Burbine, T.H. (2006) "Oxygen isotope variation in stony-iron meteorites." *Science 313*, pp. 1763-1765.

Haack, H. and T. J. McCoy (2006). "Iron and stony-iron meteorites." *Treatise on Geochemistry.* United Kingdom, Elsevier : Oxford, United Kingdom. 1: 325-345.Herzog, G.F.,Gibson, E.K. Jr.,

Heck, P.R., Hoppe, P., Huth, J. (2012). "Sulfur four isotope NanoSIMS analysis of comet 81p/wild 2 dust in impact craters on aluminum foil C2037N from NASA's stardust mission." *Meteoritics and Planetary Science 47, no. 4*, pp. 649-659.

Heger, A., Woosley, S.E., Rauscher, T., Hoffman, R.D., Boyes, M.M. (2002).

"Massive star evolution: nucleosynthesis and nuclear reaction rate uncertainties." *New Astronomy Reviews, vol. 46*, pp. 463-468.

Hoppe, P., Fujiya, W., Zinner, E. (2012). "Sulfur molecule chemistry in supernova ejecta recorded by silicon carbide stardust." *The Astrophysical Journal Letters*, 745:L26, 5pp.

Horan, M.F., Smoliar, M.I., Walker, R.J. (1998). "^{182}W and ^{187}Re-^{187}Os systematics of iron meteorites: Chronology for melting, differentiation, and crystallization in asteroids." *Geochimica et Cosmochimica Acta vol. 62*, pp. 545-554.

Huang, F., Chakraborty, P., Lundstrom, C.C., Holmden, C., Glessner, J.J.G., Kieffer, S.W., Lesher, C.E. (2010). "Isotope fractionation in silicate melts by thermal diffusion." *Nature, vol. 464*. pp. 396-400.

Hulston, J. R. and H. G. Thode (1965a). "Variations in ^{33}S, ^{34}S, and ^{36}S Contents of Meteorites and Their Relation to Chemical and Nuclear Effects." *Journal of Geophysical Research 70(14),* p. 3475.

Hulston, J. R. and H. G. Thode (1965b). "Cosmic-Ray-Produced ^{36}S and ^{33}S in Metallic Phase of Iron Meteorites." *Journal of Geophysical Research 70(18)*: p. 4435.

Kaplan, I.R. and Hulston, J.R.(1966). "The isotopic abundance and content of sulfur in meteorites." *Geochimica et Cosmochimica Acta vol. 30*, pp. 479-496.

Kita N. T., Ikeda Y., Shimoda H., Morshita Y., and Togashi S. (2003) "Timing of basaltic volcanism in ureilite parent body inferred from the ^{26}Al ages of plagioclase bearing clasts in DAG-319 polymict ureilite." *34th Lunar and Planetary Science Conference* #1557. The Lunar and Planetary Institute, Houston.

Kleine, T., Hans, U., Irving, A.J., Bourdon, B. (2012). "Chronology of the angrite parent body and implications for core formation in protoplanets." *Geochimica et Cosmochimica Acta 84,* pp. 186-203.

Kleine T., Mezger K., Palme H., Scherer E. and Mu¨nker C. (2005). "Early core formation in asteroids and late accretion of chondrite parent bodies: evidence from ^{182}Hf–^{182}W in CAIs, metal-rich chondrites, and iron meteorites." *Geochimica et Cosmochimica Acta* 69, pp. 5805–5818.

Kruijer, T.S., Fischer-Godde, M., Kleine, T., Sprung, P., Leya, I., Wieler, R. (2013a) "Neutron capture on Pt isotopes in iron meteorites and the Hf-W chronology of core formation in planetesimals." *Earth and Planetary Science Letters 361*, pp. 162-172.

Kruijer, T.S., Touboul, M., Fischer-Godde, M., Bermingham, K., Kleine, T., Walker, R.J. (2013b) "Resolution of small differences in the time of metal segregation In iron meteorite parent bodies." *44th Lunar and Planetary Science Conference*, #1920. The Lunar and Planetary Institute, Houston.

Labidi, J., Cartigny, P., Birck, J.L., Assayag, N., Bourrand, J.J. (2012) "Determination of multiple sulfur isotopes in glasses: a reappraisal of the MORB $\delta^{34}S$" *Chemical Geology vol. 334*, pp. 189-198.

Lauretta, D.S., Lodders, K., Fegley B. Jr., Kremser, D.T. (1997). "The origin of sulfide-rimmed metal grains in ordinary chondrites." *Earth and Planetary Science letters 151*, pp. 289-201.

Lewis, J.S. (1967). "A Possible origin for sulfates and sulfur in meteorites." *Earth and Planetary Science Letters 2*, pp. 29-32.

Lipschutz, M.E. (1979). "Thermal metamorphism of primitive meteorites-VIII. Noble gases, carbon, and sulfur in Allende(C3) meteorite heated at 400-1000C." *Geochimica et Cosmochimica Acta vol. 43*, pp. 395-404.

Lipschutz, M.E., Signer, P., Anders, E. (1965). "Cosmic-ray exposure ages of iron meteorites by the $^{21}Ne/^{26}Al$ method." Journal of Geophysical Research, vol. 70, no. 6, pp. 1473-1489.

Markowski, A., Quitte, G., Halliday, A.N., Kleine, T. (2006). "Tungsten isotopic compositions of iron meteorites: Chronological constraints vs. cosmogenic effects." *Earth and Planetary Science Letters 242(1-2)*, pp. 1-15.

Masterson, A.L., Farquhar, J., Wing, B.A. (2011). "Sulfur mass-independent fractionation patterns in the broadband UV photolysis of sulfur dioxide Pressure and third body effects." *Earth and Planetary Science Letters 306*, pp. 253-260.

McCoy, T.J., Walker, R.J., Goldstein, J.I., Yang, J., McDonough, W.F., Rumble, D., Chabot, N.L., Ash, R.D., Corrigan, C.M., Michael, J.R., Kotula, P.G. (2011). "Group IVA irons: New constraints on the crystallization and cooling history of an asteroidal core with a complex history." *Geochimica et Cosmochimica Acta 75*, pp. 6821-6843.

McDermott, K. H., Greenwood, R.C., Franchi, I.A., Anand, M., Scott, E.R.D. (2011). "The Relationship between IIE Irons and H Chondrites: Petrologic and Oxygen Isotope Constraints." *Meteoritics & Planetary Science 46*: A152-A152.

McDermott, K.H., Greenwood, R.C., Franchi, I.A., Anand, M., Scott, E.R.D. (2010) "Oxygen isotopic constraints on the origin and the relationship of IIE iron

meteorites and H-chondrites." 41st Lunar and Planetary Science Conference. #2763, The Lunar and Planetary Institute, Houston.

McKeegan, K.D., Kallio, A.P.A., Heber, V.S., Jarzebinski, G., Mao, P.H., Coath, C.D., Kunihiro, T., Wiens, R.C., Nordholt, J.E., Moses, R.W.Jr., Reisenfeld, D.B., Jurewicz, A.J.G., Burnett, D.S. (2011). *"The Oxygen Isotopic Composition of the Sun Inferred from Captured Solar Wind." Science 332*, *no. 6037*, pp. 1528-1532.

McEwing, C.E., Thode, H.G., Rees, C.E. (1980). "Sulphur isotope effects in the dissociation and evaporation of troilite: a possible mechanism for ^{34}S enrichment in lunar soils." *Geochimica et Cosmochimica Acta vol. 44*, pp. 565-571.

Monster, J., Anders, E., Thode, H.G. (1965). "$^{34}S/^{32}S$ ratios for the different forms of sulfur in the Orgeuil meteorite and their mode of Formation." *Geochimica et Cosmochimica Acta vol. 29*, pp. 773 – 779.

Moskovitz, N.A. and Walker, R.J. (2011). "Size of the group IVA iron meteorite core: Constraints from the age and composition of Muonionalusta." *Earth and Planetary Science Letters 308*, pp. 410-416.

Palme, H. and Jones, A. (2003) "Solar System Abundances of the Elements." *Treatise on Geochemistry vol.1.03,* ISBN 0-08-043751-6, Elsevier, pp.41-61.

Pasek, M.A., Milsom, J.A., Ciesla, F.J., Lauretta, D.S., Sharp, C.M., Lunine, J.I. (2005). "Sulfur chemistry with time-varying oxygen abundance during solar system formation." *Icarus 175*, pp. 1-14.

Pravdivtseva, O.V., Meshik, A.P., Hohenberg, C.M., Petaev, M. (2009) "Interpreting the I-Xe system in individual silicate grains from Toluca IAB"; *Meteoritics and Planetary Science 44*, pp. 1787-1796.

Qin, L., Dauphas, N., Wadhwa, M., Masarik, J., Janney, P. E. (2008). "Rapid accretion and differentiation of iron meteorite parent bodies inferred from ^{182}Hf- ^{182}W chronometry and thermal modeling." *Earth and Planetary Science Letters 273(1-2),* pp. 94-104.

Rai, V. K. and M. H. Thiemens (2007). "Mass-independently fractionated sulfur components in chondrites," *Geochimica et Cosmochimica Acta 71(5)*, pp. 1341-1354.

Rai, V. K.. Jackson, T.L., Thiemens, M.H. (2005). "Photochemical mass-independent sulfur isotopes in achondritic meteorites." *Science 309 (5737),* pp. 1062-1065.

Rauscher, T., Heger, A., Hoffman, R. D., &Woosley, S. E. (2002). "Nucleosynthesis

in Massive Stars with Improved Nuclear and Stellar Physicas." *Astrophysical Journal, 576*, pp. 323-348.

Rees, C.E. and Thode, H.G. (1977). "A ^{33}S anomaly in the Allende meteorite." *Geochimica et Cosmochimica Acta, vol. 41*, pp. 1679-1682.

Rees, C.E. and Thode, H.G. (1974) "Sulfur concentrations and isotope ratios in Apollo 16 and 17 samples." *Proceedings of 5th Lunar Science Conference*, pp. 1269-1286.

Roosbroek, N.V., Goderis, S., Debaille, V., Hublet, G., Claeys, P. (2011). "Mont Dieu a IIE non-magmatic iron meteorite with chondrules." *74th Annual Meteoritical Society Meeting*, #5330.

Rubin, A.E. (1997) "Mineralogy of Meteorite Groups." *Meteoritics and Planetary Science 32*, pp. 231-247.

Rubin, A.E. (2002). "Smyer H-Chondrite impact-melt breccia and evidence for sulfur vaporization." *Geochimica et Cosmochimica Acta vol. 66, no. 4*, pp. 699-711.

Schersten, A., Elliot, T., Hawkesworth, C., Russel, S., Masarik, J. (2006). "Hf-W evidence for rapid differentiation in iron meteorite parent bodies." *Earth and Planetary Science Letters 241*, pp. 530-542

Schoenberg, R., Kamber, B.S., Collerson, K.D., Eugster, O. (2002). "New W-isotope evidence for rapid terrestrial accretion and very early core formation." *Geochimica et Cosmochimica Acta no. 17*, pp. 3151-3160.

Schulz, T., Upadhyay, D., Munker, C., Mezger, K. (2012) "Formation and exposure history of non-magmatic iron meteorites and winonaites: Clues from Sm and W isotopes." *Geochimica et Cosmochimica Acta 85*, pp. 200-212.

Schulz, T., Munker, C., Palme, H., Mezger, K. (2009). "Hf-W chronometry of the IAB iron meteorite parent body". *Earth and Planetary Science Letter 280*, pp. 185-193.

Scott, E.R.D., Haack, H., McCoy, T.J. (1996). "Core crystallization and silicate-metal mixing in the parent body of the IVA iron and stony-iron meteorites." *Geochimica et Cosmochimica Acta, vol. 60*, *no. 9,* pp. 1615-1631.

Scott, E. R. D. and J. T. Wasson (1976). "Chemical Classification of Iron-Meteorites .8. Groups IC, IIE, IIIF and 97 Other Irons." *Geochimica et Cosmochimica Acta 40(1),* pp. 103-115.

Scott, E.R.D. (1977). "Composition mineralogy and origin of group IC iron meteorites." *Earth and Planetary Science Letters 37*, pp. 273-284.

Shu, F.H., Shang, H., Lee, T. (1996) “Towards an astrophysical theory of chondrites.” *Science 271*, pp. 1545-1552.

Tachibana, S., and Huss, G.R. (2005). “Sulfur isotopic composition of putative primary troilite in chondrules from Bishunpur and Semarkona.” *Geochimica et Cosmochimica Acta, vol. 69*, pp. 3075-3097.

Teplyakova S.N., and Humayun, M. (2011). “Siderophile elements in the Elga (IIE) metal.” *74th Annual Meeting of the Meteoritical Society*, #5286.

Thiemens, M.H. and Heidenreich, J.E. III (1983) “The Mass-Independent Fractionation of Oxygen: A Novel Isotope Effect and its Possible Cosmochemical Implications.” *Science 219, no. 4588*, pp. 1073-1075.

Tsuchiyama, A., Uyeda, C., Makoshi, Y. (1995). “Incongruent evaporation experiments on iron sulfide ($Fe_{1-\delta}S$) under H_2-rich (at 1 atm) and evacuated conditions.” *Geochemical Journal, vol. 31*, pp. 289-302.

Turro, N.J. and Kraeutler, B. (1980) “Magnetic field and magnetic isotope effects in organic photochemical reactions. A novel probe of reaction mechanisms and a method for enrichment of magnetic isotopes.”*Acc. Chem. Res. 13*, pp. 369-377.

Van Roosbroek, N., Goderis, S., Debaille, V., Hublet, G., Claeys, P. (2011). "Mont Dieu a IIE Non-Magmatic Iron Meteorite with Chondrules." *Meteoritics & Planetary Science 46*: A242-A242.

Voshage, H. and Feldmann, H. (1979). “Investigations on cosmic-ray-produced nuclides in iron meteorites, 3. Exposure ages, meteoroid sizes and sample depths determined by mass spectrometric analyses of potassium and rare gases.” *Earth and Planetary Science Letters 45*, pp. 293-308.

Walker, R.J., McDonough, W.F., Honesto, J., Chabot, N.L., McCoy, T.J., Ash, R.D., Bellucci, J.J. (2008) “Modelling fractional crystallization of group IVB iron meteorites.” *Geochimica et Cosmochimica Acta, vol. 72*, pp. 2198-2216

Wang, P. L., Rumble, D. III, McCoy, T.J. (2004). "Oxygen isotopic compositions of IVA iron meteorites: Implications for the thermal evolution derived from in situ ultraviolet laser microprobe analyses.” *Geochimica Et Cosmochimica Acta 68(5)*, pp. 1159-1171

Wasson, J. T., Huber, H., Malvin, D.J. (2007). "Formation of IIAB iron meteorites." *Geochimica et Cosmochimica Acta 71(3)*, pp. 760-781.

Wasson, J. T. and B. G. Choi (2003). "Main-group pallasites: Chemical composition,

relationship to IIIAB irons, and origin." *Geochimica et Cosmochimica Acta 67(16),* pp. 3079-3096.

Wasson, J. T. and G. W. Kallemeyn (2002). "The IAB iron-meteorite complex: A group, five subgroups, numerous grouplets, closely related, mainly formed by crystal segregation in rapidly cooling melts." *Geochimica et Cosmochimica Acta 66(13),* pp. 2445-2473.

Wasson, J. T. and J. W. Richardson (2001). "Fractionation trends among IVA iron meteorites: Contrasts with IIIAB trends." *Geochimica et Cosmochimica Acta 65(6),* pp. 951-970.

Wasson J. T. (1999) "Trapped melt in IIIAB irons: solid/liquid elemental partitioning during the fractionation of the IIIAB magma." *Geochimica et Cosmochimica Acta* 63, pp. 2875–2889.

Wasson J. T., Choi B. G., Jerde E. A., and Ulff-Møller F. (1998). "Chemical classification of iron meteorites. Part XII: New members of the magmatic groups." *Geochimica et Cosmochimica Acta* 62, pp. 715–724.

Wasson J. T., Ouyang X. W., Wang J. M., and Jerde E. (1989) "Chemical classification of iron meteorites. Part XI: Multi-element studies of 38 new irons and the high abundance of ungrouped irons from Antarctica." *Geochimica et Cosmochimica Acta 53*, pp. 735–744.

Wasson J. T. and Wang J. M. (1986) A non-magmatic origin of group IIE iron meteorites. *Geochimica et Cosmochimica Acta* 50, pp. 725–732.

Wasson J. T. and Wai C. M. (1976) "Explanation for the very low Ga and Ge concentrations in some iron meteorite groups." *Nature 261,* pp. 114–116.

Wasson J. T. (1971) "Chemical classification of iron meteorites. Part V: Groups IIIC and IIID and other irons with germanium concentrations between 1 and 25 ppm." *Icarus 14*, pp. 59–70.

Wasson J. T. (1970) "Chemical classification of iron meteorites. Part IV: Irons with Ge concentrations greater than190 ppm and other meteorites associated with group I." *Icarus 12,* pp. 407–423.

Wasson J. T. (1969) "Chemical classification of iron meteorites.Part III: Hexahedrites and other irons with germanium concentrations between 80 ppm and 200 ppm." *Geochimica et Cosmochimica Acta* 33, pp. 859–876.

Wasson J. T. (1967) "Chemical classification of iron meteorites. Part I: A study of iron meteorites with low concentrations of gallium and germanium. *Geochimica et Cosmochimica Acta 31,* pp. 161–180.

Wasson J. T. and Kimberlin J. (1967) “Chemical classification of iron meteorites. Part II: Irons and pallasites with germanium concentrations between 8 and 100 ppm.” *Geochimica et Cosmochimica Acta* 31, pp. 2065–2093.

Welton,, K.C., Nishizumi, K., Lavielle, B., Caffee, M.W., Hillegonds, D.J., Finkel, R.C., Kollar, D., Masarik, J. (2008). “The complex exposure histories of the Pitts and Horse Creek iron meteorites: Implications for meteorite delivery models.” *Meteoritics and Planetary Science 43, n. 8*, pp. 1321-1332.

Wing, B.A., and Farquhar, J. (2013) “Planetary Sulfur Isotopic Baseline from Lunar Basalts” *Geochimica et Cosmochimica Acta, (submitted).*

Wolk, S.J., Harnden, F.R. Jr., Flaccomio, E., Micela, G., Favata, F., Shang, H, Feigelson, E.D. (2005). “Stellar Activity on the Young Suns of Orion COUP Observations of K5-7 Pre-Main-Sequence Stars.” *Astrophysical Journal suppl. 160*, pp 1-49.

Woods, J.A. and Hashimoto, A. (1993) “Mineral Equilibrium in fractionated nebular systems.” *Geochimica et Cosmochimica Acta vol. 57*, pp. 2377-2388.

Woosley, S.E. and Heger A. (2007). “Nucleosynthesis and remnants in massive stars of solar metallicity.” *Physics Reports*, *vol. 442*, pp. 269-283.

Woosley, S.E. and Weaver, T.A. (1995). “The evolution and explosion of massive stars 2. Explosive hydrodynamics and nucleosynthesis.” *Astrophysical Journal Suppl. S. 101*, pp. 181–235.

Yang J., Goldstein, J.I., Michael, J.R., Kotula, P.G., Scott, E.R.D. (2010). “Thermal history and origin of the IVB iron meteorites and their parent body.” *Geochimica et Cosmochimica Acta 74*, pp. 4493-4506.

Yang , J., Goldstein, J.I., Scott, E.R.D. (2008). “Metallographic cooling rates and origin of IVA iron meteorites.” *Geochimica et Cosmochimica Acta 72*, pp. 3043-3061.